MATEUS ZANOVELLO

Recycled Portland Cement (R-PC): Water demand reduction, environmental analysis and use as engineered binder

São Paulo
2023

MATEUS ZANOVELLO

Recycled Portland Cement (R-PC): Water demand reduction, environmental analysis and use as engineered binder

Original Version

Master's Thesis presented to the Graduate Program in Civil Engineering at the Polytechnic School of the University of São Paulo for the degree of Master of Science.
Concentration area: Civil and Urban Construction Engineering.
Advisors: Prof. Dr. Sérgio Cirelli Angulo.

São Paulo
2023

Cataloging in publication
Library and Documentation Service
Institute of Civil Engineering at the University of São Paulo

Zanovello, Mateus
Cimento Portland Reciclador (R-PC): Redução da demanda de água, análise ambiental e uso como ligante otimizado / M. Zanovello -- São Paulo, 2023.

129 p.

Dissertação (Mestrado) - Escola Politécnica da Universidade de São Paulo. Departamento de Engenharia de Construção Civil.

1.Cimento Portland 2.Reciclagem 3.Economia Circular 4.Sustentabilidade I.Universidade de São Paulo. Escola Politécnica. Departamento de Engenharia de Construção Civil II.t.

Zanovello, Mateus. **Recycled Portland Cement (R-PC): Water demand reduction, environmental analysis and use as engineered binder**. 2023. 129p. Thesis (Master's in Civil and Urban Construction) - Polytechnic School, University of São Paulo, São Paulo, 2023.

Approved in:

Examination Board

Prof. Dr. Sérgio Cirelli Angulo

Institution: University of São Paulo

Judgment: _____

Prof. Dr. Qingliang Yu

Institution: Eindhoven University of Technology

Judgment: _____

Prof. Dr. Claire White

Institution: Princeton University

Judgment: _____

ACKNOWLEDGMENT

This part is mostly for my family, so it is written in Portuguese.

Meu primeiro agradecimento é destinado à minha família. Sendo assim, eu gostaria de expressar minha mais profunda gratidão aos meus pais, Flávia e Paulo. Seu amor, apoio e ensinamentos são o alicerce sobre o qual construo minha jornada. Estendo este agradecimento inicial ao meu irmão, Lucas, por seu apoio que apesar de expresso de forma singular, se fez presente. Agradeço à minha noiva, Fernanda, por todo o apoio, presença, disponibilidade e amor ao longo desta trajetória repleta de desafios. Não tenho capacidade de expressar em palavras tamanha gratidão e amor por todos vocês.

Meu segundo agradecimento é dedicado a todos os professores que desempenharam um papel fundamental na minha busca por conhecimento. Em especial, gostaria de expressar minha gratidão à Prof. Heloísa Cordon, que me apresentou ao fascinante mundo dos materiais cimentícios. Ao Prof. Leandro Sanchez, cujo intercâmbio foi um divisor de águas e me mostrou que o meu verdadeiro caminho era seguir com o mestrado. Ao Prof. Vanderley John, de quem sempre me inspirei a 'pensar fora da caixa.' E, sobretudo, ao Prof. Sérgio Angulo, meu orientador e amigo, que desempenhou um papel fundamental na minha evolução nessa área que tanto amo.

Meu terceiro agradecimento é geral, direcionado a todos que, de alguma forma, contribuíram ao longo deste trabalho. Agradeço aos colegas de pós-graduação e aos profissionais da USP. Também gostaria de expressar minha gratidão ao Laboratório de Tratamento de Minérios e Resíduos Industriais (LTM) pelo auxílio na moagem das pastas. Ao Departamento de Engenharia Metalúrgica e de Materiais (PMT), agradeço a assistência na realização das porosimetrias de mercúrio. Quero também agradecer ao Instituto de Pesquisas Tecnológicas (IPT) pela disponibilidade na realização das calorimetrias. Por fim, um agradecimento especial ao Laboratório de Microestrutura (LME), ao Innovandi Global Cement and Concrete Research Network e ao National Institute on Advanced Eco-efficient Cement-based Technologies (CEMtec).

EPIGRAPH

“A curiosidade é a fome do intelecto.”

Rubem Alves

RESUMO

Zanovello, Mateus. **Cimento Portland Reciclador (R-PC): Redução da demanda de água, análise ambiental e uso como ligante otimizado**. 2023. 129p. Dissertação (Mestrado em Construção Civil e Urbana) – Escola Politécnica, Universidade de São Paulo, São Paulo, 2023.

A cada ano, 2 bilhões de toneladas de cimento antigo proveniente de resíduos de concreto não são recuperadas pela indústria do cimento, apesar do alto potencial de redução das emissões de CO_2 provenientes da produção de cimento Portland. Nesta pesquisa, primeiro, exploramos o cimento Portland reciclado (R-PC, termoativado a 500°C) como um ligante único, reduzindo a relação água/sólidos e utilizando dispersantes. O R-PC apresentou desempenho mecânico limitado e desempenho ambiental semelhante ao cimento Portland comum (OPC). Portanto, em seguida, o R-PC foi modificado com calcário e uma quantidade reduzida de clínquer de Portland finamente moído para produzir um cimento com baixa pegada de CO_2 e alta resistência inicial (ARI). Os vazios no sistema de empacotamento granular foram reduzidos usando uma abordagem de preenchimento reverso. Os cimentos modificados exigiram menos água e dispersantes, atingindo resistências à compressão mais elevadas. O cimento modificado com 80% de cimento reciclado e 20% de cimento Portland finamente moído alcançou 73% da resistência do cimento Portland ARI (36 MPa em 28 dias, relação água/sólidos de 0,48 g/g) com uma redução de 63% nas emissões de CO_2 na fabricação (317 kgCO_2 por tonelada), oferecendo assim a maior eficiência ambiental. Os cimentos engenheirados podem igualar a resistência do cimento Portland ARI com um terço do clínquer.

Palavras-chave: Cimento reciclado. Reidratação. Cimentos ternários. Análise ambiental. Redução da demanda de água.

ABSTRACT

Zanovello, Mateus. **Recycled Portland Cement (R-PC): Water demand reduction, environmental analysis and use as engineered binder**. 2023. 129p. Thesis (Master's in Civil and Urban Construction) - Polytechnic School, University of São Paulo, São Paulo, 2023.

Every year, 2 billion tons of old cement from concrete waste go unrecovered by the cement industry, even though it has the potential to reduce CO_2 emissions from Portland cement production. In this research, first, we explored recycled Portland cement (R-PC, thermoactivated at 500°C) as a unique binder through water-to-solids ratio reduction and dispersant use. The R-PC presented a limited mechanical performance and similar environmental performance to ordinary Portland cement (OPC). Therefore, secondly, R-PC was engineered with limestone filler and a reduced quantity of finely grounded Portland Clinker to produce low-CO_2 high-initial strength engineered blended cements. The voids in the granular packing system were reduced using a reverse filling approach. The engineered cements required less water demand and dispersant content, achieving higher compressive strengths. The engineered cement with 80% recycled cement and 20% finely-ground Portland cement achieved 73% of the high-initial strength Portland cement (36 MPa at 28 days, water-to-solids ratio of 0.48g/g) with a 63% reduction in CO_2 emissions of manufacture (317 kg CO_2/ton), thereby offering the highest environmental efficiency. The engineered recycled blended cements can equalize high-initial Portland cement strength with one-third of the clinker.

Keywords: Recycled cement. Rehydration. Blended cement. Environmental analysis. Water demand reduction.

SUMMARY

1 INTRODUCTION

1.1 Background

Portland cement is a crucial material for modern society's development. The society's increasing demand for infrastructure and habitations made the pace of Portland cement production overtake not only all construction materials, but also population growth (MILLER et al., 2018; STATISTA, 2020; UNITED NATIONS, 2019). In 2020, almost 4.5 gigatons were produced (STATISTA, 2020). This elevated cement production is a cause of environmental concerns. Portland cement production involves the depletion of natural resources and greenhouse gas emissions. The cement industry contributes to 7-8% of the world's anthropogenic carbon dioxide (CO_2) emissions (SCRIVENER; JOHN; GARTNER, 2018).

The cement industry adopted the partial replacement of cement with supplementary cementitious materials (SCMs) (LOTHENBACH; SCRIVENER; HOOTON, 2011) as the main strategy to reduce the environmental impact. The cement industry annually recycles more than 400 Mt of industrial waste or co-products as SCMs, making it one of the largest recyclers in the economy. However, this waste comes from other industries and this approach only contributes to mitigate part of environmental issues and its maximum potential benefits have already been explored. Thus far, the cement industry has recycled little of its own waste in cement production.

The literature shows that concrete waste fines can be recycled as clinker raw material or recycled Portland cement (R-PC) by calcination (SHUI et al., 2008; SPLITTGERBER; MUELLER, 2003; ZHUTOVSKY; SHISHKIN, 2021). Therefore, Recycled Portland cement is the recycled cementitious materials from waste cement paste or concrete made of Portland cement, which have binding capacity after thermal treatments. R-PC characteristics primarily depend on the precursor material and dehydration temperature (CARRIÇO; BOGAS; GUEDES, 2020). In this context, researchers have adopted laboratory-made pure Portland cement pastes or concrete waste fines (containing aggregates) as precursor materials. However, a basic understanding of pure cementitious pastes is still required (XU et al., 2022). When subjected to heat treatment, the hydrated products (e.g., ettringite, other calcium aluminates, portlandite and C-S-H phases) have their free and chemically combined water partially or totally removed (CASTELLOTE et al., 2004; VYŠVAŘIL et al., 2014; REAL et al., 2020; ANGULO et al., 2022; BOGAS et al., 2022; LÜ; HE; HU, 2008). Two critical temperatures and the associated processes were identified (ALONSO; FERNANDEZ, 2004): (i) above 450 °C, portlandite dehydrates may form quick lime (a high water reactive compound that is not always desirable as a cementitious material), and (ii) approximately 650 ºC, calcite decomposes

to generate CO_2 (ZHANG; YE, 2013). Therefore, recycled cement may contain partially dehydrated phases, residual hydration products, and anhydrous cement particles, depending on the dehydration temperature among other factors (SHUI et al., 2009). In particular, recycled cement is of interest because, at calcination temperatures lower than 550 °C, CO_2 emissions of recycled cement due to decarbonation are avoided.

When anhydrous calcined fines are exposed to water again, they rapidly regain chemically bound water (XINWEI; ZHAOXIANG; XUEYING, 2010; ANGULO et al., 2015a; LIMA PACHECO et al., 2021). The R-PC generates a large amount of heat in the first few minutes of rehydration as ordinary Portland cement (OPC) (ANGULO et al., 2015a), recovering combined water in C-S-H (ANGULO et al., 2022), in part of the CaO (quicklime) formed (MENÉNDEZ; ANDRADE; VEGA, 2012). The morphologies of the hydrated and rehydrated phases are significantly different (WANG; MU; LIU, 2018). The R-PC paste showed abundant nanometric particles of C-S-H gel and $CaCO_3$. R-PC requires more mixing water than OPC to produce a workable mixture (XUAN; SHUI, 2011). This is a result of the high surface area and higher internal porosity, which include thermal cracks during dehydration (BOGAS; CARRIÇO; TENZA-ABRIL, 2020; ZHANG; YE; KOENDERS, 2013) and a tendency to agglomerate (YU; SHUI, 2013). Although the compressive strength of recycled cement can be higher at early ages (3 days), it is lower at 28 days than that of OPC (BALDUSCO et al., 2019; BOGAS; CARRIÇO; TENZA-ABRIL, 2020). No further investigation of the compressive strength and porosity relationship has been conducted so far.

R-PC exhibits high reactivity against SCMs characteristically low reactivity. Therefore, recycled Portland cement is a circular economy alternative to the cement industry. However, the elevated water demand of recycled cement may erode its high reactivity. Better strategies for improving the mechanical performance of R-PC-based materials include blending R-PC with OPC (BOGAS; CARRIÇO; PEREIRA, 2019; CARRIÇO; REAL; BOGAS, 2021; YU; SHUI, 2013) or supplementary cementitious materials (e.g., blast furnace slag (LU; HE; HU, 2009; WANG; MU; LIU, 2018; ZHANG et al., 2018), fly ash (SHUI et al., 2014; SHUI; YU; DONG, 2011) or silica fume (SERPELL; LOPEZ, 2013)) and dispersant use (BALDUSCO et al., 2019; CARRIÇO et al., 2022). However, reducing the water demand of R-PC-based materials with dispersants and through blends with cement and filler have not been explored combined and in-depth.

The reduction of mixing water demand and, consequently, the water/binder ratio reduction is a key parameter to reduce porosity (BROUWERS, 2004; POWERS, 1958) and improve strength (DE LARRARD, F., 1999), reducing the environmental impact of products

made with recycled Portland cement. For that reason, performance indices are crucial for optimizing the use and performance of cementitious materials.

1.2 Objectives

In this dissertation the use of R-PC is optimized in terms of water demand (and porosity) reduction, and of environmental performance, as (i) a solo binder, and (ii) as engineered blended binder using recycled cement, microcement and limestone filler.

1.3 Dissertation' structure

This work is divided into five chapters.

Chapter 1 contextualizes the main topics and motivations of this research. In addition, the objectives and structure of the thesis are presented.

Chapter 2 presents the recycled cement fundamentals through a literature review. Physicochemical characteristics and mechanical properties of dehydrated and rehydrated cement are approached.

Chapter 3 explores the strength-porosity relationship of recycled Portland cement and the water demand reduction through dispersant use. Binder efficiency and environmental impact are analyzed. A literature database was created to provide an overview of recycled cement behavior.

Chapter 4 demonstrates the optimizations of recycled cement through microcement, limestone filler and dispersant use. Concepts related to optimization and the associated logic are explained.

Chapter 5 shows the future outlooks.

2 RECYCLED PORTLAND CEMENT: FUNDAMENTALS

This chapter aims to review the fundamentals of recycled Portland cement. The chapter is divided into four sections: (i) Portland cement hydration, (ii) dehydration of cementitious materials, (iii) R-PC rehydration, and (iv) literature strategies to improve R-PC-based materials. The sessions allow a review of the production, characteristics, and properties of R-PC-based materials.

2.1 Portland cement hydration

Ordinary Portland cement (OPC) is composed of 95-97% clinker and 3-5% gypsum, mass percentages (TAYLOR, 1997). In clinker, 75% of the compounds are calcium silicates (i.e., alite C_3S and belite C_2S) with the other aluminates phases (i.e., C_3A and C_4AF) (MEHTA; MONTEIRO, 2014).

During the OPC hydration process, several chemical species (cations and anions) dissolve until environment saturation. Hydrated compounds (insoluble components) precipitate from the ion-rich liquid phase, which promotes an increase in the volume of solids and a progressive reduction in the void volume. Therefore, the system gains consistency and hardens (MARCHON; FLATT, 2016). The main hydration products are hydrated calcium silicates (C-S-H) and portlandite (CH), Equation 1 and Equation 2, respectively (BENTZ, 1997). The hydration of tricalcium aluminate (C_3A) is rapid, and the reaction products are crystalline hydrates. These reactions occur almost immediately, making the use of pure clinker unfeasible.

Therefore, calcium sulfate is added for initial setting reactions and the hardening control, which changes the resulting phases. Equation 3 and Equation 4 exhibits the hydrated calcium trisulfoaluminate (ettringite - AFt) and hydrated calcium monosulfoaluminate (AFm) formed through C_3A and calcium sulfate reactions, respectively. Equation 5 and Equation 6 show AFt and AFm produced through C_4AF and calcium sulfate reactions, respectively (BENTZ, 1997; MARCHON; FLATT, 2016).

$$C_3S + 5.3H \rightarrow C_{1.7} - S - H_4 + 1.3CH \quad \text{Equation 1}$$

$$C_2S + 4.3H \rightarrow C_{1.7} - S - H_4 + 0.3CH \quad \text{Equation 2}$$

$$C_3A + 3C\$H_2 + 26H \rightarrow C_6A\$_3H_{32}\ (\boldsymbol{AFt}) \quad \text{Equation 3}$$

$$2C_3A + C_6A\$_3H_{32} + 4H \rightarrow 3C_4A\$H_{12}\ (\boldsymbol{AFm}) \quad \text{Equation 4}$$

$$C_4AF + 3C\$H_2 + 30H \rightarrow CH + FH_3 + C_6A\$_3H_{32}\ (\boldsymbol{AFt}) \quad \text{Equation 5}$$

$$2C_4AF + C_6A\$_3H_{32} + 12H \rightarrow 2CH + 2FH_3 + 3C_4A\$H_{12}\ (\boldsymbol{AFm}) \quad \text{Equation 6}$$

The hydration phenomena are many and complex. It is necessary to combine several characterization techniques for a better understanding. Isothermal calorimetry is used to evaluate the cement reactivity by the heat released over time (Figure 1). Cement hydration has four stages. The first three have a behavior similar to C_3S (the main constituent of cement) (BULLARD et al., 2011). The fourth is controlled by aluminates (TAYLOR, 1997).

Figure 1 - Calorimetry curve of modern Portland cement.

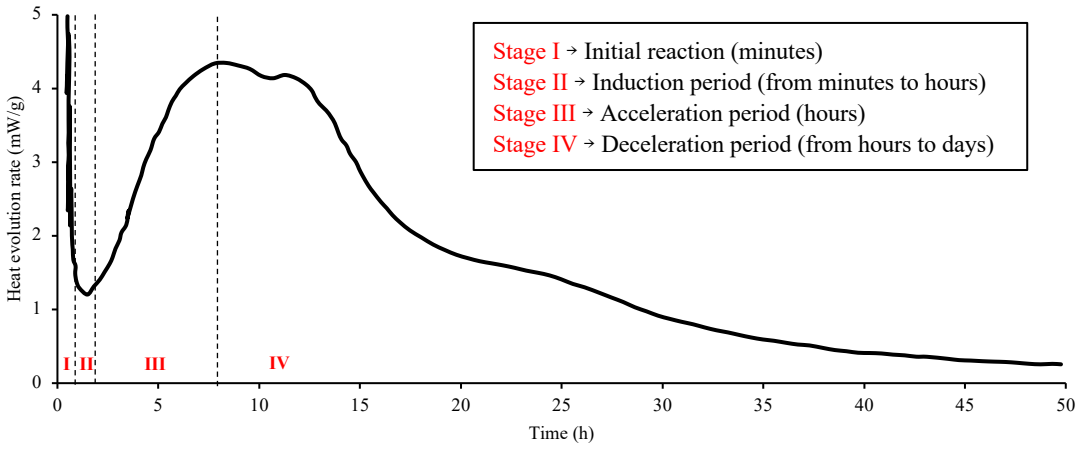

Adapted from (BULLARD et al., 2011).

In Stage I, high heat flux is observed. It is associated with particles wetting and fast hydration of alite. In the induction period (Stage II), the ions dissolution and ettringite formation occur. In the acceleration period (Stage III), the precipitation of ettringite, C-S-H, and portlandite occur. It promotes a transition in the pastes' rheological behavior from a liquid to a solid. In the deceleration period (Stage IV), part of the ettringite is converted into monosulfoaluminates. It occurs due to the reduction in the sulfate ions content in the pore solution (MARCHON; FLATT, 2016).

For advanced ages, the volume of the hydrated solids is mostly C-S-H (45% on a volumetric basis) and portlandite (25%). The other phases are sulfoaluminates and carboaluminates (20%), minor phases (e.g., magnesium compounds), and anhydrous phases (e.g., unreacted alite and belite).

Figure 2 shows the hydrated phases' transformation over time. The thermogravimetric (TG) and x-ray diffraction (XRD) data corroborate with the thermodynamic simulation. The system is dynamic during hydration, with several phases dissolving, forming, or transforming, at different rates, in a set of reactions that can occur sequentially or in parallel.

Figure 2 - Thermodynamic simulation of OPC hydration, validated with experimental data.

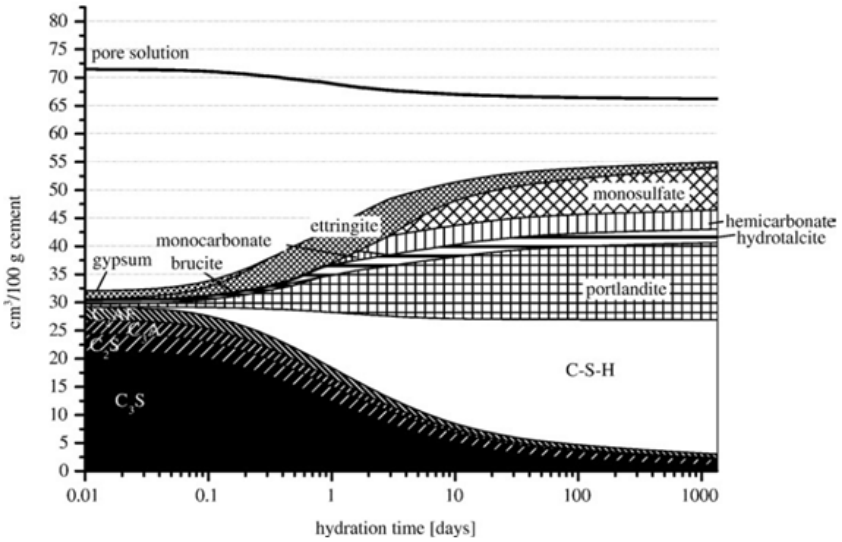

Extracted from (LOTHENBACH et al., 2008).

Table 1 presents the composition of anhydrous OPC and OPC paste at 28 days (water/cement ratio of 0.80 g/g) through Rietveld refinement of XRD (ANGULO et al., 2022). The values corroborate the literature and the thermodynamic simulation (LOTHENBACH et al., 2008).

Table 1 - Quantitative XRD of the cement and the hydrated cement.

Phase	Content (%)	
	Cement	Hydrated cement (28d)
Alite (C_3S)	50.9	
Belite (C_2S)	14.8	
Calcium aluminate (C_3A)	3.7	
Brownmillerite (C_4AF)	9.8	0.2
Calcium sulfate dihydrate	1.4	
Bassanite	8.0	
Calcite ($CaCO_3$)	11.3	16.8
Portlandite (CH)	0.1	21.3
Amorphous (C-S-H)		43.0
Ettringite (Aft)		3.6
Larnite		5.1
Rwp	6.30	6.07
Gof	1.89	1.92

Adapted from (ANGULO et al., 2022).

2.2 Dehydration of cementitious materials

Dehydration is a term used to explain the loss of water molecules from cement hydrated compounds in certain temperature ranges (Table 2). The heating process implies a succession

of transformations in the hydrated cement phases (ALONSO; FERNANDEZ, 2004; FARAGE; SERCOMBE; GALLÉ, 2003; GUILGE, 2011; SHUI et al., 2008).

Table 2 - Typical thermal events of hydrated cement compounds.

Thermal events (Decomposition of)	Temp. range (peak) [°C]	Sources
Ettringite (AFt)	70 – 114 (90)	(BAQUERIZO; MATSCHEI; SCRIVENER, 2016; SHUI et al., 2008; ZHOU; LACHOWSKI; GLASSER, 2004)
Calcium sulfoaluminates (AFm)	50 – 250 (180)	(REN et al., 2014; TAYLOR, 1997; WANG; LACARRIÈRE; SELLIER, 2019)
Brucite [$Mg(OH)_2$]	330 – 430 (360)	(REN et al., 2014; TAYLOR, 1997; WANG; LACARRIÈRE; SELLIER, 2019)
C-S-H	100 – 650	(ALONSO; FERNANDEZ, 2004; BRUTON et al., 1993; TAYLOR, 1997; ZHANG; YE, 2012)
Portlandite [$Ca(OH)_2$]	430 – 510 (480)	(MENÉNDEZ; ANDRADE; VEGA, 2012; TAYLOR, 1997; ZHANG; YE, 2012)
Calcite [$CaCO_3$]	700 – 900 (790)	(TAYLOR, 1997; ZHANG; YE, 2012)

Extracted from (ANGULO et al., 2022).

Ettringite decomposed as calcium aluminate compounds and bassanite. C-S-H decomposed progressively, becoming mostly amorphous and forming intermediate calcium silicates. Portlandite decomposes in quicklime (CaO), not necessarily in crystalline form. Calcite became free lime.

Thermal activation promotes a partial recovery of the binding capacity of cementitious materials through hydrated phases dehydration, partially recovering the original composition, non-hydrated phases (SPLITTGERBER; MUELLER, 2003).

Among the parameters present in the dehydration process, the heat treatment temperature deserves to be highlighted as it directly influences the dehydration of the phases (SHUI et al., 2009; VYŠVAŘIL et al., 2014). The influence of treatment temperature on the composition of recycled cement was studied by Zhang and Ye (ZHANG; YE, 2013) through analysis of XRD curves by the Rietveld method (Figure 3).

Zhang and Ye (ZHANG; YE, 2013) indicated that the calcium oxide produced by the decomposition of CH is present as an amorphous phase mostly at 500 °C. For increasing temperatures, calcium oxide is gradually transformed into crystalline lime. The authors infer that the C-S-H dehydration until 400 °C does not significantly change the crystalline composition. For dehydration up to 500 °C, C-S-H turned partially into β-C_2S. It indicates that the long silicate chains in C-S-H were broken. Moreover, C-S-H became linearly more crystalline as it is dehydration degree increased.

Figure 3 - Quantitative analysis of phase transition of heated Portland cement paste.

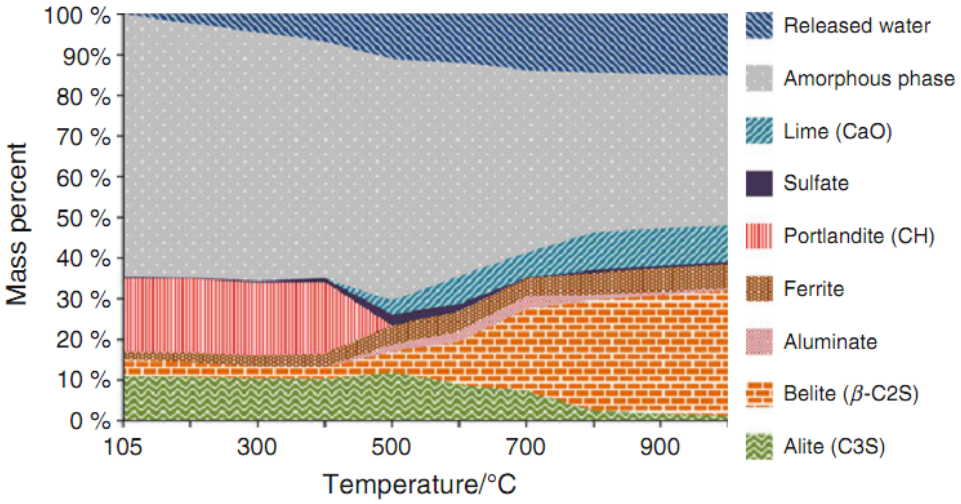

Extracted from (ZHANG; YE, 2013).

2.2.1 Dehydration of hydrated phases

2.2.1.1 Calcium silicate hydrate (C-S-H)

Hydrated calcium silicates are a set of phases with variable stoichiometry, called in a broad form of C-S-H. It is the major present phase in hydrated Portland cement (45%-55% of hydrated products by volume). Therefore, it is primarily responsible for filling voids. In addition, C-S-H directly contributes to the mechanical strength of hydrated Portland cement due to its high surface area and Van der Waals forces (MEHTA; MONTEIRO, 2014).

Lothenbach and Nonat (LOTHENBACH; NONAT, 2015) described the structure of the C-S-H phases as a function of the Ca/Si and H_2O/Si ratios (Figure 4). The C-S-H phases have a tobermorite-like structure but are defective. C-S-H structure is represented by Si-O silicate tetrahedral chains (*dreierketten structure)* associated with Ca-O polyhedral as an intermediate layer. In the interlamellar space between these structures, there are Ca^{2+} ions and water molecules (SHAW; HENDERSON; KOMANSCHEK, 2000; ZHANG et al., 2018).

C-S-H has a variable stoichiometry ($xCaO.SiO_2.yH_2O$) and chains of different sizes, amounts, and types of water within its structure. Therefore, this phase presents dehydration reactions in multiple steps (ZHANG; YE, 2012; ZHANG; YE; KOENDERS, 2013). The dehydration may collapse the microstructure of hydrated phases (Figure 5). The main cement paste compound (C-S-H) suffers densification in its interatomic structure when dehydrated. Hence, an intermediate compound type is formed, nesosilicate (ALONSO; FERNANDEZ, 2004).

Figure 4 - Schematic diagram representing the tobermorite structure showing the *dreierketten* chains of silica and evolution of the mean chain length of silica in C–S–H determined by ^{29}SiNMR in function of Ca/Si.

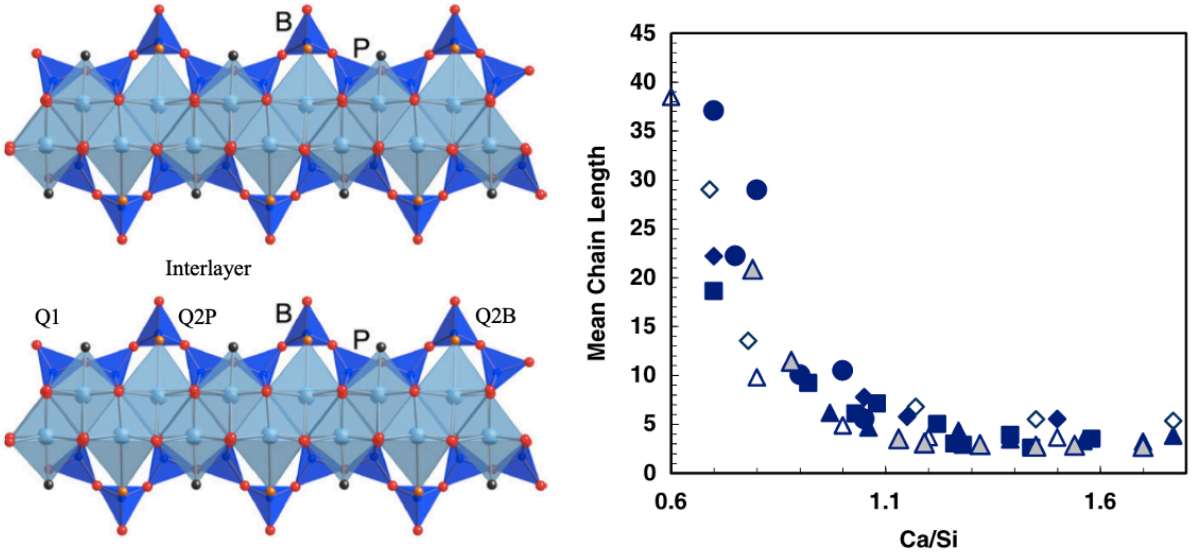

Adapted from (LOTHENBACH; NONAT, 2015; RICHARDSON, 2008).

Figure 5 - The schematic of C–S–H at high temperature.

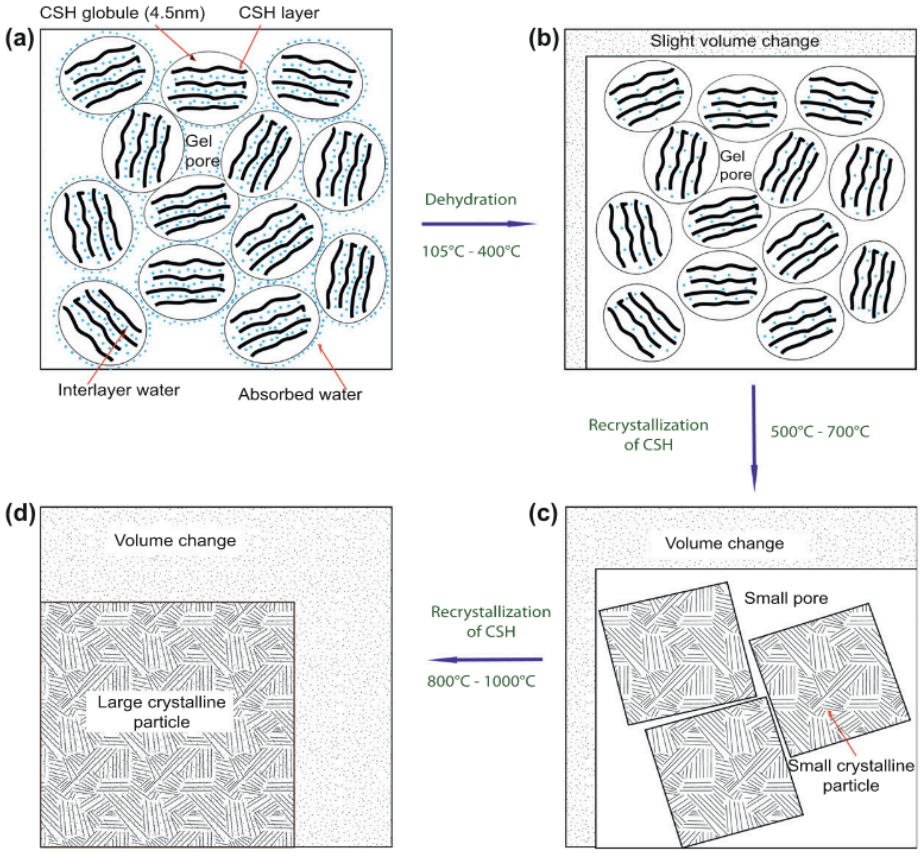

Extracted from (ZHANG; YE; KOENDERS, 2013).

2.2.1.2 Portlandite (CH)

Calcium hydroxide, also called portlandite (CH), makes up 20 to 25% of the volume of solids in hydrated Portland cement paste. Portlandite undergoes dehydration between 430 °C and 510 °C, decomposing into calcium oxide and water (Equation 7).

$$Ca(OH)_2 \rightarrow CaO + H_2O \qquad \text{Equation 7}$$

CH crystals are typically large hexagonal prismatic crystals.

2.2.1.3 Sulfoaluminates

Ettringite is composed of a two-column of cationic structure ($[Ca_3Al(OH)_6.12H_2O]^{3+}$) filled by anions (e.g., sulfate SO_4^{2-} and hydroxyl OH^-) into the interlamellar channel (ZHOU; LACHOWSKI; GLASSER, 2004) (Figure 6).

Baquerizo and coauthors (BAQUERIZO; MATSCHEI; SCRIVENER, 2016) studied the stability of ettringite as a function of temperature and water vapor pressure on synthetic samples (Figure 6). Crystalline ettringite has a water content per mol of Al_2O_3, varying from 30 to 32 H_2O, while the amorphous product formed on drying it, metaettringite, has only 9 to 13 H_2O.

Figure 6 - Crystal structures of ettringite (left) and stability of ettringite as a function of drying temperature and relative humidity (right).

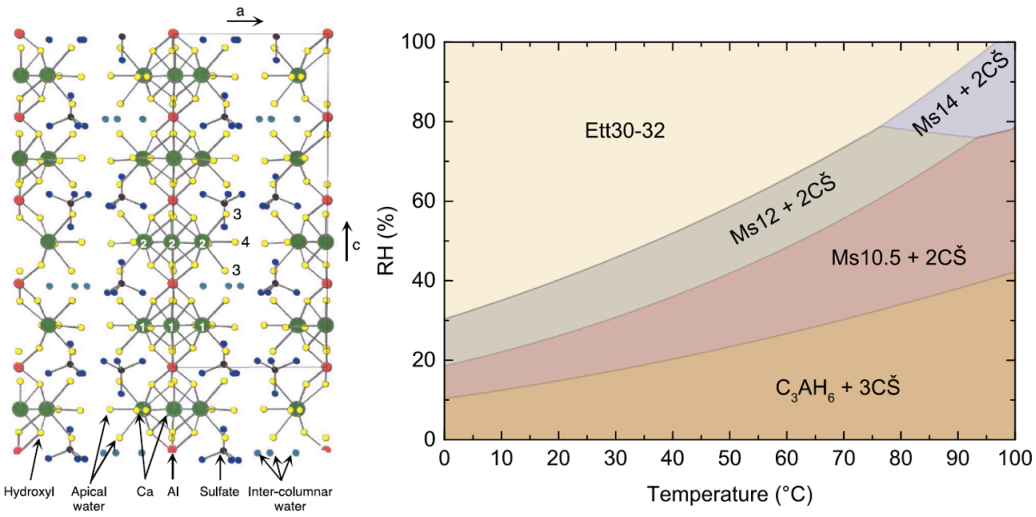

Adapted from (ZHOU; LACHOWSKI; GLASSER, 2004) and (BAQUERIZO; MATSCHEI; SCRIVENER, 2016).

The ettringite can lose 20 molecules of water of its constitution up to 100 °C without losing its structure, becoming a metastable phase. Ettringite can convert into monosulfoaluminates and anhydrite (calcium sulfate). Under more severe conditions, ettringite

decomposes into hydrogrenade (C_3AH_6) and anhydrite.

Over time, ettringite converts to monosulfoaluminates in cement pastes (MATSCHEI; LOTHENBACH; GLASSER, 2007). The ettringite becomes carboaluminate if the cement paste has limestone filler (BONAVETTI; RAHHAL; IRASSAR, 2001). Monosulfoaluminates have a lamellar structure with main layers of $[Ca_2Al(OH)_6]^+$. The interlamellar layer has SO_4^{2-} ions and water (DILNESA et al., 2012; MATSCHEI; LOTHENBACH; GLASSER, 2007). For carboaluminates, there is a CO_3^{2-} ion in the interlamellar layer, together with water and sulfate ions. Up to 260 °C, water loss occurs in the interlamellar layer. The loss of hydroxyls in the main layers occurs up to 300 °C.

Both monosulfoaluminates and carboaluminates are considered lamellar double hydroxide (LDH) structures. Therefore, those aluminates are able to reform in the presence of water, hydroxyls, and other anion compounds (sulfate, carbonate, etc.) (RAKI; BEAUDOIN; MITCHELL, 2004).

2.2.2 Characteristics of dehydrated cementitious materials

Recycled cement shows a variable behavior, depending on the recycling procedure. The recycling precursor material and the dehydration process are the most influential factors. Thus, to reduce the variables and allow a greater comparison degree, most papers define a cementitious paste with a water/solid ratio between 0.40 and 0.55 as precursor material. On the other hand, the dehydration process and all parameters involved as treatment temperature, treatment duration, heating rate, and cooling procedure remain varied. These directly influence the composition and, consequently, the characteristics of R-PC (CARRIÇO; BOGAS; GUEDES, 2020; SHUI et al., 2008, 2009). Recycled cement physicochemical changes are possible to verify through combining characterization techniques.

2.2.2.1 X-ray fluorescence (XRF)

X-ray fluorescence (XRF) allows an evaluation of the chemical elements in recycled Portland cement, and it is the most used method to describe chemical composition. Table 3 exhibits the XRF results for Portland cement and R-PC. The R-PCs were produced through different sources and dehydration temperatures. The chemical elements and contents of R-PC are similar to those of Portland cement.

Table 3 - XRF results for Portland cement and R-PC in the literature.

Ref	Binder (Temp. °C)	Source	Oxides (%)						
			CaO	SiO_2	Al_2O_3	Fe_2O_3	MgO	f-CaO	LOI
(CARRIÇO et al., 2022)	OPC		62.8	19.6	5.34	3.05	1.80	0.70	
	DCP (0)	OPC paste (w/s = 0.55)	50.1	14.7	3.97	2.49	1.29		
	DCP (700)	OPC paste (w/s = 0.55)	60.8	19.1	5.13	3.00	1.77	13.9	
	DCP (700)	OPC paste (w/s = 0.35)	64.9	20.7	5.34	3.12	1.85		
	DCW (700)	Concrete waste	47.0	19.4	4.31	2.40	1.29		
(YU; SHUI, 2013)	OPC		59.4	20.5	5.21	3.15	2.80		1.09
	DWCP (650)	Waste cement paste	58.6	22.3	5.52	3.57	0.24		3.42
(ZHANG et al., 2018)	OPC		54.6	24.6	7.77	3.62	2.68		1.20
	DCW (600)	Concrete waste	46.5	30.3	6.64	2.54	2.42		4.97
(BALDUSCO et al., 2019)	SC		49.9	25.5	5.29	1.66	5.18	1.76	3.45
	DSCP (500)	SC paste (w/s = 0.45)	48.5	25.1	6.81	1.76	5.77	3.76	5.96

Carriço and coauthors (CARRIÇO et al., 2022) evaluated the chemical composition of dehydrated cementitious materials (cement paste - CP and concrete waste - CW) at 700 °C. The XRF results of dehydrated cement pastes (DCP) were similar to OPC. The water/solids ratio of the precursor cement paste did not influence the chemical composition of the R-PC. On the other hand, heat treatment changes the composition of the R-PC. The XRF results of cement paste without dehydration showed lower CaO and SiO_2 content than that of DCP. The dehydrated concrete waste presented a significantly lower CaO content compared to OPC and DCP.

An XRF limitation is to identify the free lime (f-CaO) content, which can be made through classic inorganic chemical analyses. Literature reported that R-PC has an elevated free lime (f-CaO) content, higher than Portland cement (CASTELLOTE et al., 2004; SERPELL; LOPEZ, 2015). The DCP (700) data (CARRIÇO et al., 2022) showed higher free lime content than DSCP (500) data (BALDUSCO et al., 2019). Those data corroborate with (CASTELLOTE et al., 2004), which infers that dehydration temperatures above 600 °C promote higher levels of free CaO, a fact associated with portlandite decomposition.

XRF is a technique limited to describing the chemical composition of the material under analysis. The mineralogical understanding of cementitious materials can be complemented through the x-ray diffraction technique as well as by thermal analysis and other microstructural characterization techniques.

2.2.2.2 X-ray diffraction (XRD)

X-ray diffraction (XRD) identifies the crystal structure of a phase. Table 4 presents an

overview of dehydrated phases according to recycling parameters.

Table 4 - Treatment procedure and dehydrated phases of recycled cement. All recycled cement presented had a cement paste as precursor material.

Ref	Source material	Treatment Temp. (°C)	Cooling procedure	Dehydrated phases							
				C-S-H	Tobermorite	CH	Jennite	C_2S	C_4AF	$CaCO_3$	CaO
(SHUI et al., 2008)	CW	200	Natural	X		X		X		X	
		500				X		X		X	X
		800						X		X	X
(SERPELL; ZUNINO, 2017)	CP	700	600°C/min			X		α, γ	X		
		800						α, ß	X		X
		900							X		X
(WANG; MU; LIU, 2018)	CP	120	Natural		1.2 nm	X	X			X	
		450			0.96 nm		X			X	
		750						X			X
(LÜ; HE; HU, 2008)	CP	400	Rapid			X		ß			
		650, 900						ß			X
(VYŠVAŘIL et al., 2014)	CP	200, 400	n.m			X		X	X	X	
		600, 800				X		X	X	X	
(SERPELL; LOPEZ, 2015)	CP	660 – 940	Natural					α, ß	X	X	X
(BALDUSCO et al., 2019)	CP	500	n.m			X		X		X	

CW = concrete waste; CP = cement paste; n.m = not mentioned;

Shui and coauthors (SHUI et al., 2008) studied phase transformations in the dehydration process of fines from recycled concrete aggregates. Figure 7 shows the diffractograms of the materials at different heat treatment temperatures. At 200°C, the ettringite peak disappeared due to its loss of crystallinity (CASTELLOTE et al., 2004). After 500 °C, the C_2S peaks increased. At 800 ºC, portlandite was completely decomposed, calcium carbonate was reduced and more free CaO formed. C-S-H undergoes changes in its atomic structure when dehydrated, tobermorite was densified (BONACCORSI; MERLINO; KAMPF, 2005). The content of β-C_2S increased due to the breakage of C-S-H chains by loss of water from 500 °C.

Wang and coauthors (WANG; MU; LIU, 2018) showed that recycled cement #1 (120 °C) and #2 (450 °C) have a higher content of calcite ($CaCO_3$). Furthermore, recycled cement #3 (750 °C) and #4 (1100 °C) corroborate (SHUI et al., 2008) and Section 2.2.1, showing higher CaO contents due to the decomposition of $CaCO_3$ and $Ca(OH)_2$. There is no CaO at #2 (450 °C) and this is due to the decomposition of $Ca(OH)_2$ at 450 °C and the additional formation of $CaCO_3$.

Figure 7 - XRD of initial hardened cement paste and preheated specimens at different temperatures. Note: Ettringite (Δ); C–S–H (●); C_2S (□); Portlandite (⊕); Calcite (▼); CaO (√); Tetracacium aluminoferrite (*).

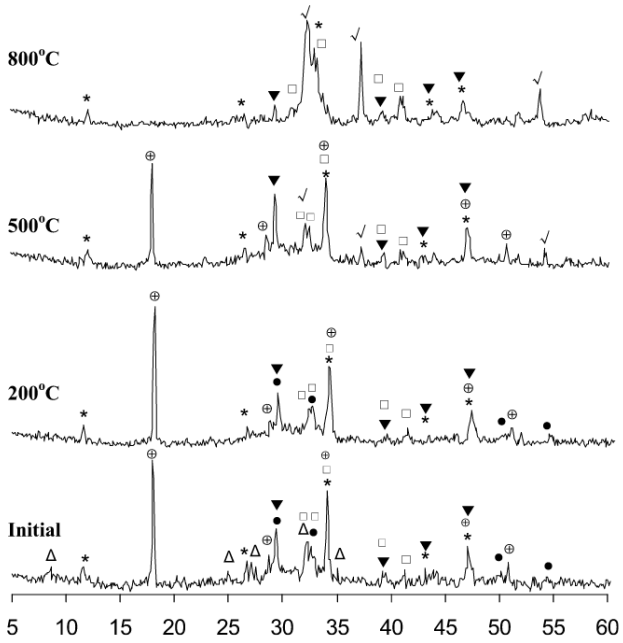

Extracted from (SHUI et al., 2008).

Wang and coauthors (WANG; MU; LIU, 2018) investigated the change in the composition of C-S-H. For dehydration at 120 °C (#1), C-S-H lost free water and showed patterns of tobermorite and jennite. Recycled cement at 450 °C (#2) showed greater water loss resulting in a change from 1.2 nm (120 °C) to 0.96 nm tobermorite (450 °C) and jennite became disordered (YU; KIRKPATRICK, 1999). In recycled cement powders #3 (750 °C) and #4 (1100 °C), only wollastonite and a small amount of larnite (C_2S) were found (YU; KIRKPATRICK, 1999). XRD results are presented in Figure 8.

Figure 8 - XRD of OPC and recycled cements at different temperatures: #1 (120 ºC), #2 (450 ºC), #3 (750 ºC) and #4 (1100 ºC). Note: C_2S (∇); C_3S (⊙); Portlandite (∗); Calcite (◆); CaO (⊗); Tobermorite (T), Jennite (J) and Wollastonite (W).

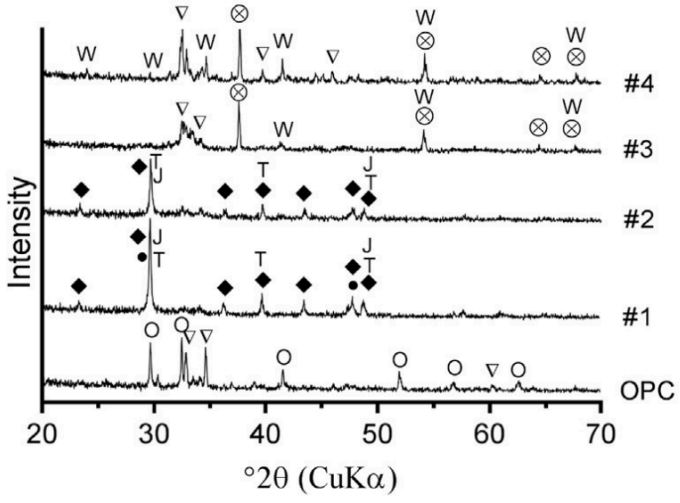

Extracted from (WANG; MU; LIU, 2018).

Angulo and coauthors (ANGULO et al., 2022) quantified the XRD data using the Rietveld refinement method (Table 5). The ettringite was decomposed at 300 °C corroborating with (SHUI et al., 2008). Most of the decomposed C-S-H remained amorphous up to 500 °C, as reported in the literature (YU; KIRKPATRICK, 1999; ZHANG; YE, 2012). The authors reinforce that the interplanar distance of C-S-H is reduced and can lead to the formation of calcium silicate intermediate (belite type) (ALONSO; FERNANDEZ, 2004; YU; KIRKPATRICK, 1999). The portlandite was fully decomposed at 650 °C. The content was reduced from 21% to 14%.

Table 5 - XRD Rietveld analyses of hydrated cement (25 ºC) and dehydrated cements (300, 500, 650 ºC).

Temp. (°C)	Phase content (% g/g)								
	Amorphous C-S-H	Tobermorite	Portlandite	Ettringite	Calcite	Larnite/Alite	Brownmillerite	C_3A	Total
25	43.0	10.0	21.3	3.6	16.8	5.1	0.2		100.0
300	40.5	11.7	27.2		14.4	6.2			100.0
500	44.5	8.3	16.1		16.3	11.3	0.2	3.3	100.0
650	28.5	1.2	14.0		13.6	32.5	2.4	7.9	100.1

Rwp were 6.07, 6.04, 7.28, and 6.39, respectively. Gof were 1.92, 1.88, 2.20, and 1.96, respectively.
Extracted from (ANGULO et al., 2022).

2.2.2.3 Nuclear magnetic resonance (NMR)

The XRD technique cannot identify amorphous materials. In this way, the analysis of recycled cement is complemented by nuclear magnetic resonance (NMR). This technique combination is crucial since recycled cement has a high amorphous materials content. The silicon nuclear magnetic resonance identifies SiO_2 fractions as SiO_4 tetrahedrons and the number of tetrahedrons connected (Q^0 to Q^4), but it is not quantitative method.

Alonso and Fernandez (ALONSO; FERNANDEZ, 2004) used this technique in dehydrated cement paste at 100, 200, 450, and 750 °C. The results are shown in Figure 9. Mass losses between 100 and 250°C was associated with changes in the C-S-H gel structure. The decrease of tetrahedral silicates promoted structure changes at 200 °C. A potentially reactive silicate intermediate was formed. At 450°C, an increase in intermediate and anhydrous silicates and C-S-H gel was observed. At the temperature of 750 °C, the C-S-H gel structure was completely restructured. The NMR results for recycled cement at 750 °C corroborate with (BOGAS et al., 2022).

Figure 9 - ^{29}Si MAS NMR spectra of the reference (initial cement paste) and the heated specimens at various temperatures. The isotropic chemical shifts are referenced to the T.M.S ($Si(CH_3)_4$). The thick solid line represents the experimental spectrum.

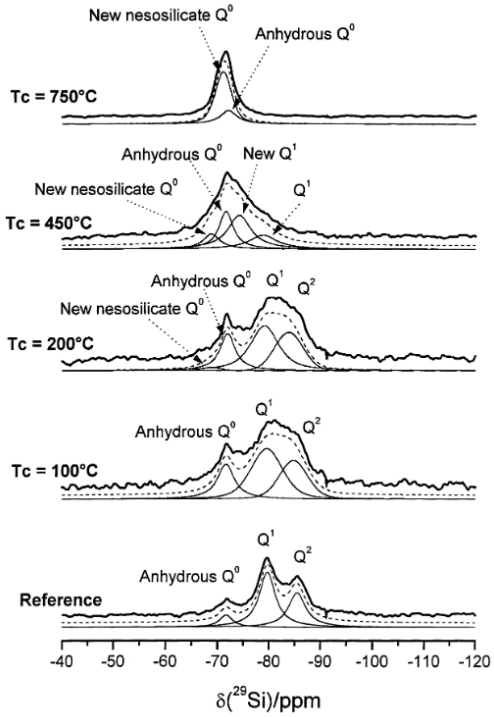

Extracted from (ALONSO; FERNANDEZ, 2004)

Real and coauthors (REAL et al., 2020) analyzed the depolymerization of C-S-H comparing Portland cement (PC), non-thermal activated recycled cement (NT), and recycled cement (RC) at 400 to 900 °C. Figure 10 expresses the results.

Recycled cement at 400 °C (RC400) had a spectrum similar to ground cement paste (NT), containing the same four main resonance peaks. RC400 showed a lower Q^2/Q^1 ratio than NT, which suggests the decomposition of the C-S-H gel, decreasing its chain length.

The complete depolymerization of C-S-H and the formation of anhydrous calcium silicates was seen at 600 °C as peaks Q^1 and Q^2 were no longer identifiable. Lu and coauthors (LÜ; HE; HU, 2008) corroborates these data. The ^{29}Si-NMR spectra of RC600 and RC700 exhibited the main Q^0 peak at a $\delta(^{29}Si)$ of -71.35 ppm, attributed to α'L-C_2S.

A progressive formation of β-C_2S (SERPELL; ZUNINO, 2017) was observed for RC800. Q^0 appeared in a $\delta(^{29}Si)$ of -70,60 ppm. At 900 °C, this resonance shifts to a $\delta(^{29}Si)$ of -70.81 ppm, narrower and more intense than RC800. Overall, the Q^0 peaks gradually became sharper with increasing treatment temperature, indicating higher crystallinity (REAL et al., 2020).

Figure 10 - ^{29}Si-NMR spectra of PC, NT and RC thermoactivated in the 400-900 °C temperature range (peak deconvolution is displayed in gray). Q^n refers to the number of orthosilicate units (*n*) attached to a SiO_4 tetrahedron (Q).

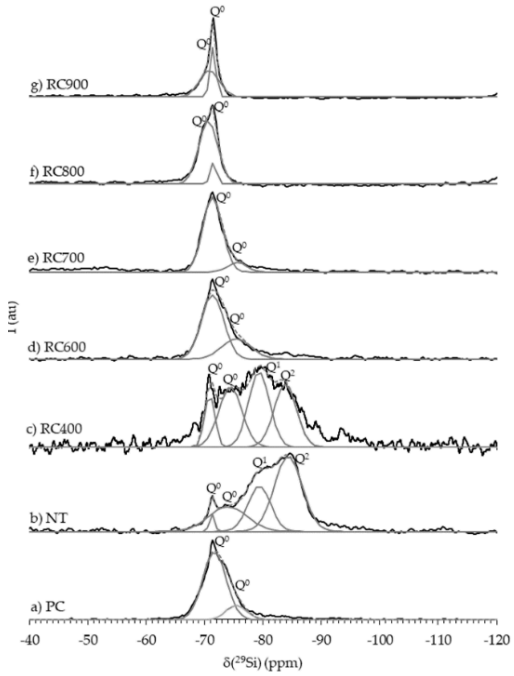

Extracted from (REAL et al., 2020).

2.2.2.4 Helium pycnometry

The density was obtained through helium pycnometry. Figure 11 exhibits the recycled cement density by dehydration temperature. Five references were used (BOGAS; CARRIÇO; PEREIRA, 2019; BOGAS; CARRIÇO; TENZA-ABRIL, 2020; REAL et al., 2020; SERPELL; LOPEZ, 2015; SPLITTGERBER; MUELLER, 2003).

Figure 11 - Recycled cement density by dehydration temperature.

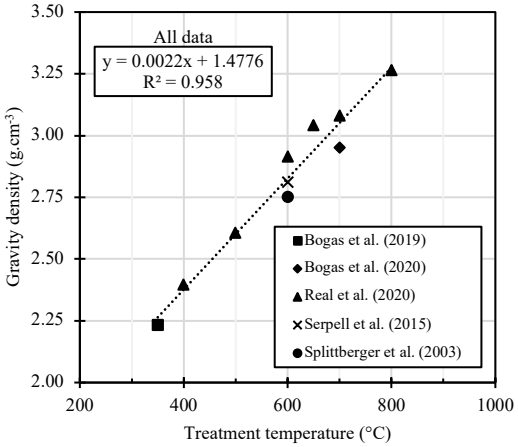

The linear correlation between the literature data was high (R^2 of 0.958). Therefore, the increase in the dehydration temperature promotes recycled cement with higher density. It is

associated with the partial removal of water from the hydrated phases, but it is lower density when compared to the clinker phases.

2.2.2.5 Thermogravimetric analysis (TG/DTG)

Thermogravimetry analysis can quantify the phases and the losses of water and CO_2 for ordinary and recycled Portland cement. Angulo and coauthors (ANGULO et al., 2022) compared the quantification of phases by quantitative XRD (QXRD) and TG (Table 6). The portlandite and calcite contents were similar. C-S-H and calcium silicate contents depends on thermal activation temperature. In addition, the QXRD can quantify aluminates properly. In general, the TG had similar values to QRXD with portlandite gradual decomposition and higher calcite content at 500 °C.

Table 6 - Quantification of phases of the hydrated (HC) and dehydrated cement (DC) by QXRD and TG.

Phases	HC		DC 300		DC 500		DC 650	
	QXRD	TG	QXRD	TG	QXRD	TG	QXRD	TG
C-S-H (amorphous, tobermorite)	53.0	53.0 (*)	52.2	60.6	52.8	69.8	29.7	75.6
Calcium silicates (larnite)	5.3	6.0 (+)	6.2		11.3		32.5	
Calcium aluminates, brownmillerite	3.7				3.5		10.3	
Brucite		2.4						
Portlandite	21.3	24.1	27.2	27.1	16.1	16.0	14.0	14.3
Calcite	16.8	14.5	14.4	12.3	16.3	14.2	13.6	10.1
Sum	100.0	100.0	100.0	100.0	100.0	100.0	100.1	100.0
Non-volatile fraction (-)	63.5	64.3	73.5	78.5	85.2	88.5	87.6	92.0
LOI	36.5	35.7	26.5 (#)	21.5	14.8 (#)	11.5	12.4 (#)	8.0

(+) estimated by hydration degree of the cement (discounting limestone content).
(*) C-S-H (% g/g) = 100 (% g/g) – phase estimated by TG (% g/g) – anhydrous (% g/g) estimated by (+).
(#) LOI (% g/g) = LOI from C-S-H (TG 25 - 420 °C) (% g/g) + Portlandite (% g/g) x (18/46) + Calcite (% g/g) x (44/100)
(-) Non-volatile fraction (% g/g) = 100 (% g/g) – LOI (% g/g).
Extracted from (ANGULO et al., 2022).

Real (REAL et al., 2020) and Angulo (ANGULO et al., 2015a) researches reported a reduction of combined water remaining in the recycled cement as the dehydration temperature increases. On the other hand, the data presented by (WANG; MU; LIU, 2018) do not corroborate this trend. Figure 12 expresses that the water remaining of recycled cement has a potential relationship with the dehydration temperature.

Figure 12 - Relationship between combined water remaining in dehydrated cement (DE WEERDT et al., 2011) and the dehydration temperature.

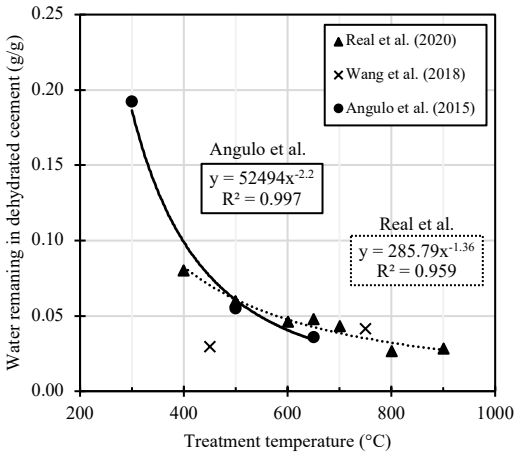

Data from (ANGULO et al., 2015a; REAL et al., 2020; WANG; MU; LIU, 2018).

In the literature, the values of combined water in recycled cement with precursor cement paste have a large range (0.027 to 0.192 g/g) associated with dehydration temperature, water/solids ratio of precursor cement paste, and hydration stoppage method.

Angulo and coauthors (ANGULO et al., 2022) analyzed the TG/DTG (Figure 13) and the mass loss at specific ranges associated with known phases (Table 7) for hydrated (HC) and dehydrated (DC) cement.

Figure 13 - DTG analyses of the hydrated (HC) and dehydrated (DC) cements. AFt – ettringite, AFm-monosulfoaluminates, CH – portlandite.

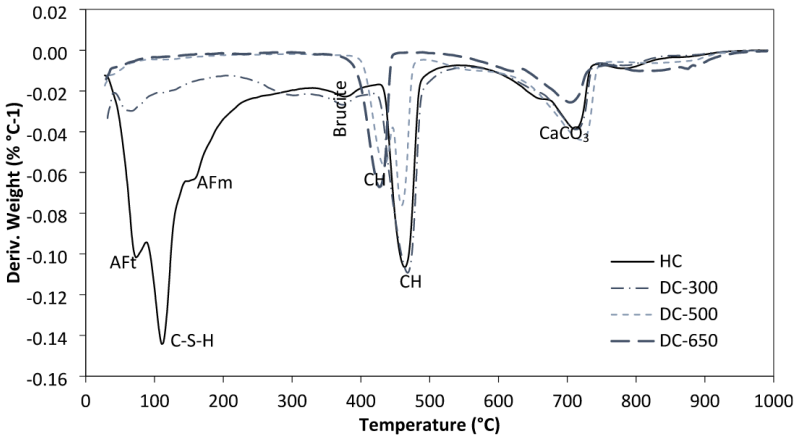

Extracted from (ANGULO et al., 2022).

Decomposition of ettringite at 95 °C, consistent with (ZHOU; LACHOWSKI; GLASSER, 2004), and subsequent decomposition of C-S-H at 120 °C and calcium monosulfoaluminates at 180 °C was observed after DTG comparison of dehydrated cement with hydrated cement. It was observed that brucite decomposed (peak of the event at 360 °C)

and C-S-H decomposed gradually with increasing temperature until 500 °C, consistent with Zhang and Ye (ZHANG; YE, 2012).

Only chemically combined water associated with portlandite was observed after 500 °C. Table 7 shows partial dehydration of portlandite (peak of event at 480 °C) which corroborates with Yu and Kirkpatrick (YU; KIRKPATRICK, 1999). The portlandite content decreased after dehydration at 500 and 650 °C, which indicates a possible quicklime formation.

Table 7 - TG analyses of the hydrated and dehydrated cements.

Sample	Water loss form C-S-H, ettringite, brucite 25 – 420 °C (% g/g)	Water loss from portlandite 330 – 550 °C (% g/g)	CO_2 loss from calcite 480 – 1000 °C (% g/g)	Total of volatiles (% g/g)
HC	23.40	5.90	6.40	35.7
DC-300	9.56	6.60	5.40	21.5
DC-500	1.35	3.88	6.25	11.5
DC-650		3.49	4.46	8.0

Portlandite (% g/g) = water loss (% g/g) x (74/18). Calcite (% g/g) = CO_2 loss (% g/g) x (100/44).
Extracted from (ANGULO et al., 2022).

2.2.2.6 Nitrogen adsorption

Zhang and coauthors (ZHANG; YE; KOENDERS, 2013) evaluated the influence of different dehydration temperatures in specific surface area and cumulative porosity measured by gas nitrogen adsorption of recycled cement, BET and BJH method, respectively.

Figure 14 demonstrates that the specific surface area (SSA) and pore volume presented a similar tendency by dehydration temperature. SSA and pore volume increased by 17% and 11% between 105-200 °C, respectively. Between 200 and 400 °C, SSA and pore volume decreased by 28% and 22%, respectively. The authors inferred that those changes are linked to C-S-H structural change.

Figure 14 - Specific surface area (a) and pore volume (b) of cement paste dehydrated at different temperatures.

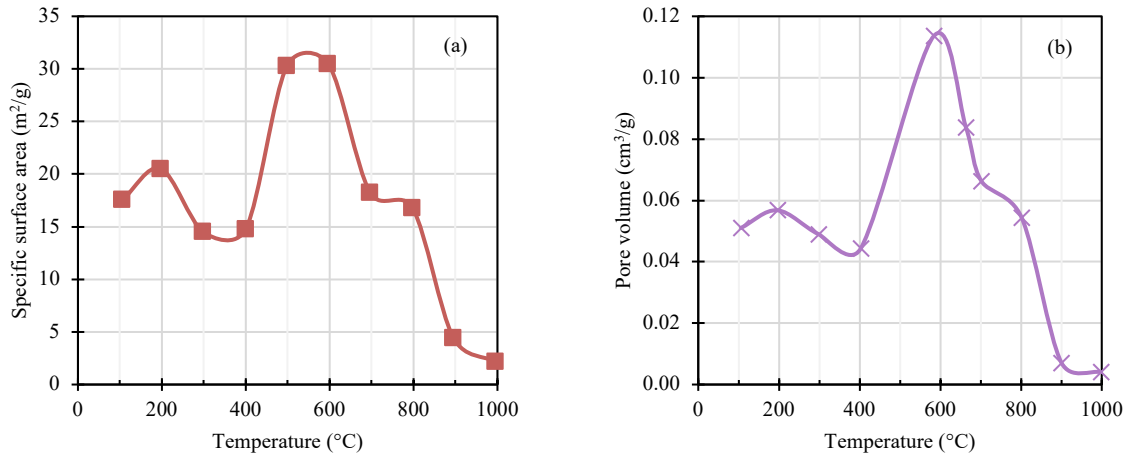

Extracted from (ZHANG; YE; KOENDERS, 2013).

In the 400-600 °C range, SSA and pore volume had increased 2.1 and 2.6 times, respectively. Up to 400 °C, there is no significant increase in the porosity of the cement paste because the main phases are not yet fully decomposed. From this temperature onwards, the paste begins to show an accentuated porosity due to the formation of connected pores.

SSA and pore volume decreased continuously from 600 °C to 1000 °C. The SSA at 1000 °C represents 12% of the SSA at 105 °C. The authors infer that it is caused by the recrystallization of C-S-H.

Zhang and coauthors (ZHANG; YE; KOENDERS, 2013) showed the cumulative pore volume and the differential pore volume curves calculated by BJH method for recycled cement at different dehydration temperature in Figure 15. The nitrogen adsorption has a limited range of pore size measurement from 3 nm to 37 nm.

Figure 15 - The pore size distribution of heated Portland cement pastes after cooling determined by nitrogen adsorption (BJH method); cumulative pore volume (a) and dV/ dlog (w) curve (b).

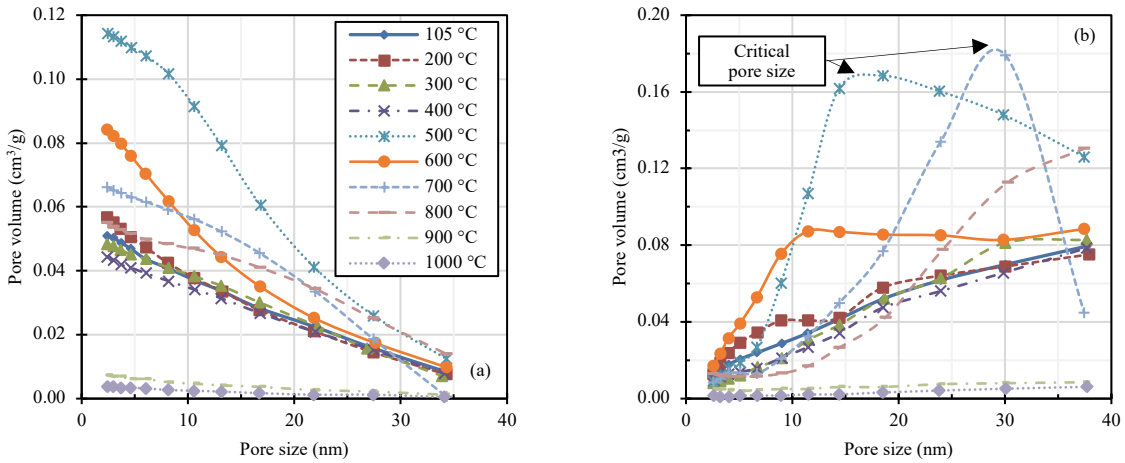

Adapted from (ZHANG; YE; KOENDERS, 2013).

Figure 15a indicates the influence of temperature dehydration on the characteristics of the cumulative pore volume curves. The cement pastes heated at 105-400 °C had a similar cumulative pore volume. The cement paste dehydrated at 500 °C presented the highest cumulative pore volume. The pore volume decreases gradually from 500 to 1000 °C.

Figure 15b exhibits the differential pore volume curves dV/dlog (w) of heated cement paste determined by BJH method. The dV/dlog (w) curves from 105 to 400 °C remain constant. The cement paste dehydrated at 500 and 700 °C had a clear peak which indicates a critical pore size of 16 and 29 nm, respectively. The authors infer that the recrystallization of C–S–H may be associated with the dV/dlog (w) curves remaining almost horizontal at 900 and 1000 °C.

Baldusco and coauthors (BALDUSCO et al., 2019) studied the recycling at 500 °C of a

slag cement paste and compared slag cement (SC) and recycled slag cement (R-SC). Table 8 shows that the specific surface area via BET for recycled cement (R-SC) is 14 times greater than that of anhydrous slag cement (SC).

Table 8 - Physical properties of anhydrous and dehydrated slag cement.

Parameters	SC	R-SC
SSA_{BET} (m^2/g) [a]	1.75	24.85
SSA_{LD} (m^2/g) [b]	0.50	0.31
Shape factor [c]	3.51	81.32

[a] *Specific surface area obtained by BET method.*
[b] *Specific surface area obtained by Laser diffraction granulometry.*
[c] *Shape factor calculated from SSA_{BET} and SSA_{LD}.*
Adapted from (BALDUSCO et al., 2019).

The ratio between the SSA via BET and the theoretical SSA obtained by laser diffraction measures how close the particle is to a sphere. This indicator is called a shape factor. The recycled cement shape factor is 23 times more irregular than anhydrous cement. It implies almost double water demand from R-SC (0.85 g/g) to standard consistency compared to SC (0.45 g/g). Moreover, the higher SSA implies a higher tendency to agglomerate leading to a higher superplasticizer content to achieve a standard consistency too.

2.2.2.7 Scanning electron microscopy (SEM)

Scanning electron microscopy technique is used to (i) analyze the morphology, (ii) identify phases, and (iii) estimate the porosity through a backscatter electron (BSE) detector of recycled cement grain.

Figure 16 presented the SEM images for an OPC powder and a recycled cement dehydrated at 450 °C (#2 powder) (WANG; MU; LIU, 2018). The recycled cement presented a larger surface area and rougher surface compared with OPC, which corroborates with SSA values determined by BET (BALDUSCO et al., 2019).

Figure 17 shows the SEM images for Portland cement, waste cement paste, and recycled cement. The influence of dehydration temperature in recycled cement is shown.

Real and coauthors (REAL et al., 2020) infer that PC grains showed angular shape, smooth surface, and a non-porous nature which promoted a lower SSA. The recycled cement had rounder and finer granules as the dehydration temperature increased. For temperatures higher than 750 °C, an SSA reduction was seen due to a progressive binding of fine granules. RC500 presents higher porosity and rougher surface than the others. The SEM images

corroborate with (ZHANG; YE; KOENDERS, 2013) (Figure 14).

Figure 16 - SEM images of OPC powder and recycled cement (dehydrated at 450 °C) powder.

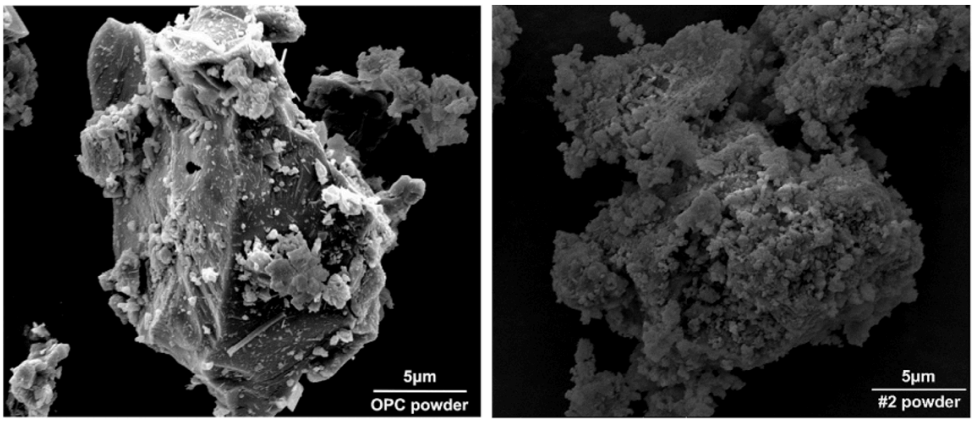

Adapted from (WANG; MU; LIU, 2018).

Figure 17 - SEM images of (a) Portland cement (PC), (b) waste cement paste (NT), and recycled cement (RC) treated at: (c) 400, (d) 500, (e) 650, (f) 700, (g) 750, (h) 800 and (i) 900 °C .

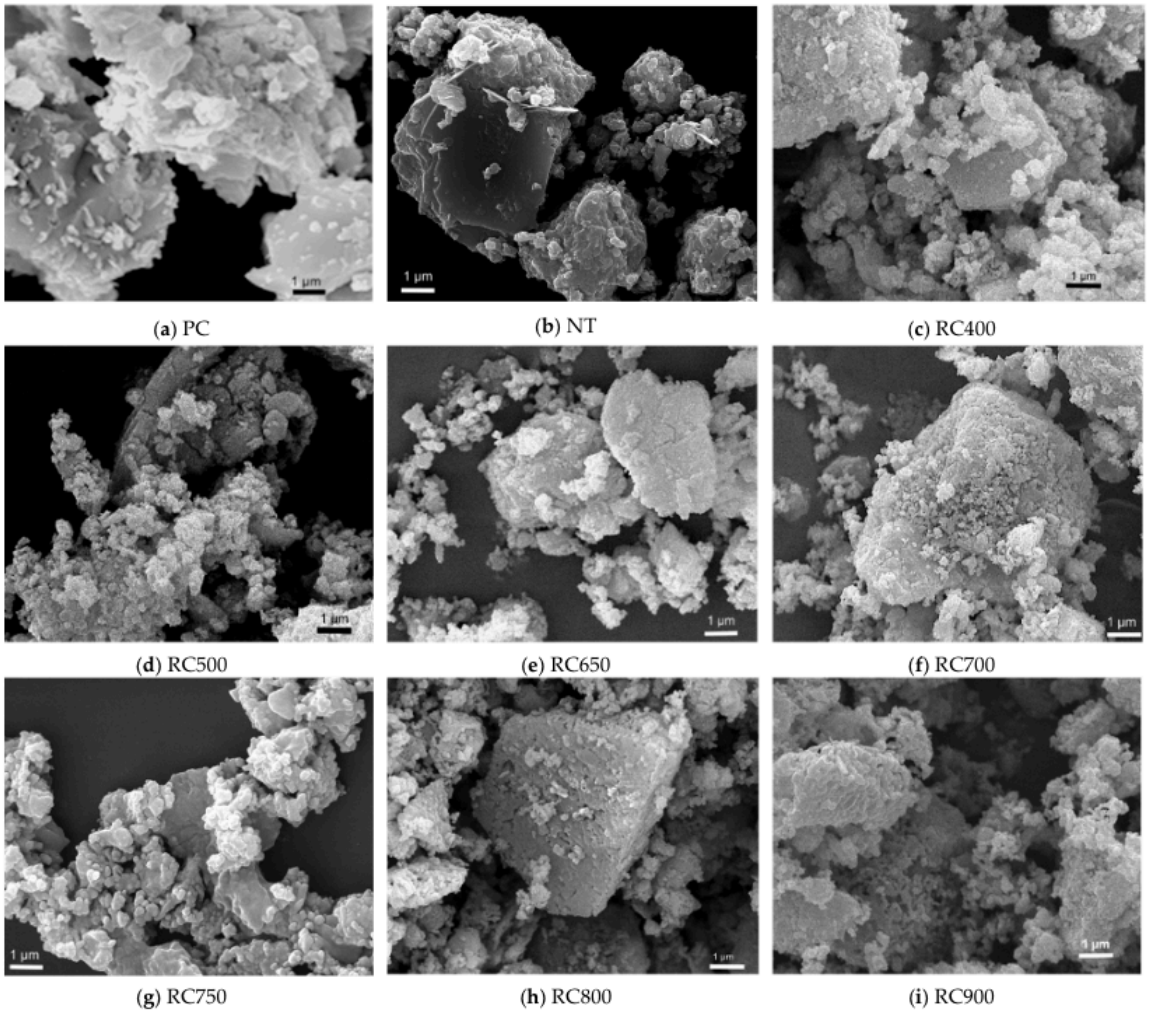

Extracted from (REAL et al., 2020).

Zhang and coauthors (ZHANG; YE, 2011) determined the porosity of cement pastes dehydrated at different temperatures for pores larger than 14 nm through SEM images with BSE and thresholding techniques. The principle of this technique is that the gray levels of digital images reflect the density difference of phases in cement paste. The porosities by SEM images are presented in Figure 18 (Section 2.2.2.8). The process used is detailed in (ZHANG; YE, 2011) and (SILVA; DE ALENCAR LOTUFO; FLORES, 2002).

2.2.2.8 Mercury intrusion porosimetry (MIP)

The pore size in cement paste and recycled cement ranges from nano to millimeter order which is difficult to determine through a single technique. Mercury intrusion porosimetry (MIP) is a technique with a broad range of analysis, from 3 nm to 200 µm.

Zhang and coauthors (ZHANG; YE, 2011; ZHANG; YE; KOENDERS, 2013) compared the cumulative pore volumes tested by MIP (3 nm to 200 µm) with the results for nitrogen adsorption (3 nm to 37 nm) and SEM (> 14 µm) for cement paste subjected to different dehydration temperatures. The comparison was strictly limited to the same pore size range (Figure 18).

Figure 18 - The comparison of the pore volumes determined by various techniques; the volumes of the pores with diameters from 3 nm to 37 nm (a) and with diameters larger than (b).

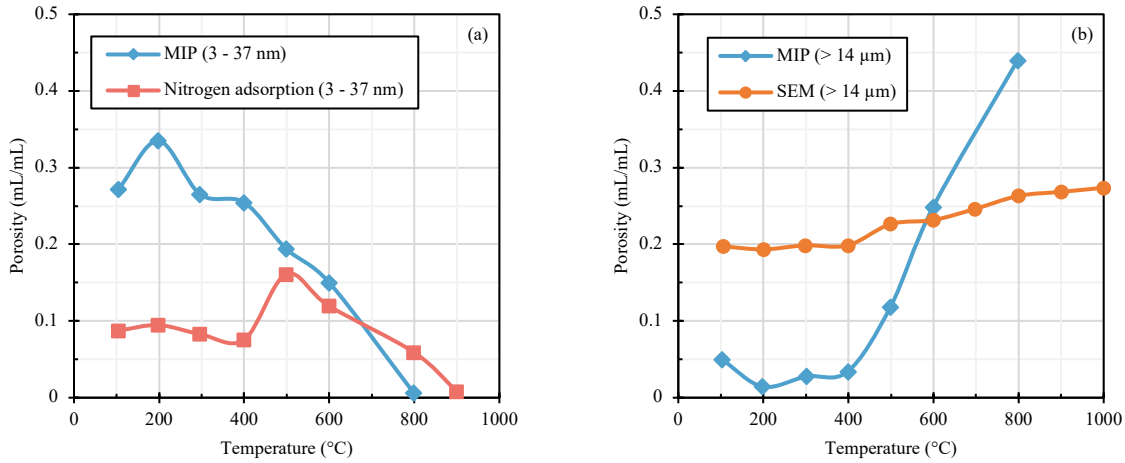

Adapted from (ZHANG; YE; KOENDERS, 2013).

Figure 18a demonstrates the MIP and nitrogen adsorption results correlation. Between 105 °C and 400 °C, MIP porosity is near the double of nitrogen adsorption porosity. For temperatures higher than 600 °C, the technique results narrow.

The authors attributed the disagreement to the different principles of these two techniques. Nitrogen adsorption can access all open pores without causing any damage.

However, the MIP technique is associated with a high pressure to intrude the mercury into the fine pores, which can damage the structure. In addition, the ink-bottle effect could lead to an overestimation of the volume of the fine pores and an underestimation of the volume of the large pores (ZHANG et al., 2019). Nitrogen adsorption measures the gel pores, while MIP measures the capillary pores due to essay limitations associated with the pressure.

Figure 18b exhibits the cumulative porosity for pore size larger than 0.14 μm determined by SEM and MIP. The pore volume by SEM is higher than MIP for temperature lower than 500 °C. This may be associated with the ink-bottle effect on the MIP technique that underestimates large pores.

On the other hand, the porosity determined by SEM was higher than MIP porosity for dehydration temperatures higher than 500 °C. The authors inferred that the solid skeleton in cement paste becomes very weak beyond 600 °C, which might break the porous matrix during the mercury intrusion process. It leads to the higher volume of porosity determined by MIP. Based on the discussion above, the cumulative porosity in the pore size range > 0.14 μm determined by SEM seems more reliable than that determined by MIP.

2.3 Rehydration of Recycled Portland Cement

Recycled Portland cement is a binder from dehydration of hydrated Portland cement based materials (e.g., waste concrete and cement paste).

The dehydration or thermal activation process changes the hydrated cementitious material. The water is removed, the morphology and physical characteristics changes, and the composition becomes a mix of anhydrous, partially dehydrated, and dehydrated phases improving its reactivity compared to a non-dehydrated cementitious material.

In this Section, the characteristics of R-PC powder (Section 2.2.2) and its variables were correlated with the properties of R-PC rehydrated (R-PC-based materials).

2.3.1 Rehydration of dehydrated phases

2.3.1.1 Layered Double Hydroxides (LDHs)

Layered double hydroxides are compounds formed by stacking layers of mixed hydroxides of divalent and trivalent cations, having hydrated anions between these layers. Figure 19 presents a schematic representation of the structure of these compounds (FORANO et al., 2013; SALOMÃO et al., 2011).

The hydration products of C_3A and C_4AF (e.g., $C_2(A,F)H_8$, $Ca_4(A,F)H_{13}$ and $C_4(A,F)H_{19}$) and the AFm phases are lamellar materials belonging to the group of LDH

compounds (RAKI; BEAUDOIN; MITCHELL, 2004). According to aluminum (Al) coordination, certain C-(A)-S-H structures can be classified as LDH (CAMETTI et al., 2015).

The dehydration process is a relevant factor for the rehydration mechanism of the phases with LDH structure and its strength. Mascolo and Mascolo (MASCOLO; MASCOLO, 2015) analyzed the influence of dehydration temperature on the reconstruction of LDHs when rehydrated.

Figure 19 - Schematic representation of the composition structure of the LDH type.

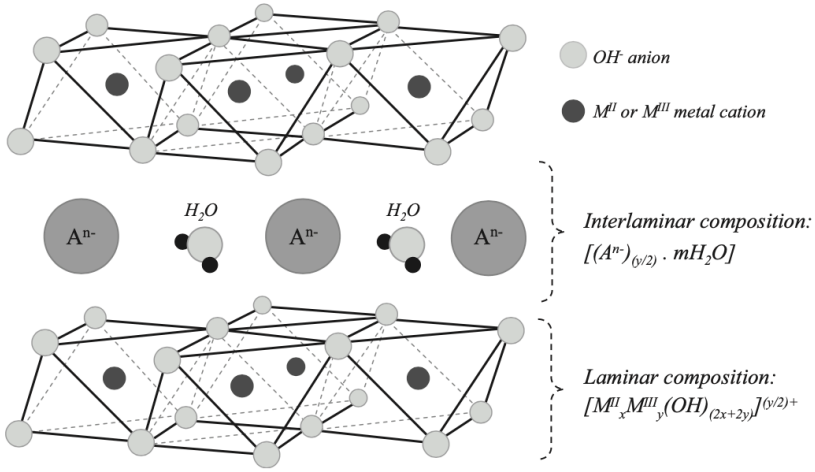

Extracted from (SALOMÃO et al., 2011).

The thermal treatment at low temperatures (about 200 °C) of LDH precursor removes the interlayer water forming a highly disordered phase. Its rehydration involves a slow reconstruction of an LDH phase similar in composition and structure to the original phase. In this case, the term “memory effect” applies.

At high temperatures (about 600 °C), dehydration results in a mixture of oxides that only partially regenerate a lamellar phase, which has a different composition, structure and morphology from the original LDH phase. The mechanism of the partial recovery of the LDH precursor involves a direct synthesis.

On the other hand, dehydration at intermediate temperatures (about 400 °C) leads to a mixture of small crystals (with low crystallinity) of oxides with a high specific area due to the crystal shuttering and to the formation of a maze micro-cracks of the ex-LDH crystals. This dehydrated material quickly rehydrates, showing a decrease in the specific area due to the regeneration of the LDH phase in the form of compact crystal aggregates. In this case, the direct synthesis appears to be the true mechanism of recovery of the layered structure.

2.3.1.2 Other phases reformation

Despite not being categorized as an LDH, the C-S-H also reforms. Its partially amorphous cationic lamellar chain structure can incorporate anions (CO_3^{2-}, $Al(OH)_4^-$), recover hydroxyls (OH^-), or interlamellar water. Much of the reformed C-S-H remains amorphous.

Portlandite (DAI et al., 2018) and hydrogarnet (ALONSO et al., 2016) are non-lamellar crystalline compounds with rehydrating ability due to the reversibility of their chemical reactions of dehydration and rehydration.

Ettringite structure is composed of lamellar chains (typically cationic) and an interlamellar layer with water, hydroxyls, and anions. Baquerizo and coauthors (BAQUERIZO; MATSCHEI; SCRIVENER, 2016) infer that decomposition and reformation of ettringite take place reversibly but with a marked hysteresis, whose occurrence can be explained by a free-energy barrier separating the transition between ettringite and metaettringite. Figure 20 expresses the decomposition and reformation zones of ettringite.

Figure 20 - Relative humidity (RH) (a) and water vapor pressure (P_{H_2O}) (b) as function of temperature showing the zones of reformation and decomposition of ettringite.

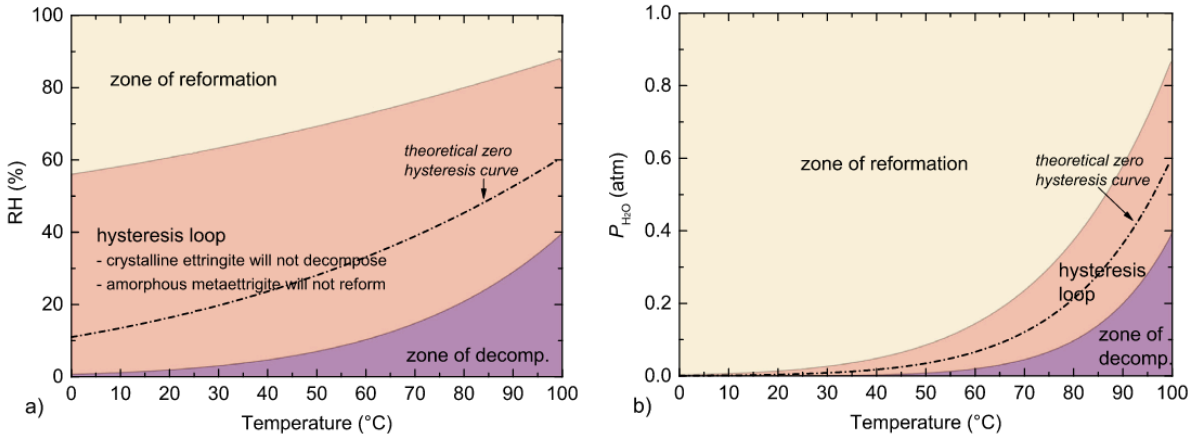

Extracted from (BAQUERIZO; MATSCHEI; SCRIVENER, 2016).

2.3.2 Characteristics of (re)hydrated recycled Portland cement

2.3.2.1 X-ray diffraction (XRD)

The dehydration temperature is the most influential parameter in cement waste recycling. In this way, the recycling procedure directly affects the composition of recycled Portland cement and its properties when rehydrated. The phases present in the R-PC pastes were studied by X-ray diffraction by several authors (ANGULO et al., 2022; BALDUSCO et al., 2019; BOGAS et al., 2022; REAL et al., 2020; SHUI et al., 2008; VYŠVAŘIL et al., 2014; WANG; MU; LIU, 2018).

Angulo and coauthors (ANGULO et al., 2022) promoted the rehydration of recycled cement produced at 300, 500, and 650 °C. These temperatures were chosen to analyze the influence of calcium sulfoaluminates, most of C-S-H, and portlandite decomposition, respectively. The rehydration of those cement was monitored over time through quantitative XRD assays through Rietveld refinement. Figure 21 shows the cumulative content of the phases present in the rehydrated cement as a function of time.

Figure 21 - Quantitative XRD by Rietveld refinement of the rehydrated cements.

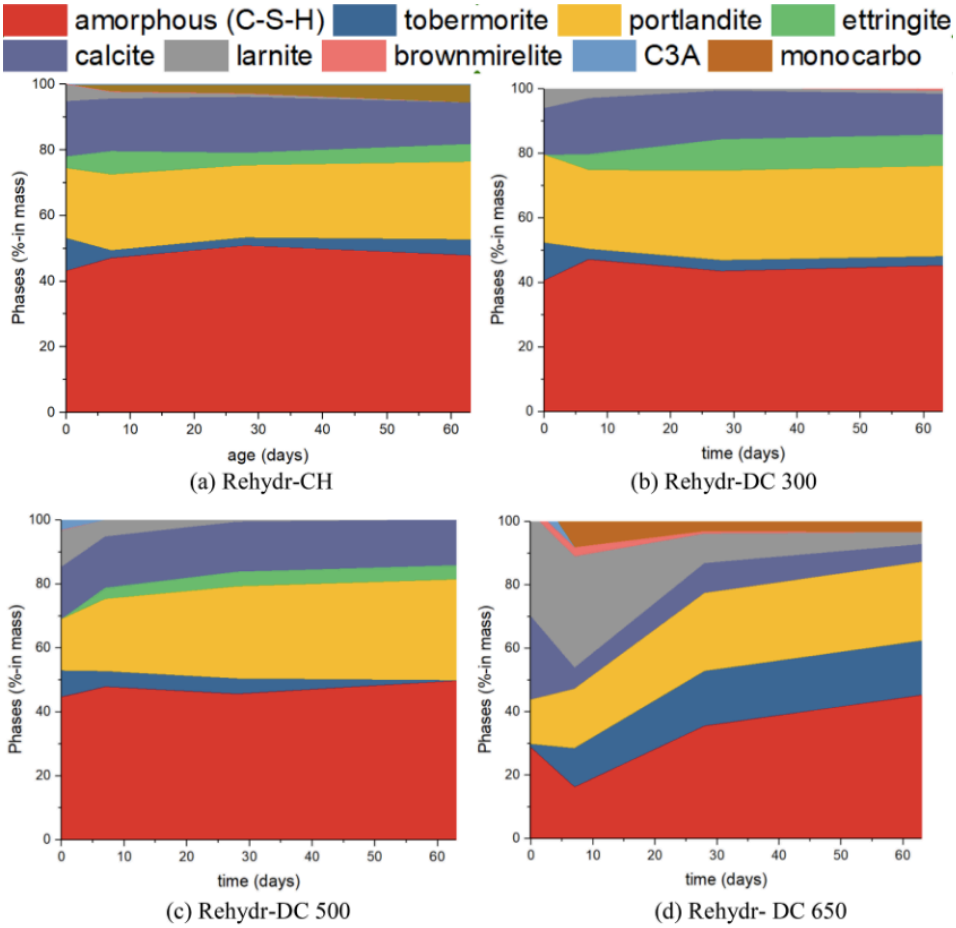

Extracted from (ANGULO et al., 2022).

For rehydrated DC 300 and DC 500, 45-47% g/g of amorphous C-S-H was observed. Tobermorite presented content lower than 5% g/g. Larnite was practically consumed in both cases. The high content of intermediate calcium silicate formed in the dehydration at 500 ◦C was also consumed. Ettringite and portlandite increased during rehydration. Calcite was kept almost constant during the aging, without carboaluminate formation.

For rehydrated DC 650, larnite was not totally consumed and had a slow consumption behavior. Different from DC 300 and DC 500 during rehydration, the content of tobermorite formed was high (17% g/g), and the content of amorphous C-S-H was low during the aging.

Portlandite and monocarboaluminate increased. Calcite content decreased to 6% g/g.

Bogas and coauthors (BOGAS et al., 2022) analyzed the rehydration of recycled cement produced at 700 °C over time through quantitative XRD by Rietveld refinement. Figure 22 shows the cumulative content of the phases present in the rehydrated cement as a function of time.

A progressive consumption of α′H–C_2S over time was confirmed, with a significant reaction between 1 and 3 days. The β-C_2S phase was almost inactive at early ages, only starting to react after 3 days. It was thus confirmed the higher initial reactiveness of the new nesosilicate.

Considering that R-PC was treated at 700 °C, CaO would be expected rather than CH, due to the dehydroxylation of the latter compound during thermal treatment. The authors infer that the high CH content at early ages is associated with fast CaO rehydration.

Figure 22 - Quantitative XRD by Rietveld refinement of the rehydrated R-PC 700.

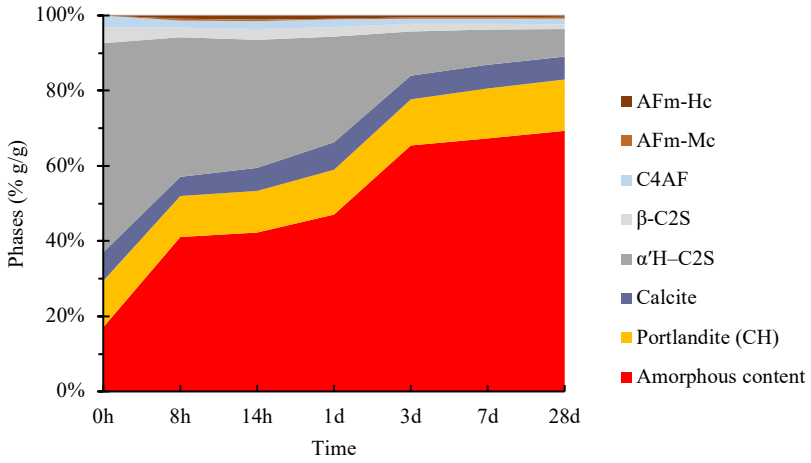

Data from (BOGAS et al., 2022).

For R-PC 650 rehydrated between 0 and 7 days, Angulo and coauthors (ANGULO et al., 2022) showed a reduction in amorphous (28 to 16% g/g) and calcite (14 to 7% g/g) content. Tobermorite (1 to 12% g/g) and monocarbo (0 to 8% g/g) increased. The portlandite and larnite content remained almost unchanged, only increasing by 3-4% g/g. Ettringite was not found.

For the same time interval, Bogas and coauthors (BOGAS et al., 2022) reported a continuous and significant increase in amorphous content (17 to 67% g/g). The α′H–C_2S was heavily consumed (56 to 9% g/g). There was no discretization of the tobermorite. The other phases remained with similar contents. Ettringite was also not found.

From the beginning of hydration (except 0h), both studies showed similar trends in larnite and α′H–C_2S consumption and amorphous production. Portlandite and calcite remained

practically constant. Bogas and coauthors (BOGAS et al., 2022) report an intensification in phase changes between 1 and 3 days. This fact is not reported by (ANGULO et al., 2022), given the time interval chosen for the analyzes (0, 7, 28, and 63 days).

Vysvaril and coauthors (VYŠVAŘIL et al., 2014) evaluated the phases present in R-PC pastes through qualitative XRD. The R-PC was produced from 200 to 1200 °C. When rehydrated, the R-PC recycled at temperatures lower than 600 °C presented ettringite, portlandite, calcite, C_2S, and C_4AF. When rehydrated R-PC treated at temperatures higher than 600 °C presented (i) ettringite absence, (ii) lower portlandite, and calcite peaks, (iii) C_2S and C_4AF presence increased, and (iv) gismondine, ternesite, katoite, and monosulfate have shown up. No anhydrite II was found. Vysvaril and coauthors (VYŠVAŘIL et al., 2014) corroborate with (ANGULO et al., 2022). Ettringite absence, calcite reduction, and larnite increase for rehydrated cement treated with temperatures above 600 °C are in accordance.

Wang and coauthors (WANG; MU; LIU, 2018) studied recycled cement pastes at 450 °C. The phases found were calcium carboaluminate, C_2S, $CaCO_3$, tobermorite, and jennite. The main difference from OPC paste was the absence of portlandite, ettringite, and C_3S. The precursor material was laboratory-made cement paste. Shui and coauthors (SHUI et al., 2008) showed the same trend for calcite, C_2S and C-S-H even with a different primary material, the fine fraction of concrete residue made in the laboratory at 500 °C. The difference was the high presence of ettringite. Angulo (ANGULO et al., 2022) and Bogas (BOGAS et al., 2022) showed a contrary trend in calcite and larnite presence over time.

2.3.2.2 Nuclear magnetic resonance (NMR)

Nuclear magnetic resonance (NMR) is used to understand the amorphous portion of cementitious materials. The ^{29}Si MAS-NMR spectra give the silicate tetrahedron named Q^n. The "Q" represents the silicon tetrahedron bonded to four oxygen atoms. The number of other Q units attached to the SiO_4 tetrahedron under study is “n”.

Therefore, Q^0 indicates a monometric orthosilicate anion, typical of anhydrous silicate (i.e., C_3S and C_2S). Q^1 represents an end group of a chain of C-S-H, Q^2 a middle group, Q^3 a chain branching site, and Q^4 a three-dimensionally fully cross-linked group. Two indicators are used in NMR analyses: (i) hydration degree (Equation 8) and (ii) mean silicate chain length of C-S-H (Equation 9).

$$\alpha_{H,NMR} = \frac{Q^1 + Q^2}{Q^0 + Q^1 + Q^2}$$ Equation 8

$$MCL = \frac{2Q^1 + 2Q^2}{Q^1}$$ Equation 9

Castellote and coauthors (CASTELLOTE et al., 2004) affirm that the rehydration of heated cement paste shows that the process is reversible. A new formation of a C-S-H gel from the new nesosilicate with a CaO/SiO_2 ratio close to the initial C-S-H gel was confirmed through the NMR technique.

Other authors investigate the rehydration of cement recycled at different temperatures and ages using NMR (ALONSO; FERNANDEZ, 2004; BOGAS et al., 2022; CARRIÇO et al., 2020; REAL et al., 2020). Table 9 exhibit the NMR analysis from (REAL et al., 2020).

Table 9 - NMR spectra analysis and indexes.

Paste ID	Binder	w/b ratio	Structural Unit	δ (^{29}Si) (ppm)	Q^2/Q^1	$\alpha_{H,NMR}$	MCL
PC1	PC	0.72	Q^0	-71.37	1.02	0.68	4.04
			Q^0	-73.00			
			Q^1	-79.16			
			Q^2	-84.30			
P600	R-PC (600 °C)	0.73	Q^0	-72.77	1.30	0.76	4.60
			Q^1	-79.18			
			Q^2	-84.04			
P700	R-PC (700 °C)	0.72	Q^0	-72.67	1.02	0.74	4.04
			Q^1	-79.32			
			Q^2	-84.51			
P800	R-PC (800 °C)	0.87	Q^0	-71.53	1.02	0.73	4.05
			Q^0	-75.00			
			Q^1	-79.18			
			Q^2	-84.22			
P900	R-PC (900 °C)	0.91	Q^0	-71.47	0.88	0.71	3.75
			Q^0	-73.40			
			Q^1	-79.20			
			Q^2	-84.12			

Adapted from (REAL et al., 2020).

The $\alpha_{H,NMR}$ was lower in PC paste than in R-PC pastes. Real and coauthors (REAL et al., 2020) inferred that those values confirm that a higher volume of C-S-H products was formed in the R-PC pastes. Moreover, the authors associated that with the higher surface area of the R-PC. The higher MCL and Q^2/Q^1 ratio for P600 indicated a faster reaction, justified by the C_2S polymorph's high reactivity. The MCL value and the Q^2/Q^1 ratio decreased with treatment temperature above 800 °C. These suggested a shorter chain length and that the RC particles

reacted slower.

Table 10 compares the NMR spectra for an R-PC (dehydrated to 700 °C) paste and a Portland cement paste over time (BOGAS et al., 2022).

The effective development of hydration products over time was indicated by the gradually increased MCL, $Q^2/Q1$ ratio, and α_{NMR} of PC/P and R-PC/P between 8 h and 28 days.

Table 10 - ^{29}Si NMR results of PC/P and R-PC/P between 8h and 28 days.

Age	Q^n	Portland Cement Paste (PC/P)				Recycled Portland Cement Paste (R-PC/P)			
		δ (^{29}Si) (ppm)	Q^2/Q^1	$\alpha_{H,NMR}$	MCL	δ (^{29}Si) (ppm)	Q^2/Q^1	$\alpha_{H,NMR}$	MCL
8h	Q^0	-71.24	0.63	0.42	3.25	-71.26	0.57	0.29	3.15
	Q^0	-73.40				-73.40			
	Q^1	-79.43				-79.30			
	Q^2	-84.50				-84.80			
14h	Q^0	-71.44	0.66	0.43	3.32	-71.42	0.65	0.44	3.29
	Q^0	-73.50				-74.02			
	Q^1	-79.64				-79.60			
	Q^2	-84.40				-84.80			
1d	Q^0	-71.24	0.67	0.47	3.33	-71.19	0.67	0.46	3.35
	Q^0	-73.20				-73.40			
	Q^1	-79.20				-79.48			
	Q^2	-84.00				-84.40			
3d	Q^0	-71.17	0.70	0.52	3.40	-71.55	0.86	0.64	3.72
	Q^0	-73.40				-73.72			
	Q^1	-79.00				-79.27			
	Q^2	-82.95				-84.31			
7d	Q^0	-71.26	0.81	0.61	3.61	-71.53	1.12	0.69	4.24
	Q^0	-73.30				-72.74			
	Q^1	-78.88				-79.23			
	Q^2	-83.23				-84.40			
28d	Q^0	-71.00	1.05	0.69	4.11	-71.53	1.14	0.75	4.28
	Q^0	-73.60				-72.74			
	Q^1	-79.03				-79.23			
	Q^2	-84.20				-84.40			

Adapted from (BOGAS et al., 2022).

Between 8 h and 28 days, PC/P presented two Q^0 peaks of remaining unreacted calcium silicates. For the same period, R-PC/P displayed broader and less defined Q^0 peaks. These indicate that the calcium silicates were of lower crystallinity and associated with the Q^0 peak transformation attributed to the more reactive α′H-C_2S.

A polymerization (transformation of Q^0 into Q^n) is observed at one day old. The authors attributed this to the α′H-C_2S reaction. From 3 days on, the α_{NMR} was higher in R-PC/P than in PC/P. It was related to the high surface area and high reactivity of α′H-C_2S and the lower content of β-C_2S in R-PC/P than in PC/P.

2.3.2.3 Thermogravimetric analysis (TG/DTG)

Thermogravimetry (TG/DTG) is used to (i) measure the phases' reformation through their thermal events and (ii) estimate the reactivity of R-PC-based materials through their loss of free and chemically bound water.

Table 11 displays the mass loss over specific temperature ranges to analyze the reactivity of recycled cement when rehydrated.

Angulo and coauthors (ANGULO et al., 2022) compared the rehydrated phase quantification through TG and quantitative XRD through the Rietveld method. The results were similar. Moreover, the authors analyzed (i) the chemically bound water of C-S-H, calcium sulfoaluminates, and brucite through the mass loss between 25 °C and 420 °C; and (ii) the portlandite content through the 330-430 °C mass loss for rehydrated cement. Chemically bound water of C-S-H, calcium sulfoaluminates, and brucite were similar for the hydrated cement (R-PC 0) and the rehydrated fines (R-PC 300, and R-PC 500), near 20% (g/g). It indicated that phases reform almost completely when dehydrated until 500 °C. The content was 15% (g/g) for the R-PC 650 rehydrated. The authors inferred it to the low reactivity of calcium silicate formed. The portlandite content was near the same for hydrated and rehydrated cements, 25% g/g. Values in parentheses represent the loss of water associated with C-S-H from the R-PC paste minus the water of C-S-H in anhydrous R-PC. Therefore, R-PC (500 °C) shows the highest reactivity. This consideration is needed since the water not removed from the dehydrated cement will not contribute to strength when rehydrated.

Bogas and coauthors (BOGAS et al., 2022) evaluated the rehydration of recycled cement at 700 °C from the first hours to 28 days. The data showed a similar trend to (ANGULO et al., 2022), a gradual increase in water combined with C-S-H, AFt, brucite, and portlandite. Furthermore, the loss of CO_2 from calcite showed a variation also seen in (ANGULO et al., 2022). For the initial ages, fast recombination of water was observed. The water combined by C-S-H, AFt, brucite, and portlandite with one day of hydration was 67% and 79% of the total at 28 days, respectively.

Real and coauthors (REAL et al., 2020) showed that recycled cement dehydrated between 400-500 °C and 800-900 °C had greater reactivity, recombining more water. Cementitious materials heated at 600-700 °C presented low reactivity when rehydrated, corroborating the data from (ANGULO et al., 2022). Wang and coauthors (WANG; MU; LIU, 2018) presented more reactive recycled cement when dehydrated at 750 °C and 450 °C than at 120 °C and 1100 °C.

Table 11 - TG analyses of the rehydrated cements at different ages.

Reference	Rehydrated cement	Age	Water loss from C-S-H, Aft and brucite	Water loss from portlandite	CO_2 loss from calcite	Total of volatiles
			[25-420 °C] % (g/g)	[330-550 °C] % (g/g)	[480-1000 °C] % (g/g)	% (g/g)
(ANGULO et al., 2022)	R-PC (0 °C)	0	20.8	5.9	6.4	33.1
		7d	19.4	6.1	7.7	33.2
		28d	19.8	5.8	6.9	32.5
		63d	20.2	6.3	6.4	32.9
	R-PC (300 °C)	0	9.6	6.6	5.4	21.6
		7d	20.3 (10.7)	5.7	7.6	33.6
		28d	20.7 (11.1)	6.1	6.6	33.4
		63d	20.2 (10.6)	6.4	6.4	33.0
	R-PC (500 °C)	0	1.4	3.9	6.3	11.6
		7d	20.0 (18.6)	5.8	7.0	32.8
		28d	19.5 (18.1)	6.7	6.8	33.0
		63d	18.2 (16.8)	7.3	5.9	31.4
	R-PC (650 °C)	0	1.0	3.5	4.5	9.0
		7d	14.2 (13.2)	5.2	5.8	25.2
		28d	15.9 (14.9)	5.7	5.9	27.5
		63d	14.6 (13.6)	6.2	5.3	26.1
(BOGAS et al., 2022)	R-PC (700 °C)	0	2.6	3.3	3.7	7.9
		8h	6.9 (4.3)	4.1	5.0	14.9
		14h	7.8 (5.2)	4.3	5.2	16.0
		1d	9.6 (7.0)	5.0	5.7	18.6
		3d	12.7 (10.1)	5.9	6.3	22.7
		7d	13.3 (10.7)	6.3	5.8	23.0
		28d	14.3 (11.7)	6.4	5.7	23.9
(REAL et al., 2020)	R-PC (400 °C)	28d	13.4	6.4	8.3	20.8
	R-PC (500 °C)		11.4	6.5	8.5	21.0
	R-PC (600 °C)		11.3	5.9	8.2	20.7
	R-PC (650 °C)		11.4	5.8	8.4	21.2
	R-PC (700 °C)		11.5	5.8	8.6	21.1
	R-PC (800 °C)		11.6	6.4	7.0	20.5
	R-PC (900 °C)		12.4	6.6	6.5	20.6
(WANG; MU; LIU, 2018)	R-PC (120 °C)	1d	10.3	4.4	12.7	23.8
		28d	10.2	4.9	15.3	27.0
	R-PC (450 °C)	1d	9.6	3.9	12.4	22.8
		28d	10.9	4.6	13.5	25.3
	R-PC (750 °C)	1d	9.6	3.8	6.8	16.8
		28d	12.8	5.2	9.1	22.9
	R-PC (1100 °C)	1d	7.3	4.1	3.8	11.4
		28d	9.9	4.6	3.3	14.2

In literature, the most reactive recycled cement was obtained from dehydration between 400-500 °C or 750-900 °C. These two dehydration ranges promote distinct changes in the characteristics of the recycled cement and, consequently, in the R-PC-based materials. The temperature influence R-PC properties as water demand, mechanical properties and the environmental impact of R-PC-based materials will be analyzed in Sections 2.3.2.8 and 2.3.2.9.

Angulo and coauthors (ANGULO et al., 2022) founded a correlation between the combined water and the strength of cement pastes. This relation applies as the same water/binder ratio was used for all pastes. The dehydration temperature affects the reactivity and water demand of recycled cement. Therefore, it is necessary to use an index that evaluates both criteria. In Chapter 3, the combined water fraction (*cwf*) was used to evaluate the binder efficiency of recycled cement in the literature.

2.3.2.4 Isothermal calorimetry (IC)

The hydration process of cementitious materials is an exothermic reaction. It is studied through the heat released from the material during its hydration. The OPC hydration process is divided into four main stages: dissolution, induction, acceleration, and deceleration (Figure 1) (SCRIVENER; JUILLAND; MONTEIRO, 2015). This process has a dissolution-precipitation mechanism of the phases in the anhydrous grains. Recycled cement presents a different behavior indicating a different (re)hydration process to OPC. Recycled cement shows an intense peak of heat release in the initial moments of hydration (dissolution). This behavior is widely reported in the literature (ANGULO et al., 2015a, 2022; BALDUSCO et al., 2019; BOGAS; CARRIÇO; TENZA-ABRIL, 2020; CARRIÇO et al., 2020; REAL et al., 2020; WANG; MU; LIU, 2018; ZHANG et al., 2018).

Figure 23 expresses the heat flux of OPC and recycled cement at different temperatures during their (re)hydration in a calorimeter (ANGULO et al., 2015a, 2022). The calorimetry was performed in situ. Therefore, the heat released was captured in the first moments of hydration.

Figure 23 - Heat flux and cumulative heat released of rehydrated cement pastes.

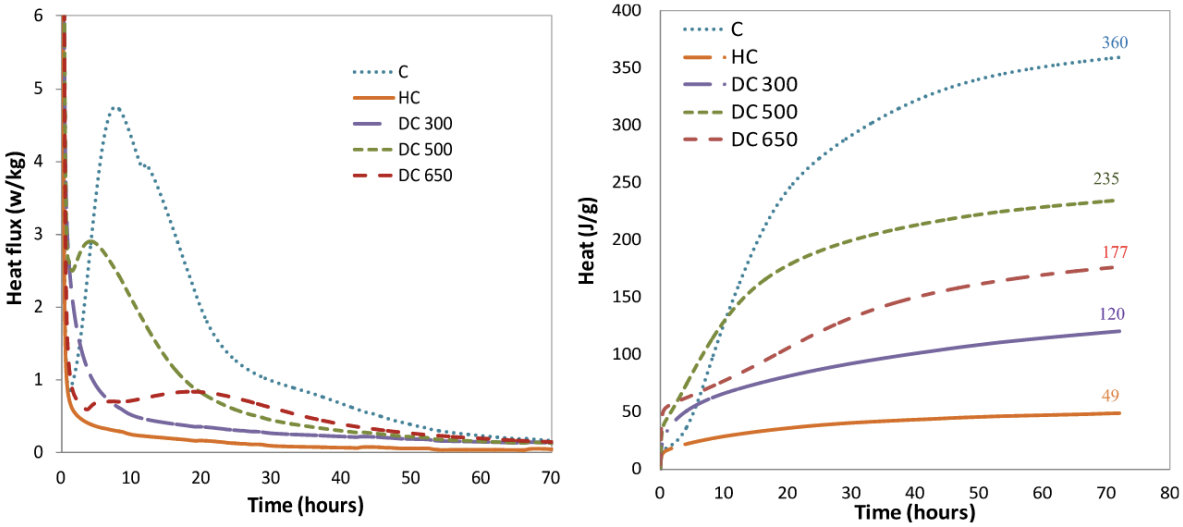

Extracted from (ANGULO et al., 2015a, 2022).

The behavior of recycled cement in calorimetry presents variable data in the literature. Figure 24a illustrates the calorimetry of rehydrated cement with OPC-like heat release peaks, indicating a dissolution-precipitation-like mechanism. Figure 24b shows a behavior with an intense peak of heat release followed by a continuous and gradual deceleration with no more prominent peaks. The behavior shown in Figure 24 is more reported in the literature, corroborate with (ANGULO et al., 2022; BALDUSCO et al., 2019; ZHANG et al., 2018).

Figure 24 - Heat flow over time of pastes produced Portland cement (OPC or PC) and recycled cement (RC). For data from (a) #1, #2, #3 and #4 are cement dehydrated at 120, 450, 750 and 1100 °C.

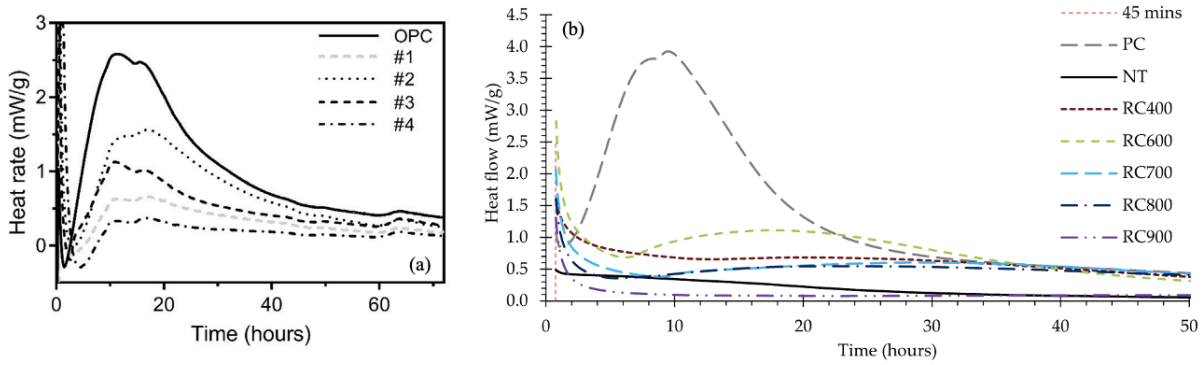

Extracted from (a) (WANG; MU; LIU, 2018) and (b) (REAL et al., 2020).

Table 12 shows the heat release of anhydrous and recycled cement. Two intervals to analyze the heat release were defined, 0-1h and 1h-72h. The cumulative heat was also studied. Baldusco (BALDUSCO et al., 2019) and Angulo (ANGULO et al., 2015a, 2022) performed in situ calorimetry obtaining more reliable data. Wang (WANG; MU; LIU, 2018) and Carriço (CARRIÇO et al., 2020) took 30 s and 45 min between the beginning of (re)hydration and the measurement of the heat released, respectively.

For the first hour of (re)hydration, the heat released is higher as the dehydration temperature of the recycled cement increases. It is valid for dehydrated cement up to 750 °C. Recycled cement at temperatures that promote clinkerization (such as 1100 °C) showed a reduction in heat emission between 0-1h. For Angulo and coauthors (ANGULO et al., 2015a, 2022), recycled cement presents a heat release in the first hour between 1.8 and 2.8 times greater than OPC. Baldusco and coauthors (BALDUSCO et al., 2019) presented a recycled cement that emitted 10 times more heat than slag cement (SC) between 0-1h.

For heat release between 1 and 72 hours, recycled cement released less heat than Portland cement (OPC and SC). Furthermore, the recycled cement at 450-500 °C showed the highest heat release among the rehydrated R-PC (ANGULO et al., 2015a, 2022; WANG; MU;

LIU, 2018). Recycled cement released lower total accumulated heat than Portland cement when rehydrated. The only exception was recycled slag cement (R-SC).

Table 12 - Partial and total accumulated heat values of Portland and recycled cement pastes in the literature.

Reference	Binder (re)hydrated	Cumulative heat (J/g)		
		0-1h	1-72h	Total (0-72 h)
(BALDUSCO et al., 2019)	SC	4	162	166
	R-SC (500 °C)	41	146	187
(ANGULO et al., 2015a, 2022)	OPC	19	341	360
	R-OPC (0 °C)	17	33	49
	R-OPC (300 °C)	34	86	120
	R-OPC (500 °C)	44	191	235
	R-OPC (650 °C)	54	123	177
(WANG; MU; LIU, 2018)	OPC	0	261	261
	R-OPC (120 °C)	0	74	74
	R-OPC (450 °C)	39	179	218
	R-OPC (750 °C)	53	127	180
	R-OPC (1100 °C)	23	51	74
(CARRIÇO et al., 2020)	OPC	0	244	244
	R-OPC (700 °C)	2	174	176

Baldusco and coauthors (BALDUSCO et al., 2019) argued that the high initial peak of R-PC is associated with its elevated specific surface area and the higher amount of calcium aluminates present in the amorphous phases of the dehydrated cement. This agreed with De Rooij and Scher (DE ROOIJ; SCHER, 2011). The authors founded that the higher the surface area of the cement, the higher the rate of dissolution of the anhydrous phases and the greater the heat release. The aluminates and silicates content were regardless.

Therefore, Baldusco and coauthors (BALDUSCO et al., 2019) inferred that rehydration occurs through a simple wetting mechanism. The adsorption of water molecules in dehydrated phases and reformation of phases (containing some microstructural similarity to previously hydrated phases). Guilge and coauthors (GUILGE, 2011) proved that the dehydrated phases (calcium silicates or calcium aluminates intermediates) in contact with water rehydrate in a shorter time.

Overall, there is consensus about elevated heat liberation in the first minutes of rehydration of R-PC between the researchers. On the other hand, the reactions and process involved in the heat release of rehydration still undefined (CARRIÇO; BOGAS; GUEDES, 2020).

Figure 25 shows the relationship between heat released with (a) recombined water and

(b) compressive strength of recycled cement pastes elaborated by (ANGULO et al., 2022).

The heat released by cement during its rehydration is a way of measuring the reactivity of the material, as is the calculation of combined water presented in Section 2.3.2.3. In this way, the two reactivity parameters must be analyzed to obtain recycled cement with better mechanical properties. Based on Table 11 and Table 12, it is possible to see that cement with greater reactivity was recycled at temperatures near 500 °C.

Figure 25 - Heat released relation to bound water in (re)hydrates (a) and 7-days compressive strength (b) for recycled and ordinary Portland cement pastes.

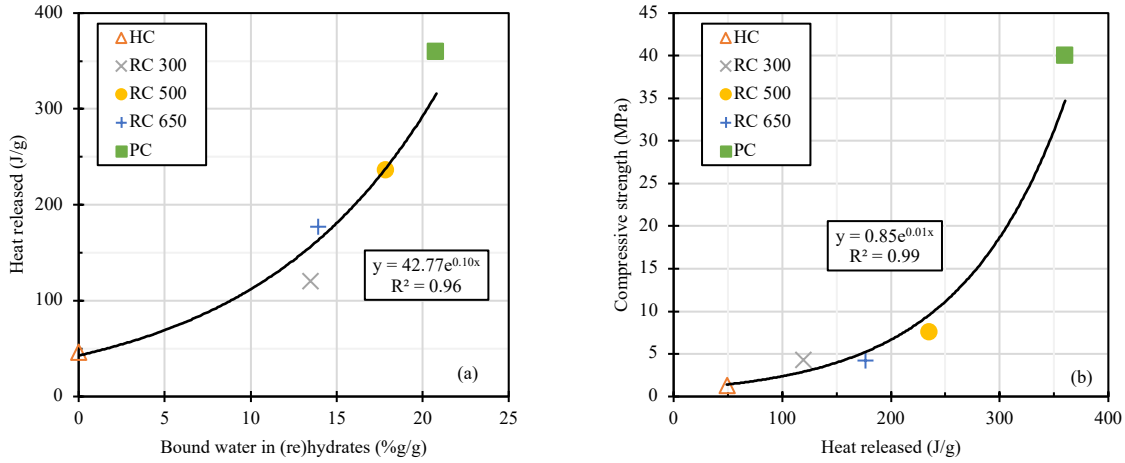

Extracted from (ANGULO et al., 2022).

2.3.2.5 Setting time

The setting time is a crucial parameter for R-PC feasibility in future applications. In general, R-PC presents a setting time shorter than OPC (BOGAS; CARRIÇO; PEREIRA, 2019; CARRIÇO et al., 2020; REAL et al., 2020; SERPELL; LOPEZ, 2015; WANG; MU; LIU, 2018), which might be harmful to the fresh and long-term mechanical properties of the materials (XU et al., 2022). The setting time of R-PC paste also showed a dependence on precursor material characteristics. Xuan and Shui (XUAN; SHUI, 2011) observed a decrease in the setting time of R-PC pastes with the precursor material's water/binder ratio increase. This behavior occurs due to a higher content of dehydrated phases.

Figure 26 shows the initial and final setting time for rehydrated pastes. The methods used in the works are provided for in the standard and use the same principle, needle penetration of the Vicat device.

Shui and coauthors (SHUI et al., 2009) showed a decrease in the initial and final setting time as the cement was recycled at higher temperatures. In addition, the setting time was short, 33-36 min. Vysvaril and coauthors (VYŠVAŘIL et al., 2014) showed a similar tendency for

dehydrated cement up to 1000 °C. However, the setting time was 5-10 times longer than (SHUI et al., 2009), between 165 and 400 min. Exception for the R-PC (800 °C), with a short setting time, 13 min.

Carriço (CARRIÇO et al., 2020) and Real (REAL et al., 2020) showed an opposite trend, with an increase in the initial and final setting time as the cement was recycled at higher temperatures. The setting time presented a wide range of values, between 37 min and more than 12 hours. R-PC (750 °C) had a short set time, 37 min.

Figure 26 - Initial (a), final (b) and total (c) setting time for rehydrated recycled Portland cement.

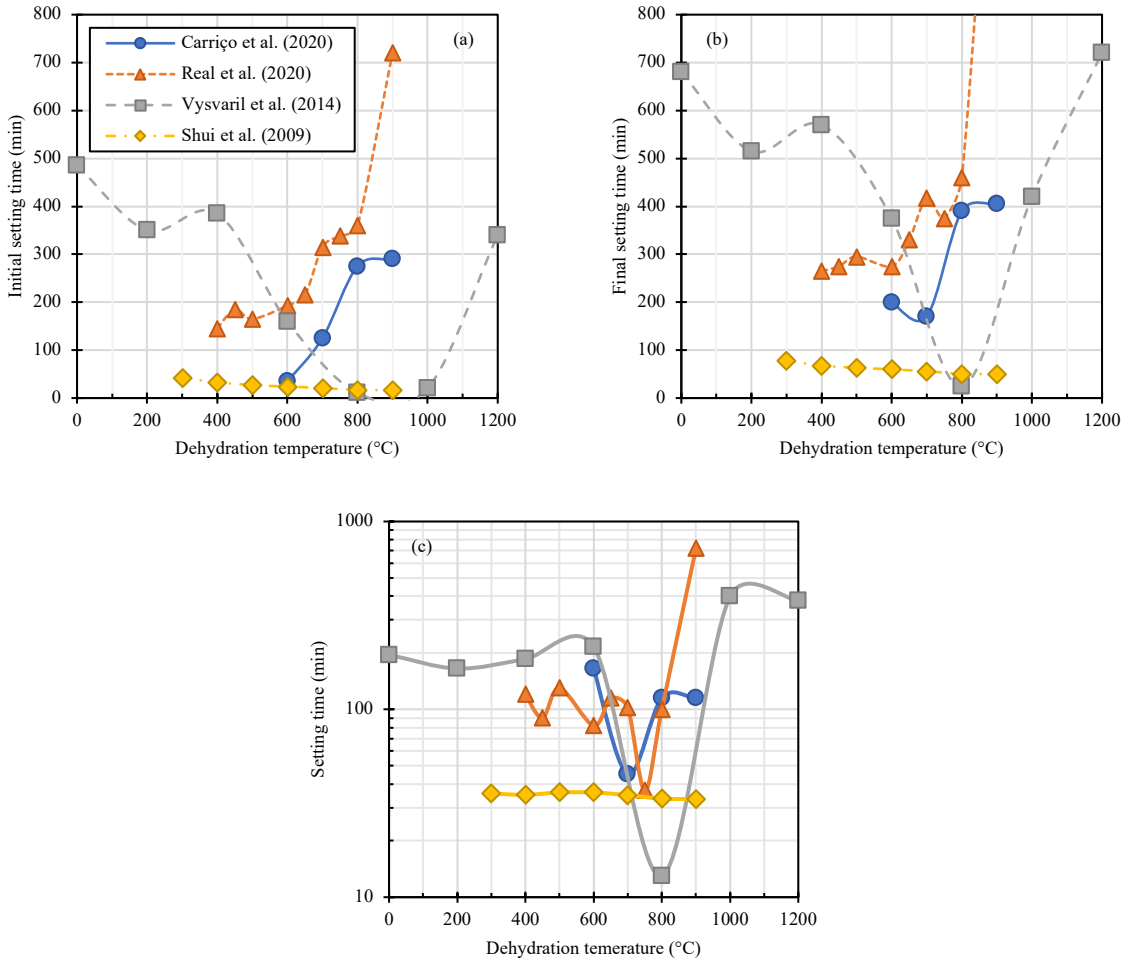

Data from (CARRIÇO et al., 2020; REAL et al., 2020; SHUI et al., 2009; VYŠVAŘIL et al., 2014).

In general, the literature data showed distinct trends. Several authors argued about the rehydration and consolidation mechanisms of recycled cement. Carriço and coauthors (CARRIÇO et al., 2020) reported a false setting phenomenon. The authors also argued that the setting time may not depend on the CaO content but may be more related to the reactivity of the dehydrated products.

Shui and coauthors (SHUI et al., 2009) suggested that in contact with water, the dehydrated phases rapidly polymerize to form a new C-S-H network, without the need for dissolution and nucleation, justifying the rapid setting behavior observed. The high heat peak reported in the first moments of rehydration (Section 2.3.2.4) and the rapid paste consolidation, allowing the verification of the compressive strength with 8 hours (BOGAS et al., 2022), corroborate this view. More research is needed for a better understanding of the consolidation mechanism of recycled cement.

2.3.2.6 Water demand

It is widely reported that recycled Portland cement requires, on average, twice as much water as OPC for standard consistency (BALDUSCO et al., 2019; BOGAS et al., 2022; BOGAS; CARRIÇO; TENZA-ABRIL, 2020; REAL et al., 2020). The main reasons for this are (i) high specific surface area, (ii) grain and phase morphology, and (iii) intragranular porosity (SHUI et al., 2009; XUAN; SHUI, 2011; YU; SHUI, 2013). In addition, these physicochemical characteristics promote a high tendency to agglomerate. The water trapped between the particles reduces the amount of available water, increasing the water demand.

Figure 27 shows the trend of water demand of recycled cement as a function of dehydration temperature. There is a clear linear trend of increase in water demand as a function of the dehydration temperature increase. This trend does not apply to recycled cement at temperatures above 900 °C.

Figure 27 - Water/binder ratio of rehydrated recycled Portland cement for standard consistency.

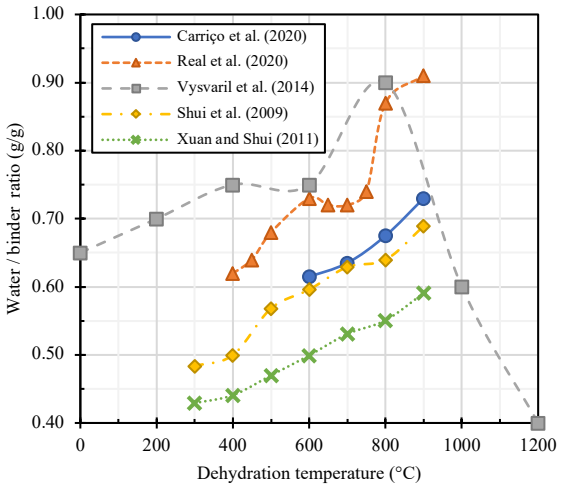

Data from (CARRIÇO et al., 2020; REAL et al., 2020; SHUI et al., 2009; VYŠVAŘIL et al., 2014; XUAN; SHUI, 2011).

Xuan and Shui (XUAN; SHUI, 2011) indicated a lower water demand trend for recycled cement with precursor material with a lower water/cement ratio. The behavior is corroborated by the comparison of the water demand of the R-PC in (CARRIÇO et al., 2020) and (REAL et al., 2020) who had cement pastes with a water/binder ratio of 0.40 and 0.55 g/g, respectively.

2.3.2.7 Compressive strength

The literature presents a wide range of compressive strength values for pastes and mortars made with 100% recycled cement. This wide range is associated with the various parameters involved in recycled cement production as precursor material, treatment temperature, particle fineness, dispersion efficiency, and the water/binder ratio (CARRIÇO; BOGAS; GUEDES, 2020).

The compressive strength analysis was based on cement recycled from cement pastes. Recycled cement with other precursor materials as concrete residues has low reactivity and high variability. Besides, the separation process of aggregate/hydrated cement paste is very influential (SHUI et al., 2014; XINWEI; ZHAOXIANG; XUEYING, 2010).

Figure 28 shows the relationship between the evolution of strength of recycled cement (R-PC) and Portland cement (PC) pastes. The early strength development of R-PC pastes is broadly documented in the literature (BALDUSCO et al., 2019; BOGAS et al., 2022; SHUI et al., 2009; WANG; MU; LIU, 2018). The authors associate this behavior with the fast rehydration mechanism.

Figure 28 - Compressive strength of R-PC pastes relative to OPC pastes over time.

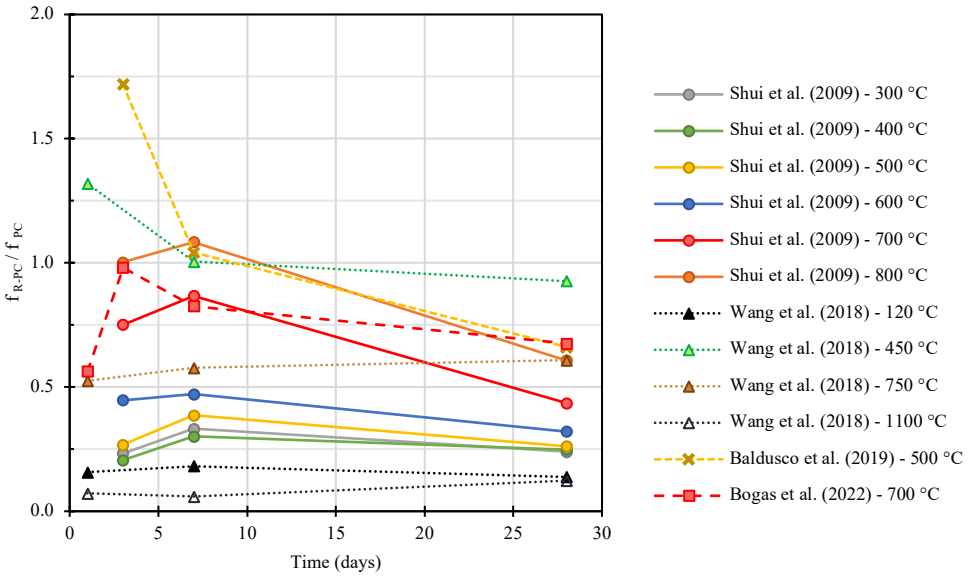

Data from (BALDUSCO et al., 2019; BOGAS et al., 2022; SHUI et al., 2009; WANG; MU; LIU, 2018).

The dehydrated cement at 450-500 C presented 32% and 72% strength development higher than the PC when rehydrated for 1 and 3 days, respectively (BALDUSCO et al., 2019; WANG; MU; LIU, 2018). Other authors report an elevated strength development of R-PC at 7 days (BOGAS et al., 2022; SHUI et al., 2009). The results presented in the literature are variable. Wang (WANG; MU; LIU, 2018) and Shui (SHUI et al., 2009) showed opposite trends. These will be discussed in-depth forward.

Overall, the fast strength evolution can be an advantage in the R-PC application as the main binder or SCM. This behavior enhances the agility in the formwork and, consequently, the productivity of conventional constructions.

Figure 29 shows the compressive strength at 28d of pastes made with the same standard consistency using cement recycled at different temperatures. Only cubic-shaped cement pastes were analyzed. The standard consistency varied among the studies (REAL et al., 2020; SHUI et al., 2009; VYŠVAŘIL et al., 2014; XUAN; SHUI, 2011).

Figure 29 - Water demand for standard consistency vs. compressive strength at 28d of cubic-shaped recycled cement pastes. The data was divided by the dehydration temperature of recycled cement. Each circle represents data for a specific article. The thick lines represent the potential trend of the behavior of recycled R-PC at 400 °C (green) and 800 °C (orange).

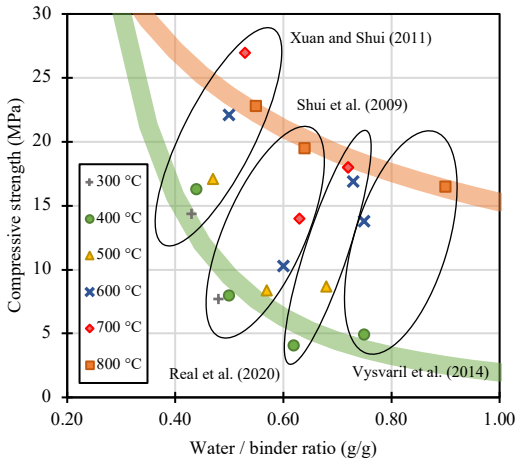

Data from (REAL et al., 2020; SHUI et al., 2009; VYŠVAŘIL et al., 2014; XUAN; SHUI, 2011).

There is a trend towards an increase in water demand due to the dehydration temperature increase, which corroborates Figure 27. The data analysis per article shows an increase in compressive strength with the dehydration temperature increase, regardless of the also increasing w/b ratio trend.

However, by analyzing the data by dehydration temperature, it is possible to see that the compressive strength depends on the porosity generated by the water demand. Therefore, the lower the water/binder ratio, the lower the strength of the R-PC paste for the same dehydration

temperature, respecting the standard behavior of cementitious materials.

Data analysis by the w/b ratio indicates that cement dehydrated at lower temperatures tends to have more fluid consistencies. For the same water/binder ratio, the higher the dehydration temperature of the recycled cement, the higher its compressive strength tends to be.

From another point of view, different dehydration temperatures promote different internal porosity (microcracks), which affects the water demand and the initial porosity of the system. Therefore, the water/binder ratio is not the best parameter to investigate the compressive strength of R-PC-based materials. Further studies must be done to analyze in-depth the relations between the initial porosity (internal porosity of the R-PC), reactivity, hydration degree, final porosity of the system (R-PC-paste), and compressive strength.

Figure 30 shows the relation between the dehydration temperature and the compressive strength of those recycled cements rehydrated with a fixed water/binder ratio. Wang and coauthors (WANG; MU; LIU, 2018) used w/b of 0.55 and recycled cement pastes in cubic molds. Angulo and coauthors (ANGULO et al., 2022) used w/b of 0.63 and mortars (1:3) in cylindrical molds.

As each study fixed the water demand, the strength variation is exclusively associated with the material's reactivity. The R-PC recycled at 450-500 °C obtained the highest strength, which indicates a greater reactivity than the others. The TG/DTG results (Table 11), calorimetry results (Table 12), and their correlation with the compressive strength (Figure 25) corroborate with the analysis.

Figure 30 - Dehydration temperature vs. compressive strength of R-PC-based materials with constant water/binder ratio.

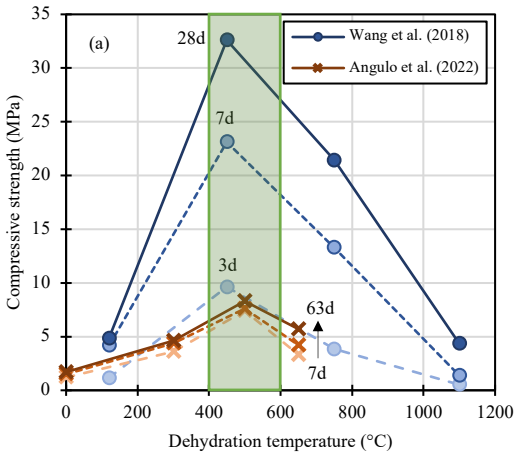

Data from (ANGULO et al., 2022; WANG; MU; LIU, 2018).

Differently from the trend presented in Figure 29, for the same water/binder ratio, an optimum point (450-500 °C) of greater reactivity appeared. Consequently, recycled cement in this temperature range has the highest performance potential when rehydrated.

Therefore, the data present in the literature show different behaviors when analyzed from different perspectives (standard consistencies vs. fixed w/b ratio). More data is needed to understand the relationship between water demand, strength, and dehydration temperature.

2.3.2.8 Porosity of R-PC-based materials

The porosity of recycled cement pastes varies from nano to micrometer scale. Therefore, many techniques are used to evaluate the cement matrix porosity.

The scanning electron microscopy technique estimates the porosity of the paste through a backscattered electron (BSE). In the SEM images, the pores are black, the clinker is bright, and the remaining hydrated phases appear in different levels of gray. In this way, the pore area and phase are estimated by their color. The area fraction of each phase determined by the images is assumed equal to the volumetric fraction. The resolution of this method is limited to 1 μm, pixel size. Therefore, this image analysis only estimates the total porosity, having less accuracy in the range of smaller pores up to about 1–10 μm.

Only one study was found (BOGAS; CARRIÇO; TENZA-ABRIL, 2020) that evaluated porosity SEM-BSE for rehydrated pastes. The results obtained are shown in Figure 31.

Figure 31 - Porosity by SEM-BSE in time (a) and its relationship with compressive strength of pastes (b).

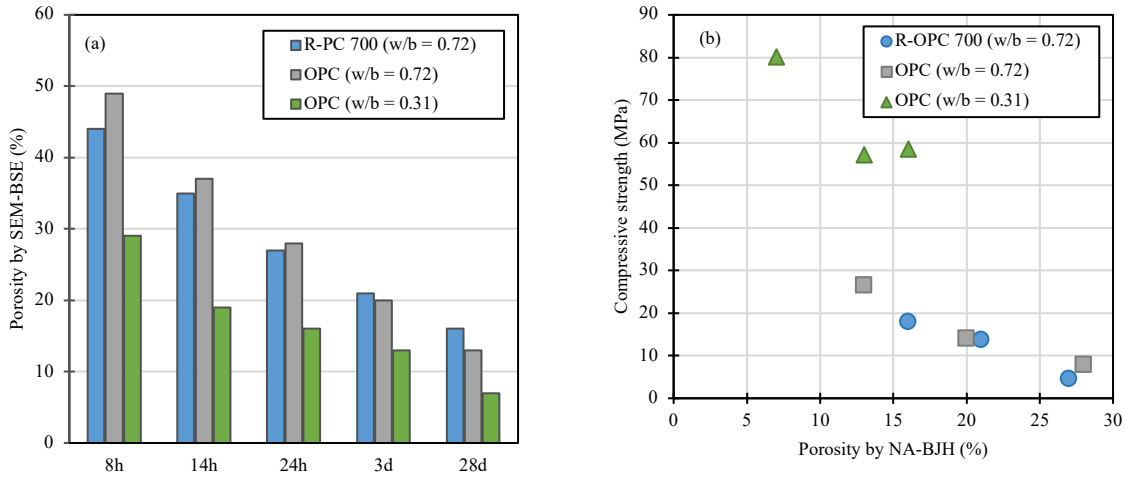

Date from (BOGAS; CARRIÇO; TENZA-ABRIL, 2020).

In the study, the cement recycled at 700 °C required 0.72 g/g of water for standard

consistency. For comparison, an OPC paste with the same water/binder ratio (0.72 g/g) and another with the same consistency (0.31 g/g) were made.

Figure 31a shows a tendency to reduce porosity over time for all pastes, standard behavior as a function of the (re)hydration of the phases. R-OPC 700 showed lower porosity than hydrated OPC with the same w/b up to 1 day. The OPC paste of the same consistency showed lower porosity values due to its lower water demand.

Figure 31b shows that for the same w/b ratio, the R-OPC 700 and OPC pastes obtained similar porosities and strength. It indicates regular hydration of the RC paste over time. Between 24 h and 28 days, the total porosity of the recycled cement paste was reduced by up to 41%. However, between 3 and 28 days, the reduction was lower than that found in the OPC folder of the same w/b (26 vs 34%). The authors infer that this leads to faster formation of C-S-H and lower density in RC pastes.

2.3.2.9 Environmental impact analysis

Recycled cement emerges as an alternative for the disposal of fine construction and demolition waste (CDW). Furthermore, its application as a main binder or SCM allows its reuse in the primary product (concrete).

CDW has no CO_2 emissions linked to it. However, by promoting the dehydration of this residue, two sources of CO_2 emission arise: (i) the burning of the fuel necessary to heat the CDW and (ii) the decarbonation to temperatures from 600 °C.

In this way, recycled cement at temperatures below 600 °C has a smaller CO_2 footprint than others. Moreover, the fuel consumption is proportion to the heat needed. Therefore, the R-PC has lower CO_2 emissions as lower its dehydration temperature.

As shown throughout this chapter, the dehydration temperature plays a key role in the characteristics of R-PC and R-PC-based materials. Different temperatures affect phase reactivity, specific surface area, water demand, porosity, and strength.

In this work, the dehydration temperature to produce the R-PC was 500 °C. This temperature was chosen for two reasons: (i) it does not promote the extra emissions caused by decarbonation, and (ii) it promotes the R-PC with the highest reactivity in the literature.

The CO_2 emissions by a ton of R-PC do not represent the best way to assess the environmental impact. The proper way to evaluate is to divide the environmental impact by its performance. Chapter 3 analyzes the environmental performance of recycled cement present in the literature through the CO_2 index proposed by (DAMINELI et al., 2010).

2.4 Literature strategies overview

Table 13 lists the main strategies used in the literature to increase the compressive strength of pastes containing recycled Portland cement. This analysis was based on cement paste as the precursor material. Two scenarios with concrete waste as the precursor material are used for comparison. The precursor material composition is informed by (i) cementitious material type, (ii) water/binder ratio, and (iii) dehydration temperature for recycled Portland cement production. The R-PC-based material composition was detailed through (iv) the type of cementitious material, (v) substitution used, (vi) substitution content, (vii) water/binder ratio, and (viii) superplasticizer content. An analysis of the mechanical performance of R-PC-based materials is presented through the (ix) sample shape, (x) test age, (xi) compressive strength, and (xii) relationship between the compressive strength of R-PC and OPC pastes or mortar with same water/binder ratio or consistency.

Baldusco and coauthors (BALDUSCO et al., 2019) explored the use of superplasticizers to reduce the water demand of R-OPC. Strengths of 12-15 MPa were obtained and a ratio of 1.72 to OPC paste of the same water/solids at three days.

Shui (SHUI; YU; DONG, 2011) and Wang (WANG; MU; LIU, 2018) researches showed that the synergy between R-OPC and SCMs can achieve high strengths. This approach has a low environmental impact. However, fly ash and slag are not widely available materials.

The strategy that presented the best performance was the combination of R-OPC with OPC. For paste studies, Yu and Shui (YU; SHUI, 2013) reported a strength increase of 1.38 and 1.88 compared to that obtained by OPC for 3 and 28 days, respectively. Although effective, this strategy uses R-OPC in low amounts. For studies on mortar, Carriço (CARRIÇO et al., 2022) and Bogas (BOGAS; CARRIÇO; PEREIRA, 2019) works exhibited good performance but none surpassed the strength of OPC-based mortar.

There is a clear research gap where no reducing the water demand of R-PC-based materials with dispersants and through blends with cement and filler have not been explored combined and in-depth.

Table 13 - Literature overview of most used strategies for R-PC-based materials improvement.

Reference	Precursor material information			R-PC-based material composition					Compressive strength analysis			
	Type	w/b	Dehydration temperature (°C)	Type	Substitution		w/b	SP (%)	Sample shape	Age (days)	fc (MPa)	$f_{R\text{-}PC}/f_{OPC}$
					Type	Content						
(BALDUSCO et al., 2019)	Cement Paste	0.45	500	Cement Paste			0.60	1.0	Cylinder (27x54 mm)	3	13.6	1.72
										7	12.5	1.04
										28	14.6	0.66
(YU; SHUI, 2013)	Cement Paste	n.m	650	Cement Paste	OPC	95.0%	0.30	0.5	Cube (40 mm)	3	33.7	1.29
					OPC	92.5%					42.2	1.62
					OPC	90.0%					49.1	1.88
					OPC	87.5%					42.7	1.64
					OPC	85.0%					38.9	1.49
					OPC	95.0%				28	67.0	1.18
					OPC	92.5%					72.3	1.27
					OPC	90.0%					76.3	1.34
					OPC	87.5%					69.9	1.23
					OPC	85.0%					64.1	1.13
(SHUI; YU; DONG, 2011)	Cement Paste	0.50	650	Cement Paste	Fly ash	47.0%	0.40	1.0	Cube (40 mm)	28	20.1	
					Fly ash	52.0%					35.9	
					Fly ash	57.0%					39.7	
					Fly ash	62.0%					45.6	
					Fly ash	67.0%					59.0	
					Fly ash	72.0%					54.5	
(WANG; MU; LIU, 2018)	Cement Paste	0.50	450	Cement Paste			0.55		Cube (25 mm)	1	9.7	1.28
			750				0.55				4.1	0.54
			450				0.55				9.8	1.29
			450		Slag	30.0%	0.55				3.9	0.52
			450				0.55			28	32.4	0.92
			750				0.55				21.9	0.62
			450				0.55				35.4	1.00
			450		Slag	30.0%	0.55				38.2	1.08
(CARRIÇO et al., 2022)	Cement paste	0.55	700	Mortar (1:3)			0.90		Cube (40 mm)	28	15.4	0.26
							0.72	2.0			28.3	0.49
					OPC	95.0%	0.47				52.6	0.90
					OPC	85.0%	0.55				38.9	0.67
					OPC	70.0%	0.58				38.7	0.66
					OPC	59.0%	0.64				36.0	0.62
					Fly ash	15.0%	0.85				13.4	0.23
					Fly ash	30.0%	0.75				14.2	0.24
					OPC	85.0%	0.60	2.0			47.1	0.93
					OPC	70.0%	0.60	2.0			44.3	0.87
					OPC	50.0%	0.60	2.0			39.7	0.78
(BOGAS; CARRIÇO; PEREIRA, 2019)	Concrete	0.45	350	Mortar (1:3)	OPC	80.0%	0.60		Cube (40 mm)	28	30.6	0.73
					OPC	50.0%	0.60				12.5	0.30
					OPC	25.0%	0.60				2.5	0.06
			650	Mortar (1:3)	OPC	80.0%	0.60				32.8	0.78
					OPC	50.0%	0.60				13.8	0.33
					OPC	25.0%	0.60				4.1	0.10
	Cement paste	0.45	350	Mortar (1:3)	OPC	80.0%	0.60				31.2	0.74
					OPC	50.0%	0.60				10.3	0.25
					OPC	25.0%	0.60				2.8	0.07
			650	Mortar (1:3)	OPC	80.0%	0.60				32.9	0.79
					OPC	50.0%	0.60				17.9	0.43
					OPC	25.0%	0.60				5.1	0.12

3 RECYCLED PORTLAND CEMENT AS A SOLO BINDER

This chapter explores the influence of water/binder ratio reduction by dispersant use in porosity and compressive strength of recycled Portland cement paste. Experimental and literature data were analyzed to investigate (i) a correlation between compressive strength and total porosity of ordinary, blended, and recycled Portland cement pastes and (ii) binder efficiency index and dioxide carbon intensity index of the recycled cement in comparison with traditional Portland cement.

This chapter was based on a paper published by "Resources, Conservation and Recycling" named "Strength-porosity correlation and environmental analysis of recycled Portland cements" (https://doi.org/10.1016/j.resconrec.2022.106763).

Figure 32 presents the experimental flow chart of this chapter.

Figure 32 - Flow chart of the experimental program of Chapter 3.

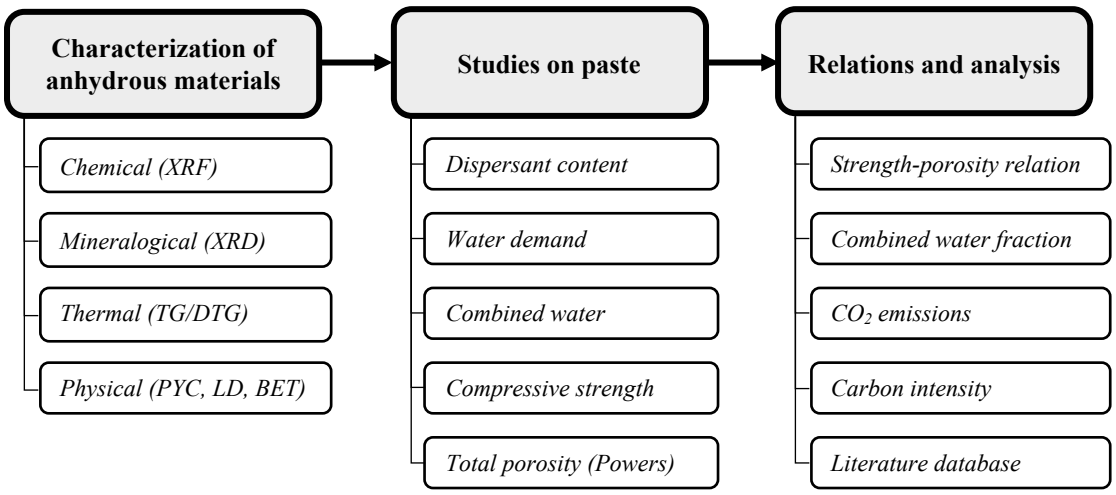

3.1 Materials and Methods

Ordinary Portland cement (CPV, the cement with the highest content of clinker) available in the Brazilian market was used (Table 14). OPC paste was prepared with water/cement ratio of 0.45. The specimens were cured in a controlled room at a temperature of 23±2 °C and relative humidity above 95%. After 28 days of curing, the specimens were oven-dried for 24 hours at 70 °C to facilitate crushing and grinding. After drying, the specimens were crushed in a jaw crusher, resulting in a material with a particle size of less than 4.75 mm. The crushed pastes were then ground in a disk mill until all the material passed through a 150-μm sieve.

The sieved powder of hydrated cement paste was calcined in a furnace at a rate of 10 °C/min from room temperature to 500 °C and maintained at this temperature patamar for 2 h to

remove the chemically combined water from the hydrated products. The dehydrated cement was cooled outside the furnace through a forced air current to room temperature, recycled ordinary Portland cement (R-OPC) was obtained.

Table 14 - General information: code, cement type, general description and clinker, slag and filler contents.

Code	Type of cement	Description	Clinker content + $CaSO_4$	Slag content	Filler content
OPC	CPV - ARI [a]	High early strength cement	95 – 100 [a]	0 – 5 [a]	0 – 5 [a]
R-OPC	Recycled OPC	Dehydrated at 500°C	–	–	–

[a] According to Brazilian standards (BRAZILIAN ASSOCIATION OF TECHNICAL STANDARDS, 2018).

3.1.1 Characterization of OPC and R-OPC

The chemical composition of the cement was evaluated using X-ray fluorescence (XRF) and expressed quantitively in terms of the main oxides. For loss on ignition (LOI) analysis, the samples were melted at 1200 °C at a sample/flux ratio of 1:6.75.

The crystalline phases were identified using X-ray diffraction (XRD) (Windmax 2000, Rigaku). The samples were ground, sieved to 0.045 mm, and pressed into aluminum support. The operating conditions were CuKα radiation (40kV/30mA), 1° divergent slit, 1° scattering slit, 0.02° 2θ angular pitch, 2°/min, 5° to 65.90° sweep and 2,000 counts/s. The compounds were identified using Panalytical X-Pert HighScore Plus software (version 2.2) according to the International Center for Diffraction Data (ICDD).

Thermogravimetry was performed by SDT 2960 (TA Instruments). The samples were placed in a 110 µL alumina crucible, without a lid. Gas flow was 50 mL/min of ultra-pure nitrogen (N), with a constant heating rate of 10 °C/min up to 1000 °C. Data from thermogravimetric analyzes (TG) and their respective first-order derivatives (DTG) were calculated using Universal Analysis 2000 software (TA Instruments, version 4.1D).

The particle size distribution of the cement was quantified using a laser granulometer (Helos KR, Sympatec) with an analysis range between 0.1 and 350 µm. The sample was dispersed in water using a mixer (RW20, IKA) at a constant speed of 1000 rpm/min before being added to the granulometer. A helium gas pycnometer (Accupyc 1340, Micromeritics) was used to determine the density. The specific surface area was measured by nitrogen gas intrusion and data processing by the Brunauer–Emmett –Teller (BET) method.

3.1.2 Water demand reduction and rheological analysis

A continuous flux rheometer was used to determine viscosity (RUSSELL, 2012) and yield stress (FLATT, 2004; FLATT; BOWEN, 2003; MACIEL, 2017; OLIVEIRA et al., 2000)

of cementitious suspension (TEIXEIRA et al., 2014). It measures the stress at a given strain rate, or vice-versa. The multi-point curve behavior can be described by variating of the strain rates; a more precise approach compared to a single point (e.g., mini-slump).

Rheometry was used to ensure fully dispersed conditions in the pastes. Initially, the hydrated (OPC/P – Ordinary Portland Cement Paste) and rehydrated pastes (R-OPC/P – Recycled Ordinary Portland Cement Paste) were produced with the same consistency (mini-slump spread of 50±5 mm), without dispersant, by changing the water/binder ratio. The procedure was identical to that of (BALDUSCO et al., 2019).

The rheometer used was a Thermo Haake, with parallel plate geometry, a diameter of 40 mm and a plate spacing of 1 mm. A polycarboxylate-based superplasticizer TecFlow 8000, with a density of 1.10 g/cm³, GCP was used. The sequence of paste preparation was: (i) adding superplasticizer to the water, (ii) adding the binder into the water plus superplasticizer, and (iii) mixing the paste in the stirrer at 10,000 rpm for 60 s. After mixing, the paste was placed in the rheometer for approximately 30 s. The paste shear rate was accelerated from 0 to 50 s^{-1} at a constant rate for a minute, then decelerated with the same rate. This cycle was repeated because measurements of the first cycle may be influenced by agglomeration (MACIEL, 2017). Data from the second cycle were used for analysis.

The dispersant saturation contents on the cement pastes were determined by rotational rheometry while keeping the water/binder content constant. The apparent viscosity was obtained at a shear rate of 50 s^{-1} for each mix for yield stress versus shear rate curves. The criteria used included the lowest superplasticizer content for an apparent viscosity lower than 0.50 Pa.s (DAMINELI et al., 2016a).

The minimum mixing water demand for a fully dispersed paste was determined by fixing the optimum dispersant content and decreasing water content. The minimum water/binder ratio selection criterion was based on apparent viscosity conservation of paste with higher water content. The selected water/binder ratio was within 15% of the relative standard deviation of the paste with higher water content.

3.1.3 Characterization of OPC/P and R-OPC/P

3.1.3.1 Thermogravimetric analysis

Thermogravimetric analysis was used to quantify the chemically bound water. For pastes without dispersant, hydration was interrupted by freezing a cylindrical sample in total immersion in nitrogen for 5 min (-196 °C). Thereafter, the pastes were kept in a scientific freezer at -33 °C until lyophilization (GUILGE, 2011).

For pastes with dispersants, hydration stoppage was achieved by solvent exchange with isopropyl alcohol (SNELLINGS et al., 2018). The pastes were then placed in a vacuum desiccator over silica gel and soda lime to mitigate carbonation. All pastes were ground below 0.045 mm for the TG essay.

The chemically combined water content of ordinary cement ($w_{n,o}$) was calculated based on (DE WEERDT et al., 2011) (Equation 10).

$$w_{n,o} = \frac{W_{40} - W_{550}}{W_{550}} \qquad \text{Equation 10}$$

Where Wx corresponds to the percentage of mass lost under temperature X in °C.

For recycled cement, a correction on the chemically combined water content ($w_{n,r}$) must be made (Equation 11).

$$w_{n,r} = w_{n_{RC/P}} - w_{n_{RC}} \qquad \text{Equation 11}$$

Where $w_{n_{RC/P}}$ is the rehydrated paste combined water and $w_{n_{RC}}$ is the recycled cement combined water. This correction is needed because the combined water present in the cement does not contribute to the reactivity and strength evolution of the rehydrated paste.

3.1.3.2 Compressive strength

Fresh cement paste was cast into cylindrical molds of reduced dimensions (diameter x height): 27 x 54 mm. The reduced-dimension samples containing only cement paste (without sand) correlated significantly with the standard method (normalized sand), with a dimension of 50 x 100 mm. For further details, refer to (BALDUSCO et al., 2019).

Six specimens were molded for each age of interest. A vibrating table was used for 30 s to ensure proper compaction. The specimens were cured in a controlled room at a temperature of 23±2 °C and relative humidity above 95%.

At the age of interest, the specimens were demolded to measure their compressive strengths. The compressive strength test of the hydrated and rehydrated pastes was performed using a press (BPP20/2, Mohr & Federhaff) with an electronic load cell having a capacity of 20,000 kN, resolution of 0.01 kN, and loading speed of 0.25 MPa/s.

The pastes without dispersant were subjected to mechanical tests at 28 days. The pastes with dispersant were tested at 12 h, 24 h, 7 and 28 days to evaluate the strength and porosity evolution.

3.1.4 Strength-porosity correlation

3.1.4.1 Literature database

A literature review was conducted for the strength-porosity and environmental analyses of ordinary, blended, and recycled Portland cement pastes. To be part of the database, the reference should satisfy three criteria: (i) the tests should be performed on pastes, (ii) compressive strength of the paste should be informed, and (iii) mercury intrusion porosimetry (MIP) data and/or thermogravimetry tests should be informed. Rehydrated cement pastes have additional criteria: (iv) the predecessor material must be a cement paste and (v) dehydration with calcination temperature below 900 °C (without clinkerization of phases). Table 15 presents the database references.

Table 15 - References used in the database.

Reference	Code	Compressive strength	MIP	TG
(JEONG et al., 2015)	Jeong et al. (2015)	X	X	X
(KIM et al., 2019)	Kim et al. (2019)	X	X	X
(REAL et al., 2020)	Real et al. (2020)	X	X	X
(DU et al., 2021)	Du et al. (2021)	X	X	X
(LAM; WONG; POON, 2000)	Lam et al. (2000)	X	X	-
(VYŠVAŘIL et al., 2014)	Vysvaril et al. (2014)	X	X	-
(HOU et al., 2019)	Hou et al. (2019)	X	X	-
(BOGAS; CARRIÇO; TENZA-ABRIL, 2020)	Bogas et al. (2020)	X	X	-
(WANG; MU; LIU, 2018)	Wang et al. (2018)	X	-	X

As the shapes of literature data varied, the compressive strength of the pastes was standardized using the following steps. The standard format consisted of a 27 x 54 mm cylinder, as was the specimen used in our experimental data.

First, the cubic samples were converted to 27 mm cubes using a scale factor index. Equation 12 was deducted from the trend presented in (OLIVEIRA et al., 2021). It was used for cubic samples with size of 20-70 mm. For more details see Supplementary material A.

$$SF_{index} = 1.2935 - 0.089 \ln(d) \qquad \text{Equation 12}$$

Where "SF_{index}" is the scale factor index and "d" is the side of the cube in mm.

After the first conversion, the height/diameter coefficient (h/d_{coef}) was applied to transform the cubes into a 27 x 54 mm cylinder. For this, the coefficient was considered to be 1.15 (NEVILLE; BROOKS, 1987; YI; YANG; CHOI, 2006). Equation 13 must be used to

obtain the compressive strength for 27 x 54 mm cylinders.

$$f_{cylinder_{27x54}} = \frac{SF_{index}}{h/d_{coef}} \cdot f_{cube} \quad \text{Equation 13}$$

3.1.4.2 Total porosity estimation

The Powers model allowed an estimation of the volumetric composition of hardened cement paste through calculations (POWERS; BROWNYARD, 1947). The model can estimate the total porosity, which strongly correlates with the mechanical properties of cementitious pastes (HANSEN, 1986).

Mercury intrusion porosimetry and Powers' total porosity estimative were compared determine their agreement. When some experimental data was unavailable, this comparison enabled an inference when the correlation was considered good. The Powers model was applied only to pastes with a water/solid ratio higher than 0.35.

Equation 14 - Equation 17 show the total porosity calculations.

$$V_{paste} = V_{solids} + V_{water} \quad \text{Equation 14}$$

$$V_{hydrates\ solids} = V_{solids} + 0.75w_n \quad \text{Equation 15}$$

$$V_{pores} = V_{paste} - V_{hydrate\ solids} \quad \text{Equation 16}$$

$$P = \frac{V_{pores}}{V_{paste}} \quad \text{Equation 17}$$

Where V_{paste} is the volume of paste; V_{solids} is the volume of solids; V_{water} is the volume of water; $V_{hydrates\ solids}$ is the volume of hydrates solids; w_n is non-evaporable (the chemically bound) water; V_{pores} is the volume of all pores; P is the total porosity.

For literature data with mercury intrusion porosimetry and without TG data, the MIP porosity was converted to total porosity through the relation presented in Equation 18. In total, 33 data points were used (DU et al., 2021; JEONG et al., 2015; KIM et al., 2019; REAL et al., 2020). The trend has a good fit, (R^2 = 0.975). For further details, see Supplementary data.

$$P = 1.487 \cdot MIP \quad \text{Equation 18}$$

3.1.4.3 Combined water fraction (cwf)

The combined water fraction (*cwf*) was derived from a discussion between Dr. Ellis Gartner and Dr. Vanderley John. They identified that every SCM has a double effect on cement, changing its reactivity (chemical effect) and water demand (physical effect) (JOHN et al., 2019). Consequently, to express binder efficiency, *cwf* was created by combining these two effects (Equation 19). Moreover, *cwf* strongly correlates with cement pastes' porosity and compressive strength (ABRÃO; CARDOSO; JOHN, 2020).

$$cwf = \frac{w_n}{w_{mix}} \quad \text{Equation 19}$$

Where w_n is the non-evaporable (combined) water of the material at the age under analysis, and w_{mix} is the amount of water used in the mixture.

Powers and Brownyard (POWERS; BROWNYARD, 1947) briefly presented this coefficient. However, the authors preferred to use the geo-space ratio because of its greater precision. Owing to the easy application of *cwf*, which requires only chemically combined water (measured by thermogravimetric testing) and mixing water, this coefficient was suggested as an improvement over the current cement standard. The *cwf* evaluates the binder use efficiency and presents a good correlation with the mechanical properties of the cementitious materials (compressive strength and porosity) (ABRÃO et al., 2020; ABRÃO; CARDOSO; JOHN, 2020; JOHN et al., 2019). We verified whether this parameter is valid for recycled cement by combining our experimental data with the literature data.

3.1.5 Environmental analysis

The CO_2 emissions of the studied binders were calculated to assess their environmental impact. To simplify the analysis and determine the CO_2 emissions of the recycled and ordinary cements, we ignored the CO_2 emissions from crushing and grinding processes were disregarded. To establish the CO_2 emission during the binder production, we considered three parameters: (i) CO_2 emissions to heat the system through fuel burn, (ii) the volatile fraction of CO_2 resulting from the decarbonation process, and (iii) CO_2 emissions from supplementary cementitious material. These three parameters yield the total CO_2 emission per binder (Equation 20).

$$CO_{2_{binder}} = CO_{2_{fuel}} + CO_{2_{decarb}} + CO_{2_{SCM}} \quad \text{Equation 20}$$

To determine the CO_2 emissions of fuel burn for heating process, the following equations are required: the quantity of energy needed and required to heat the system (furnace) (Equation 21 - Equation 22), the mass of fuel and (Equation 23) and its emission of CO_2 (Equation 24). This method used was proposed by (QUATTRONE; ANGULO; JOHN, 2014). Petroleum coke was used as the fuel.

$$Q_b = c \cdot m \cdot (\theta_t - \theta_{amb}) \quad \text{Equation 21}$$

Where Q_b is the amount of heat needed to increase the temperature of the binder [kJ]; c is the specific heat of the binder, fixed at 0.80 kJ/kg°C for ordinary cement and 1.85 kJ/kg°C for recycled cement (WANG, 2016); m is the amount of material at the beginning of the process to guarantee a ton of binder at the end [kg]; θ_t is the treatment operating temperature; and θ_{amb} is the ambient temperature, fixed at 25 °C.

For ordinary cement, the material before the thermal treatment for clinker production includes limestone, clay, sand, iron ore, and more. Therefore, the initial material mass was fixed at 1600 kg to produce a clinker ton (HUNTZINGER; EATMON, 2009). For blended cement, the mass required was determined proportionally to the clinker content. Moreover, the treatment operating temperature was set to 1500 °C for clinker production.

For recycled cement, the initial amount of paste to produce one ton of recycled cement was determined by multiplying the recycled cement mass (1000 kg) by the predecessor material mass loss at 25 °C, divided by the mass loss at the dehydration temperature. If the recycled cement has an SCM addition after its dehydration process, the mass of recycled cement must be proportional to its content in the binders' final composition. Mass loss was obtained using TG/DTG. The operating temperature of the treatment was set equal to the dehydration temperature.

$$E_s = \frac{Q_b}{\eta_f} \quad \text{Equation 22}$$

Where E_s is the amount of heat required by the system (furnace) to heat the binder [kJ] and η_f is the efficiency of the furnace, determined as 0.55 (TRINKS et al., 2003).

$$m_{fuel} = \frac{E_s}{H}$$ Equation 23

Where m_{fuel} is the mass of fuel [kg] and H is the net heating value of the fuel used in the heating system. For petroleum coke, it was 34.2 MJ/kg (GUADAGNI, 2003).

$$CO_{2_{fuel}} = m_{fuel} \cdot CO_{2_{factor}}$$ Equation 24

Where $CO_{2\ fuel}$ is the amount of CO_2 emitted per ton of binder produced in the heating step [$kgCO_2$/ton of binder] and $CO_{2\ factor}$ is the CO_2 emission obtained from burning the fuel, 3.17 $kgCO_2$/kg fuel.

Equation 25 was used to calculate the CO_2 emission from the decarbonation of clinker process and recycled cement. For OPC, 1200kg of limestone was used for the calculation (HUNTZINGER; EATMON, 2009). For blended cement, the required limestone mass required was determined to be proportional to the clinker content. For recycled cement, CO_2 emissions were obtained through predecessor material loss of mass between 550 °C and the dehydration temperature. At dehydration temperatures below 550 °C, there is no decarbonation.

$$CO_{2_{decarb}} = m_{limestone} \cdot \frac{M_{CO_2}}{M_{CaCO_3}}$$ Equation 25

Where Mx is the molar mass of the component. M_{CO_2} and M_{CaCO_3} are equal to 44 and 100 g/mol, respectively.

Equation 26 presents the CO_2 emission related to the supplementary cementitious material.

$$CO_{2_{SCM}} = SCM_{emission} \cdot SCM_{content}$$ Equation 26

Where $SCM_{emission}$ is the CO_2 emission per ton of SCM during its production and $SCM_{content}$ is the percentage by mass of SCM in the final binder.

The emissions associated with the heating granular blast furnace slag, fly ash, and limestone fillers were disregarded. Therefore, there were no CO_2 emissions associated with those SCMs and binders without SCM. The CO_2 emission related to the metakaolin and nanoclay have process emissions owing to the heat treatment near 800 degrees, equivalent to 270 $kgCO_2$/ton of SCM (MILLER et al., 2018).

Equation 27 was used to determine CO_2 (kg/m^3) emitted to produce all cementitious

paste raw materials.

$$CO_{2_{paste}} = \left[CO_{2_{binder}} + (SP_{emisson} \cdot SP_{content})\right] \cdot B_m \qquad \text{Equation 27}$$

Where $SP_{emission}$ is the CO_2 emission per kg of dispersant during its production, adopted as the maximum value of 2.0 $kgCO_2$/kg dispersant (CHEUNG; ROBERTS; LIU, 2018; EUROPEAN FEDERATION OF CONCRETE ADMIXTURES ASSOCIATIONS LTD. (EFCA), 2015). $SP_{content}$ is the percentage by mass of dispersant in the binder. B_m is the binder mass needed to produce one cubic meter of paste. The binder mass was the sum of the cement and SCM masses. The $CO_{2_{paste}}$ unit is $kgCO_2$. m^{-3} paste.

For an overall analysis, the CO_2 index was estimated for 300 dm^3 of paste (Equation 28). This paste volume is commonly used in concrete.

$$CO_{2\ index} = \frac{0.30\ CO_{2_{paste}}}{f_{paste}} \qquad \text{Equation 28}$$

Where CO_2 index unit is $kgCO_2$. m^{-3}. MPa^{-1} and f_{paste} is the compressive strength of cementitious paste in 27x54 mm cylinder.

3.2 Results and discussions

3.2.1 Characterization of OPC and R-OPC

Figure 33 presents XRD qualitative results of OPC and R-OPC. The OPC presented its usual phases (e.g., alite, belite, aluminates, quartz, and calcite). Probably due to exposure of the material to the environment, portlandite and ettringite were found in anhydrous cement.

Figure 33 - Diffractograms: OPC (left) and R-OPC (right).

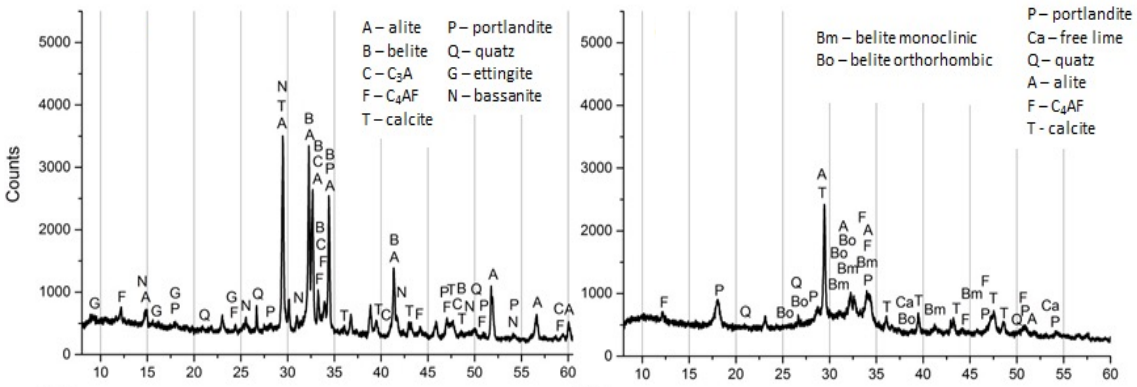

The R-OPC presented similar phases to the anhydrous OPC, such as alite, belite, aluminates, quartz, and calcite. In addition, R-OPC had portlandite phases because the

dehydration temperature used cannot remove all the bound water of the precursor paste. R-OPC showed higher amounts of free lime and absence of tricalcium silicates compared to OPC, which corroborates the literature (BOGAS; CARRIÇO; PEREIRA, 2019) and XRF (Table 16).

Table 16 - Chemical analysis of anhydrous and recycled cement (dehydrated at 500ºC).

Oxides (%)	OPC	R-OPC
CaO	59.0	56.3
SiO_2	20.9	18.9
Al_2O_3	5.09	4.23
Fe_2O_3	2.67	2.49
MgO	2.73	2.46
SO_3	3.06	3.05
K_2O	0.90	0.98
Mn_2O_3	0.20	0.16
TiO_2	0.23	0.22
P_2O_5	0.18	0.16
SrO	0.16	0.15
ZnO	0.01	0.01
Cr_2O_3	0.01	0.01
S_2^-	-	-
CaO (free)[c]	1.94	9.93
LOI	4.06	8.83

[c] Determined using ethylene glycol (BRAZILIAN ASSOCIATION OF TECHNICAL STANDARDS, 2013).

TG/DTG results are shown in Figure 34. Anhydrous cement (OPC) undergoes three thermal events: (i) dehydroxylation of calcium sulfate, (ii) dehydroxylation of portlandite (residual hydration due to environmental exposure of the material), and (iii) decarbonation of calcite (limestone filler of the cement). For dehydrated cement (R-OPC), the first prominent peak is between 400 and 500 °C, indicating the substantial presence of portlandite from the hydration of cement paste. The second peak is close to 750 °C and demonstrates the decarbonation of calcite, similar to that found in OPC.

Figure 34 - TG (a) and DTG (b) results of cements used in this work (OPC and R-OPC).

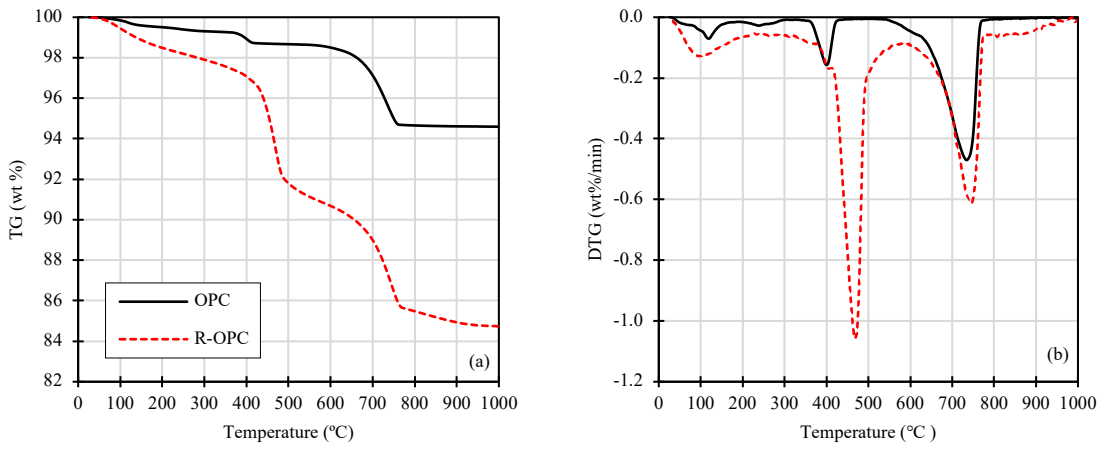

Recycled cement presented TG/DTG results similar to literature with a mass loss between 430-550 and 550-1000 °C of 3.5-5.5% and 4.5-9.0%, respectively (ANGULO et al., 2015a; REAL et al., 2020; WANG; MU; LIU, 2018). For recycled cement, the combined water remaining was 0.097 g/g. The R-OPC result is higher than the literature data, between 0.03 and 0.06 g/g for recycled cements with similar dehydration (ANGULO et al., 2015a; REAL et al., 2020; WANG; MU; LIU, 2018). Table 17 shows the combined mass and water loss values for cements recycled from the literature.

Table 17 - Mass losses of recycled cements in literature for TG/DTG temperature ranges.

Reference	Binder	w/b ratio (Precursor)	Cure (days)	Rate (Time)	Mass loss (%)				Wn (g/g)
					W25-W330[a]	W330-W430[b]	W430-W550[c]	W550-W1000[d]	
Our data (2022)	OPC	-	-	-	0.72	0.57	0.07	4.04	-
Our data (2022)	R-OPC	0.45	90	10 (2h)	2.28	1.24	5.34	6.40	0.097
Angulo et al. (2015)	R-OPC	0.48	28	10 (2h)	1.35	0.00	3.88	6.25	0.032
Wang et al. (2018)	R-OPC	0.50	720	7 (8h)	0.67	1.81	0.66	9.47	0.030
Real et al. (2020)	R-OPC	0.55	100	10 (3h)	0.90	0.24	4.66	4.50	0.060

(a) Dehydroxilation of Aft, C-S-H, C-A-H, AFm
(b) Dehydroxilation of hydrotalcite
(c) Dehydroxilation of portlandite (CH)
(d) Decarbonation of calcite ($CaCO_3$)

Table 18 lists the physical properties of OPC and R-OPC. Recycled cement has a lower density than anhydrous cement because it is not composed by clinker phases but dehydrated cement compounds (ANGULO et al., 2022). The BET-specific surface area of recycled cement was 12 times greater than that of anhydrous cement. The intrinsic porosity of C-S-H due to dehydration is probably the main responsible for the higher surface area of recycled cements (BOGAS; CARRIÇO; TENZA-ABRIL, 2020).

The shape factor measures the closeness of a particle shape to a sphere. The indicator was obtained by dividing the specific surface area via BET by the theoretical specific surface area obtained by laser diffraction (HUNGER; BROUWERS, 2009). The particle is closer to a sphere when the shape factor is closer to 1. The OPC shape factor agrees with the literature data (ABRÃO; CARDOSO; JOHN, 2020). However, the shape factor of the R-OPC is 26 times higher than OPC, which indicates that this material is irregular. There are no records in the literature of such a high factor. The elevated water demand of recycled cements is directly related to their morphology and surface area, with open (accessible) pores in the grains.

Table 18 - Physical properties of the used binders.

Parameters	OPC	R-OPC
ρ (g/cm^3) [a]	3.06	2.64
D_{10} (µm) [b]	1.87	4.52
D_{50} (µm) [b]	14.00	26.50
D_{90} (µm) [b]	40.45	62.27
SSA_{BET} (m^2/g) [c]	1.53	18.76
SSA_{LD} (m^2/g) [d]	0.47	0.22
Shape factor [e]	3.25	86.11

[a] *Particle specific gravity from He pycnometer.*
[b] *D-Values obtained by Laser diffraction granulometry.*
[c] *Specific surface area obtained by BET method.*
[d] *Specific surface area obtained by Laser diffraction granulometry.*
[e] *Shape factor calculated from SSA_{BET} and SSA_{LD}.*

3.2.2 Water demand reduction and rheological analysis

3.2.2.1 Dispersant demand for full dispersion

Figure 35 presents the deflocculation curves (apparent viscosity versus dispersant content) of hydrated (w/b 0.45) and rehydrated pastes (w/b 0.85). The water/binder ratios were determined for a mini-slump consistency of 50 mm without dispersant.

For OPC/P, dispersant saturation (minimum viscosity) was observed for 0.3% superplasticizer content. R-OPC/P required 10 times more, 3.0% to reach saturation. On the other hand, the relation between the surface areas was higher, 18.76 per 1.53 m^2/g. Therefore, the specific dispersant saturation was slightly higher for OPC than R-OPC, 1.96 mg/m^2 compared with 1.60 mg/m^2. The high dispersant demand for R-OPC has raised environmental and financial concerns. A dispersant admixture is commonly the most expensive constituent of cementitious materials, a ten-times increase in its ratio can make R-OPC unfeasible as a solo binder.

Figure 35 - Deflocculation curves for ordinary cement and recycled cement.

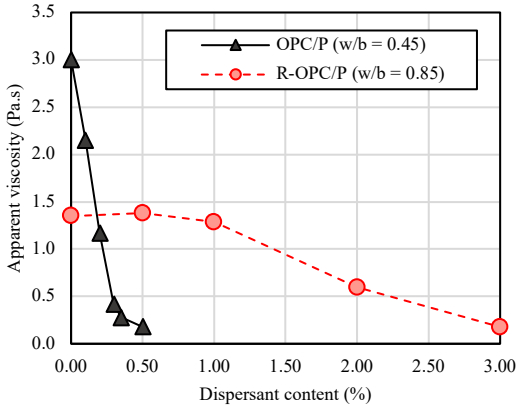

3.2.2.2 Water demand for a set rheological behavior

Subsequently, the reduction in water demand of each cement type with the optimal dispersant content fixed was investigated by rotational rheometry (Figure 36). The w/b reduction promoted viscosity and yield stress increase for all pastes, as it reduced the interparticle distance (IPS) between the grains, increasing their friction (DAMINELI et al., 2016a). The recycled cement pastes had lower apparent viscosities and yield stresses.

Figure 36 - Apparent viscotiy (a) and yield stress (b) of cement pastes in fuction of w/b ratio.

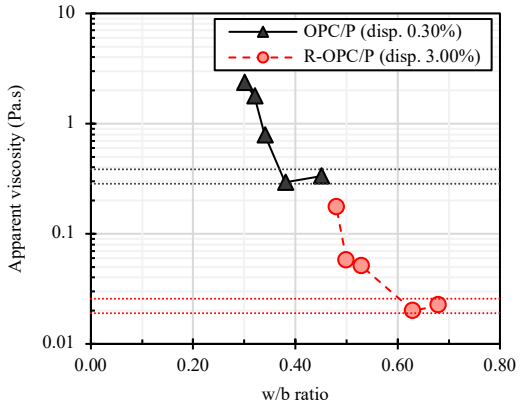

The minimum water/binder ratio chosen were 0.38 and 0.63 for OPC/P and R-OPC/P, respectively. The yield stress tended to zero. The recycled cement paste achieved a higher w/b reduction (25.9% vs 15.5% of OPC) and lower viscosity increase than ordinary cement pastes. Therefore, the reduction in water demand was more striking for recycled cement owing to agglomeration caused by elevated surface area.

3.2.3 Characterization of OPC/P and R-OPC/P

Figure 37a,b shows the TG/DTG results of the pastes without dispersant at 28 days. Figure 37c-e shows the pastes with dispersant at different ages.

Hydrated (OPC/P) and rehydrated (R-OPC/P) cement pastes presented similar peaks in DTG. The four prominent peaks are near 100, 150, 450 and 750 °C. The first two peaks indicate the presence of ettringite, C-S-H, C-A-H, and calcium monosulfoaluminates. The third and fourth peaks indicate the presence of portlandite and calcite, respectively.

Figure 37 - TG and DTG paste results: pastes without (a,b) and with dispersant pastes by dispersant (c-e).

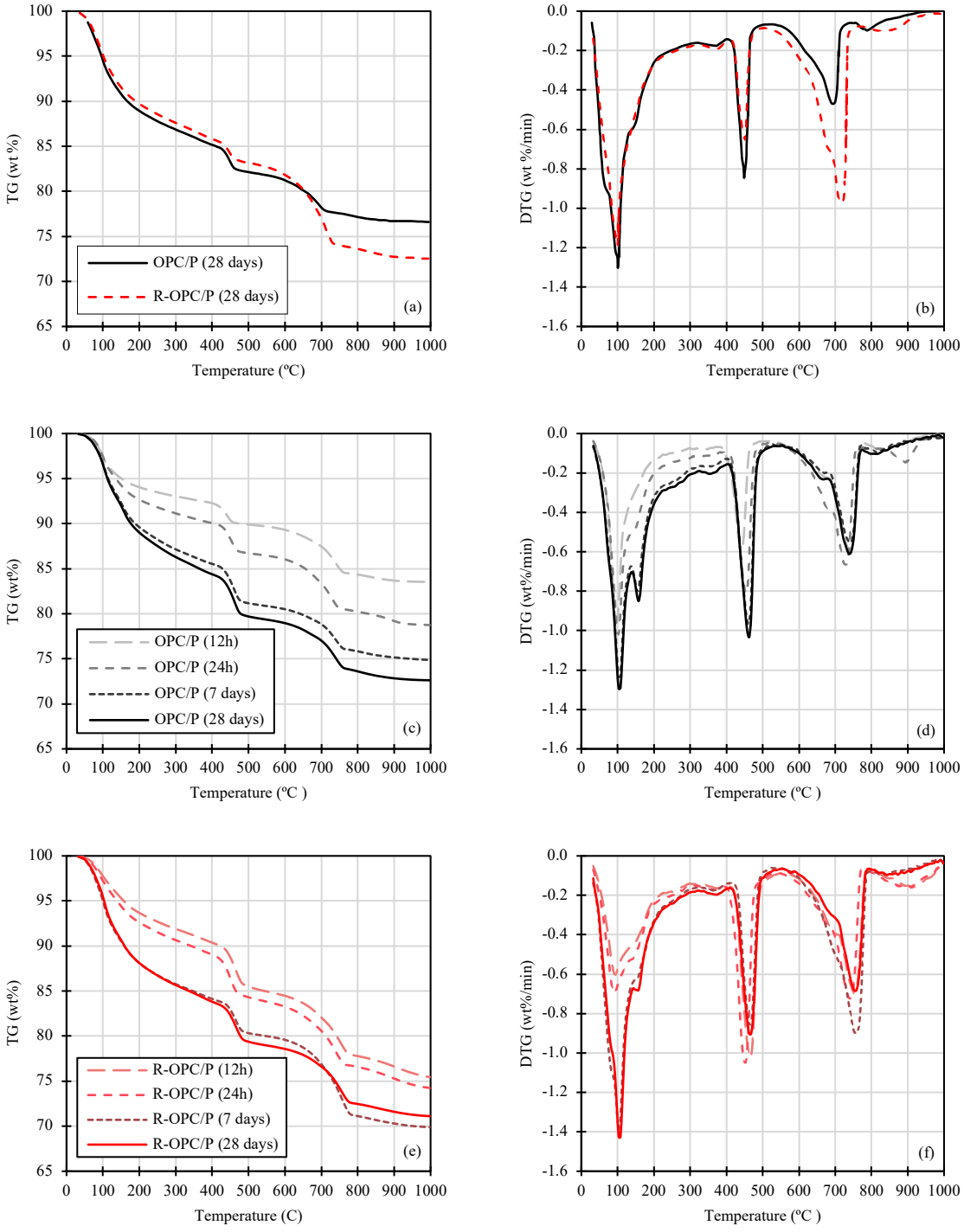

R-OPC reformed 65% of the hydrated compounds (C-S-H, C-S-A-H, and hydrotalcite) in the first 12 hours. The reformation of hydrated compounds was close to 80% at 7 and 28 days (Table 19). As expected, no differences were found in the reformation of hydrated compounds due to the use of paste dispersants after 28-day of age.

Table 19 - Mass losses of pastes for TG/DTG temperature ranges.

Paste	Scenario	Age (days)	Mass loss (%)					Wn (g/g)
			W25 - W330[a]	W330 - W430[b]	W430 - W550[c]	W550 - W1000[d]	LOI	
OPC/P	noSP	28	13.68	1.75	2.79	5.18	23.40	0.208
OPC/P	SP	0.5	7.19	1.30	1.82	6.16	16.48	0.114
OPC/P	SP	1	9.21	1.25	3.10	7.70	21.26	0.156
OPC/P	SP	7	13.37	1.70	4.08	5.99	25.14	0.235
OPC/P	SP	28	14.31	1.99	4.36	6.73	27.39	0.259
R-OPC/P	noSP	28	12.93	1.94	2.41	10.18	27.46	0.155
R-OPC/P	SP	0.5	8.54	1.63	4.89	9.50	24.55	0.079
R-OPC/P	SP	1	9.80	2.04	4.33	9.58	25.76	0.095
R-OPC/P	SP	7	14.72	1.58	3.71	10.10	30.10	0.151
R-OPC/P	SP	28	14.88	1.87	4.29	7.85	28.89	0.167

(a) Dehydroxilation of Aft, C-S-H, C-A-H, AFm

(b) Dehydroxilation of hydrotalcite

(c) Dehydroxilation of portlandite (CH)

(d) Decarbonation of calcite ($CaCO_3$)

The literature data range from 0.117 to 0.135 g/g of combined water for 28-day recycled cement pastes with precursor materials and dehydration processes similar to this work. The combined water in R-OPC/P with dispersant at 28 days was 0.167g/g.

3.2.4 Strength-porosity correlation

3.2.4.1 Compressive strength vs Total porosity

Figure 38 shows a single trend for strength-porosity correlation, regardless of the cement type (ordinary, blended or recycled). Therefore, the mechanical properties of recycled cement pastes can be optimized by reducing their porosity.

The recycled cement pastes produced in this study had one of the lowest porosity values reported in the literature. Water demand reduction through superplasticizer use and rheological analysis successfully reduced free water (water demand) and porosity in recycled cement. The total porosity was reduced by 15%. The compressive strength was increased by 2.5 times. However, the recycled cement paste with superplasticizer was only approximately 15 MPa at 28 days. Therefore, recycled cement has limitations when used as a solo binder.

The recycled cement pastes showed the same range of values, showing that the factor that governs the high water demand of the recycled cement is the high specific surface area arising from the dehydration process (BALDUSCO et al., 2019; SHUI et al., 2009). The high specific surface area required more water to fill grain pores to cover and spread (by a water layer) during the fluid state. Therefore, the optimization of recycled cement depends on controlling water demand.

Figure 38 - Correlation between Powers' total porosity vs compressive strength of paste with the cylindrical shape of 27x54 mm. The data used are from pastes between 12h and 180 days old.

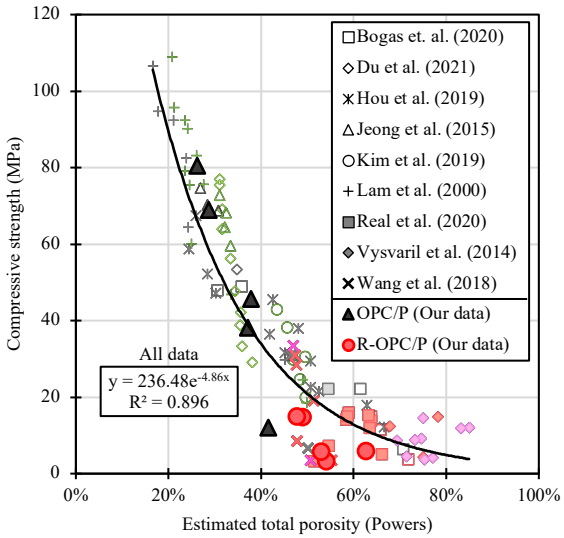

Literature data from nine sources (BOGAS; CARRIÇO; TENZA-ABRIL, 2020; DU et al., 2021; HOU et al., 2019; JEONG et al., 2015; KIM et al., 2019; LAM; WONG; POON, 2000; REAL et al., 2020; VYŠVAŘIL et al., 2014; WANG; MU; LIU, 2018) and our experimental data were used. Gray, green, red, and pink represent OPC/P, BC/P, R-OPC/P and R-BC/P, respectively.

All data were used in the analysis, including experimental and literature data. Data from ten references were used to assess the relationship between the total porosity and compressive strength of ordinary, blended and recycled Portland cement pastes. A total of 106 data points were used, and 4 outliers were removed. For more details, see Supplementary Data.

For the literature data, the pastes were divided into four categories. Pastes made from anhydrous cement are ordinary Portland cement paste (OPC/P) or blended Portland cement paste (BC/P). Blended cement is cement with an SCM content. Rehydrated pastes are recycled ordinary Portland cement paste (R-OPC/P) or recycled blended Portland cement paste (R-BC/P). R-BC/P can be: (i) an R-OPC blended with SCM and rehydrated or (ii) a BC/P that was dehydrated and rehydrated.

For experimental data with low ages, it is possible to observe a high strength gain for a small porosity variation. We understand that this is associated with microstructure consolidation over time. For ages of 12 h or 24 h, the microstructure contained a high free water content and millimeter-order pore structure.

3.2.4.2 Combined water fraction (cwf)

Table 20 presented the water/binder ratio (w/b), dispersant/superplasticizer (SP) content, non-evaporable water (w_n), combined water fraction (*cwf*), total porosity estimated by the Powers model (P) and average compressive strength of the pastes (f_{paste}) for study's

experimental data from this work.

Table 20 - Experimental and estimated data of ordinary and recycled cement pastes produced in this work.

Name	w/b	SP (wt%)	Age	w_n (g/g)	*cwf* (g/g)	P (%)	f_{paste} (MPa)
OPC/P	0.45	-	28 days	0.208	0.46	37.8	45.7
OPC/P	0.38	0.3	12h	0.114	0.30	41.6	12.1
OPC/P	0.38	0.3	24h	0.156	0.41	37.2	38.1
OPC/P	0.38	0.3	7 days	0.235	0.62	28.7	68.9
OPC/P	0.38	0.3	28 days	0.259	0.68	26.2	80.6
R-OPC/P	0.85	-	28 days	0.107	0.13	62.7	5.9
R-OPC/P	0.63	3.0	12h	0.079	0.13	54.1	3.2
R-OPC/P	0.63	3.0	24h	0.095	0.15	53.0	5.8
R-OPC/P	0.63	3.0	7 days	0.151	0.24	49.0	14.7
R-OPC/P	0.63	3.0	28 days	0.167	0.27	47.8	14.9

Figure 39a presented the relationship between the mixing water (water demand for a set rheological condition) and the combined water; both parameters are used to calculate the *cwf* index. Recycled cement showed a high water recombination capacity. R-OPC/P and R-BC/P presented similar or higher combined water contents than blended cement with SCMs such as slag, limestone filler, or metakaolin. For the experimental data, recycled cement combined 35-49% less than OPC, probably owing to the high reactivity when exposed to atmospheric humidity.

Moreover, recycled cement pastes showed a high water demand compared to hydrated pastes of the same consistency as reported in the literature (SHUI et al., 2008, 2009; CARRIÇO; BOGAS; GUEDES, 2020). The data show R-OPC demands significantly more water and dispersant than OPC and BC to produce a workable paste, partially eroding the benefits of its relatively high-bound water content.

Figure 39b shows the correlation between *cwf* and compressive strength for this experimental work and literature data. In total, 54 data points were used. The experimental data of this work showed a high linear fit owing to the standard methods it employed (e.g., TG/DTG process and hydration stop process).

Literature data indicate that BC/P and OPC/P *cwf* results are mostly between 0.30 and 0.60. Meanwhile, *cwf* results for R-OPC/P and R-BC/P range are 0.10 to 0.30. These values

indicate a low binder efficiency of recycled cement owing to its high water demand. This observation reinforces a limitation of using recycled cement as the sole binder.

R-OPC/P with SP presented a *cwf* of 0.27 g/g at 28 days, the highest binder efficiency of recycled cement in the literature. Evidence shows that reducing the mixing water was well developed and effective compared to recycled cement pastes in the literature.

The combined water fraction of recycled and ordinary cement showed a similar trend, reinforcing the unique relationship between porosity and strength. The combined water fraction (*cwf*) index applies to recycled cement.

The relationship between *cwf* and compressive strength presented a slope similar to that reported by (ABRÃO; CARDOSO; JOHN, 2020). The trend is different because Abrão et al. (2020) developed a correlation based on mortars (50x100 mm), whereas this study used pastes (27x54 mm). Check the database in Supplementary Data.

Figure 39 - Mixing water vs. combined water (a), the two variables that generate *cwf*. Combined water fraction (*cwf*) vs. compressive strength of pastes in cylindrical shape of 27x54 mm (b).

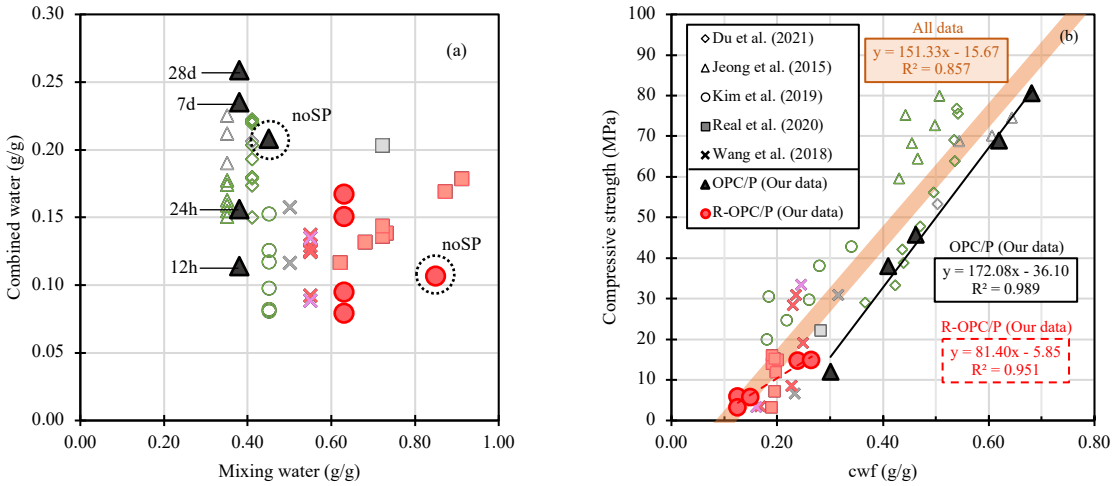

Literature data from nine sources (BOGAS; CARRIÇO; TENZA-ABRIL, 2020; DU et al., 2021; HOU et al., 2019; JEONG et al., 2015; KIM et al., 2019; LAM; WONG; POON, 2000; REAL et al., 2020; VYŠVAŘIL et al., 2014; WANG; MU; LIU, 2018) and our experimental data were used. Gray, green, red, and pink represent OPC/P, BC/P, R-OPC/P and R-BC/P, respectively. There are four icons for OPC/P and R-OPC/P pastes with dispersant of this work, corresponding to 12h, 24h, 7, and 28 days of hydration. The data used are from pastes between 12h and 180 days old.

3.2.5 Environmental analysis

The potential CO_2 emissions for recycled cement dehydrated at 500 and 750°C (below and above decarbonation) were compared to OPC. The values were obtained from the database (our data and (WANG; MU; LIU, 2018)) using the equations described in Section 2.4.3.

The OPC was considered 90% clinker (BRAZILIAN ASSOCIATION OF TECHNICAL STANDARDS, 2018). Its emission was estimated as 846 $kgCO_2$/ton of binder. Recycled cement produced at 750 °C showed an estimated total emission of 335 $kgCO_2$/ton of binder, representing a 60% reduction in OPC emissions. Emissions from decarbonation were very low, approximately 15% of total emissions (51 $kgCO_2$/ton of binder). The cement recycled at 500 °C showed a total emission of 184 $kgCO_2$/ton of binder, saving 662 $kgCO_2$/ton of binder, a 78% reduction in OPC emissions.

Figure 40a shows the compressive strength and total CO_2 emission relation for 300 dm^3 of paste at 28 days old; both parameters are used to calculate the CO_2 intensity index. The recycled cement pastes had the lowest CO_2 emissions and strength, with values between 38-116 $kgCO_2.m^{-3}$ and 4-31 MPa, respectively. The dehydration temperature of the paste used for recycled cement production is a relevant environmental factor. If the dehydration temperature is above 550 °C, decarbonation occurs, which increases the emissions of the final material. Pastes with recycled cement produced below the decarbonation temperature (400-550 °C) presented an average emission of 49 $kgCO_2.m^{-3}$ against 86 $kgCO_2.m^{-3}$ of other recycled cement pastes. The average compressive strength was roughly the same for all recycled cement pastes. The dehydration temperature had no clear influence on it. The OPC/P and BC/P results corroborate the literature (DAMINELI et al., 2010). For the recycled Portland cement paste used in this study (R-OPC), 25% of CO_2 emissions were associated with dispersant (17 of 69 $kgCO_2.m^{-3}$). Therefore, dispersant demand is relevant in environmental analysis. For further details, see Supplementary Data.

Figure 40b presents the relationship between the compressive strength and CO_2 intensity index for 300 dm^3 of paste with 28-day-old. The CO_2 index shows that despite the low environmental impact of recycled cement, its low strength makes the environmental efficiency of R-OPC similar to that of conventional binders (OPC and BC). The OPC/P and BC/P results corroborate the literature (DAMINELI et al., 2010; SCRIVENER; JOHN; GARTNER, 2018). The experimental data were 4.48 and 4.65 $kgCO_2.m^{-3}.MPa^{-1}$ for OPC/P and R-OPC/P, respectively, with superplasticizer at 28 days. For experimental pastes without dispersant, the CO_2 indices were 7.15 and 7.49 $kgCO_2.m^{-3}.MPa^{-1}$ for OPC/P and R-OPC/P, respectively. R-OPC presented a similar environmentally efficient to OPC for both scenarios (with and without SP). In contrast, R-OPC/P had a compressive strength of 5-8 times lower than that of OPC/P. Wang et al. (2018) obtained the best recycled cement performance with R-BC dehydrated at 450 °C and with the addition of 30% granulated blast furnace slag, 0.98 $kgCO_2.m^{-3}.MPa^{-1}$ and 33 MPa (WANG; MU; LIU, 2018).

Figure 40 - Compressive strength of paste (27x54 mm) vs. CO_2 emissions for 300 dm^3 of paste (a), both CO_2 intensity index components. Compressive strength of paste (27x54 mm) vs. CO_2 intensity index for 300 dm^3 of paste (b).

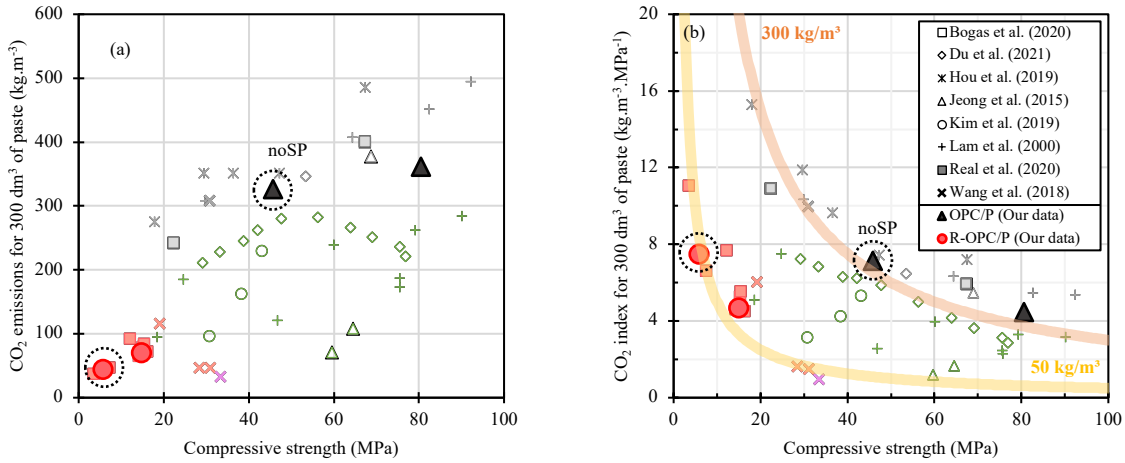

Literature data from nine sources (BOGAS; CARRIÇO; TENZA-ABRIL, 2020; DU et al., 2021; HOU et al., 2019; JEONG et al., 2015; KIM et al., 2019; LAM; WONG; POON, 2000; REAL et al., 2020; VYŠVAŘIL et al., 2014; WANG; MU; LIU, 2018) and our experimental data were used. Gray, green, red, and pink represent OPC/P, BC/P, R-OPC/P and R-BC/P, respectively. Only 28-day pastes were used for this analysis.

3.3 Conclusion

This study presents the porosity-strength relationship, binder efficiency (*cwf*), and CO_2 intensity index for recycled cement (dehydrated at 500 °C) pastes. Pastes with similar rheological conditions and decreasing water content were prepared using dispersants. Data from the literature complemented the analyses. The following conclusions were drawn:

- The total porosity-compressive strength relationship presented a single trend for both hydrated and rehydrated pastes. Therefore, reducing porosity by minimizing mixing water content using dispersant use for a set rheological condition can improve the mechanical performance of recycled cement paste.

- The R-OPC/P after the water demand reduction process presented a *cwf* of 0.27 g/g at 28 days, the highest binder efficiency of recycled cement in the literature. The total porosity was reduced by 15%. The compressive strength was increased by 2.5 times. However, R-OPC/P was near 15 MPa after 28 days. Therefore, recycled cement has limitations when used as a solo binder.

- The cement recycled at 500 °C showed a total binder emission of 184 $kgCO_2$/ton of binder, a 78% reduction in OPC emissions. The recycled cement pastes exhibited the lowest CO_2 emissions and strength values. These low values make the R-OPC environmental efficiency similar to conventional binders (OPC and BC). CO_2 indices were 4.48 and 4.65 $kgCO_2.m^{-3}.MPa^{-1}$ for OPC/C (SP) and R-OPC/C (SP) at 28 days, respectively.

4 ENGINEERED RECYCLED PORTLAND CEMENT SYSTEMS

This chapter investigates recycled cement (thermoactivated at 500°C) in combination with limestone filler and a reduced quantity of finely grounded Portland Clinker to produce low-CO_2 high-initial strength engineered blended cements. The voids in the granular packing system were reduced using a reverse filling approach. The blended composition and dispersant use influence on water demand and compressive strength of pastes were analyzed. Environmental analysis was assessed by CO_2 emissions per ton of binder.

This chapter will be refined to become a publication and no patent was found with the main concepts presented: (i) heat treatment of hydrated cementitious waste and (ii) use of R-PC as SCM. Therefore, this chapter presents engineered cementitious materials with patent potential.

Figure 41 presents the experimental flow chart of this chapter.

Figure 41 - Flow chart of the experimental program of Chapter 4.

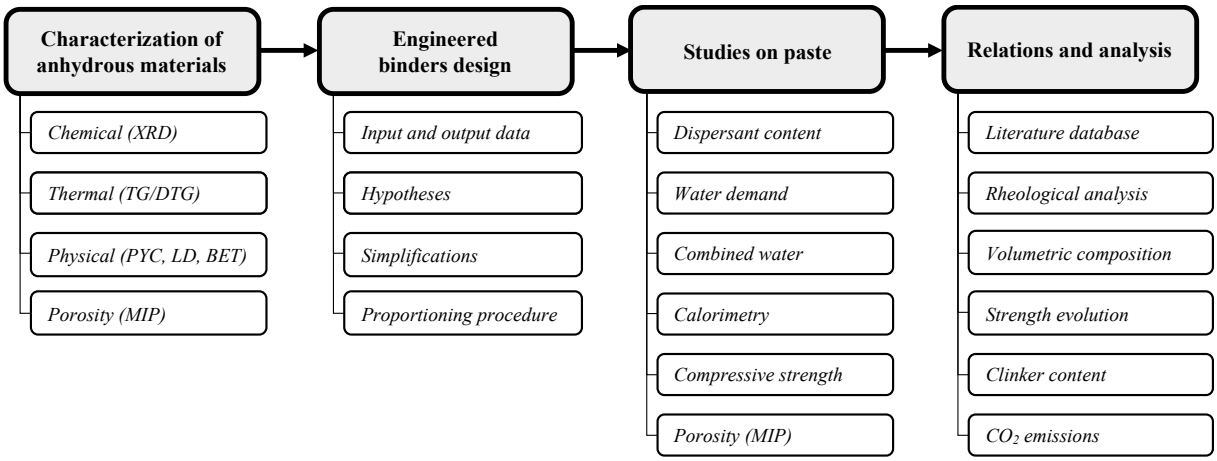

4.1 Experimental design, materials, and methods

4.1.1 Engineered cements

4.1.1.1 Material selection and characterization

The purest clinker Portland cement commercially available in Brazil (90% g/g of clinker and calcium sulfate partially hydrated) was used. It is the high-initial strength cement in the Brazilian market (CPV type). By Brazilian standards (BRAZILIAN ASSOCIATION OF TECHNICAL STANDARDS, 2018), the minimum compressive strength required at 1, 3, and 7 days are 14, 24, and 34 MPa, respectively. For this work, we named as high-initial strength

cement (HIS-C).

The HIS-C was hydrated with a water-to-solids ratio of 0.45. The cement paste was cured in a controlled room at 23±2°C and relative humidity above 95%. After 90 days of curing, the hardened cement paste was oven-dried for 24 hours at 50 °C to facilitate crushing and grinding. This drying temperature avoids ettringite decomposition in the hydrated cement paste. The hardened cement paste was crushed in a jaw crusher, resulting in a material with a particle size of less than 1.18 mm. Then it was grounded in a bar mill until pass through a 150-μm sieve. The sieved powders of hydrated cement paste were calcined in a furnace using a rate of 10 °C/min from room temperature to 500 °C and kept at this temperature patamar for two hours. This calcination temperature achieves the highest mechanical strength without decarbonation of the material; so, no CO_2 emissions from the raw materials in the manufacture. The dehydrated powder was cooled outside the furnace until room temperature. Therefore, recycled ordinary Portland cement (R-PC) was obtained.

A finely-ground (micronized) Portland cement with smaller granulometry than that of HIS-C was used to produce the engineered cements. It was produced by Holcim Brazil and named herein as Micro Portland Cement (MPC).

Two limestone fillers were used: (i) a thinner filler than HIS-C called as micro limestone filler (MLF), and (ii) a filler with granulometry similar of that of HIS-C called as ordinary limestone filler (OLF). All powders were then characterized by density, surface area, particle size distribution, thermogravimetry, quantitative X-ray diffraction and porosimetry.

A helium gas pycnometer (Accupyc 1340, Micromeritics) was used to determine the density. The specific surface area was measured by nitrogen gas intrusion and data processing by the BET method.

The particle size distribution was quantified using a laser granulometer (Helos KR, Sympatec), analysis range between 0.1 and 350 μm. The sample was dispersed in deionized water using a mixer (RW20, IKA) at a constant speed of 1000 rpm/min before being added to the granulometer.

Crystalline phases were identified by the XRD assay (PW 1830, Philips). The samples were ground, sieved to 0.075 mm and pressed into aluminum support. The operating conditions were CuKα radiation (40kV/40mA), 1° divergent slit, 1° scattering slit, 0.02° 2θ angular pitch, 2°/min, 5° to 65.90° sweep and 2,000 counts/s. The compounds quantification by Rietveld method used the Panalytical X-Pert HighScore Plus software (version 4.9) and the COD (Crystallography Open Database). See Supplementary material, Table C1.

Pore size distribution of R-PC was obtained using mercury intrusion porosimetry. The

other powders are non-porous and do not require this test method. The equipment used was an Auto Pore III (Micromeritics) with an intrusion and extrusion cycle, from low pressure (0.5-30 psia) to high pressure (30 to 60,000 psia). See Supplementary material, Figure C1.

Thermogravimetry was performed by TG 209 F1 Libra, Netzsch. The samples were placed in an 85 μL alumina crucible, without a lid. Gas flow was 20 mL/min of ultra-pure nitrogen with a constant heating rate of 10 °C/min up to 1000 °C. See Supplementary material, Figure C2.

4.1.1.2 Mix proportion design

The engineered cements (EC) were designed to fill the porosity of the R-PC paste and increase the packing density using Portland cement and limestone fillers with different particle size distributions. Our mix design goal was to achieve a final paste with a total porosity comparable to that of HIS-C paste with 0.45 g/g water.

Supplementary material B outlines the steps for determining the initial mix design proportions of engineered cements. First, we estimated the volumetric composition and porosity of the HIS-C paste with 0.45g/g of water using simplified Powers equations (BROUWERS, 2004; T. C. POWERS AND T. L. BROWNYARD, 1946). Second, we used the R-PC to estimate its granular volumetric composition by identifying the minimum amount of water required for paste formation, further discussed in items 4.2.1.1 and 4.2.2.1. Third, we determined the porosity of the R-PC paste by Powers concepts and our assumptions. Finally, we optimized the hypothetical R-PC paste based on the specified scenario.

The mix design used the concept of reverse filling (ZHENG et al., 2020) (cement is the finest fraction and used to occupy the lowest voids volume from the granular packing) and it was formulated considering three scenarios (*Mix design concepts illustration*): (i) combined use of R-PC and MPC, with the MPC content defined through the volume of hydrated solids required to cover the excess porosity of the R-PC paste to meet the objective (a total porosity comparable to that of HIS-C paste with 0.45 g/g water); (ii) addition of MLF to the first scenario to fill granular voids, reducing the water demand and the demand for volume occupied by Portland cement (clinker); and (iii) using OLF, R-PC and MPC respectively to promote granular packing and reduce the surface area of the engineered cements, consequently, reduce quantity of voids, size of voids, water demand and increase the hydration degree and the ability of volume filling over time of the system.

Table 21 presents the final composition of HIS-C, R-PC and engineered cement pastes for a standard consistency. The procedures and values for water-to-solids ratio (w/s) and

dispersant content (SP) are discussed and presented further, items 4.1.2.1 and 4.2.2.1.

Table 21 - Composition of experimental pastes.

Pastes	HIS-C	R-PC	MPC	MLF	OLF	w/s	SP (%)
HIS-C/P	100%					0.48	0.10
R-PC/P		100%				0.56	1.00
R80-C20/P		80%	20%			0.48	1.00
R75-C10/P		75%	10%	15%		0.43	1.00
R35-C15/P		35%	15%		50%	0.36	0.60

Pastes were referred to as the name of the binder followed by the suffix "/P". The nomenclature for engineered cements adhered to this pattern: "R" signifying recycled cement (R-PC), followed by its mass percentage, and "C" representing micronized cement (MPC), followed by its respective mass percentage.

4.1.2 Engineered cement pastes

4.1.2.1 Water demand and Rheological analysis

Initially, the lowest water/solids ratio possible to obtain a paste (turning point (WONG; KWAN, 2008; KWAN; LI, 2014; CHU et al., 2021; DE LARRARD, 1999)) was experimentally determined for HIS-C, R-PC and the engineered binders. The procedure consisted of water gradual addition to the binder composition (100 g) until mixing was possible; a paste (suspension) needs to be formed. A mixer RW 20 (IKA) was used under a constant shear rate of 1000 rpm. The higher solids concentration makes the suspension dispersion harder as the distance between particles (IPS) becomes smaller; scenarios that require superplasticizer (SP) addition.

For the determination of dispersant saturation content, a continuous flux rheometer was used to determine viscosity of cementitious suspension (DAMINELI, 2013; DAMINELI et al., 2016b; DAMINELI; JOHN; PILEGGI, 2023; RUSSELL, 2012; TEIXEIRA et al., 2014). The rheometer used was a Thermo Haake, with parallel plate geometry, with a diameter of 40 mm and spacing between plates of 1 mm. A polycarboxylate-based superplasticizer (ADVA CAST 527, GCP) with a density of 1.075 g/cm³ was used. The SP content increased as a function of each mixture. The sequence of paste preparation was: (i) add SP to the water, (ii) add the water plus SP into the binder, (iii) homogenize the mixture with a spatula for 120 s and (iv) mix the paste in the stirrer at 1000 rpm for 120 s. With the mixture carried out, it took approximately

180 s to place the paste in the rheometer. The paste shear rate was accelerated from 0 to $50s^{-1}$ with a constant rate for a minute, then decelerated with the same rate. The cycle was repeated, as the measurements of the first cycle may be influenced by agglomeration (MACIEL, 2017). The second cycle data were used for analysis.

The dispersant saturation content was determined by varying the superplasticizer content in pastes with the water/solid ratio determined before. Therefore, the selected dispersant content corresponds to the smallest amount of superplasticizer needed to obtain the lowest viscosity at $50s^{-1}$ without segregation. A relative percentage error of 10% was defined as a confidence interval for the viscosity values.

Finally, the minimum water content for a fully dispersed paste with a mini-slump of 100 ± 10 mm was determined. For this, pastes with the dispersant saturation content fixed and decreasing water content were produced until the desired spread was obtained.

For HIS-C, a water/solid ratio of 0.48 was used, as recommended to classify the cement compressive strength class by the Brazilian cement standard (BRAZILIAN ASSOCIATION OF TECHNICAL STANDARDS, 2019) – and similar of that adopted in other countries; (AMERICAN SOCIETY FOR TESTING AND MATERIALS, 2002) (0.485) and (EUROPEAN STANDARDS, 2005) (0.50). The dispersant content was determined to ensure the same consistency of other pastes.

All the final pastes had their rheological behavior assessed by shear stress and apparent viscosity over shear rate.

4.1.2.2 Kinetics and Reactivity

4.1.2.2.1 Isothermal calorimetry (IC)

The heat flux and total heat released by each paste over time were measured using an isothermal calorimeter (TAM Air - 8 channel, TA Instruments). The process of mixing, placing the paste, and starting data acquisition took less than four minutes. The measurement was conducted for a period of 72 hours, with data collected at a frequency of 16 seconds.

4.1.2.2.2 Thermogravimetric analysis (TG/DTG)

Thermogravimetric analysis was used to quantify the chemically bound water. For all pastes, hydration stoppage was made by solvent exchange by isopropyl alcohol (SNELLINGS et al., 2018). Then, the pastes were kept in a vacuum desiccator over silica gel and soda lime to mitigate carbonation. All pastes were ground below 0.045 mm. The age of analysis was at 6 and 12 hours, as well as at 1, 7, and 28 days.

The effective chemically combined water content of all pastes (w_n) was calculated based on (DE WEERDT et al., 2011) with a proportional mass correction associated with the remaining combined water of the anhydrous material (powder) (Equation 29). This correction is needed because the combined water in the powder (cement or filler) does not contribute to the reactivity and strength evolution of the (re)hydrated paste.

$$w_n = \left(\frac{W_{40} - W_{550}}{W_{550}}\right)_{Paste} - \sum_{i=1}^{n} M_i \cdot \left(\frac{W_{40} - W_{550}}{W_{550}}\right)_{Powder} \quad \text{Equation 29}$$

Where Wx corresponds to the percentage of mass lost at temperature X in °C.

M is the mass percentage of the powder (cement or filler) to the final binder. For pastes with only one binder, the value is 1.

4.1.2.3 Phases' volumetric composition and porosity over time

4.1.2.3.1 Quantitative X-ray diffractometry (QXRD)

Quantitative X-ray diffraction was used to analyze the phases' content and behavior over time (1, 7 and 28 days) for each experimental paste. The QXRD tests were conducted under standardized conditions for both powders and pastes. The hydration stoppage was also made by solvent exchange by isopropyl alcohol (SNELLINGS et al., 2018).

The Rietveld method was used to quantify the compounds using the Panalytical X-Pert HighScore Plus software (version 4.9) and the Crystallography Open Database (COD) (see Table B1). Portlandite content defined by TG was used as an external standard to quantify the amorphous phases. The refinement procedure followed the steps outlined in (ANGULO et al., 2022).

The volumetric composition of the experimental pastes was accessed by (i) converting the QXRD mass percentage values through the density of the phases (Table B2) and (ii) adjusting the total volume of paste based on the MIP porosity results per age. For the initial porosity of each engineered cement, the MIP porosity of the R-PC grain and the water demand were used. The density of amorphous was adopted as C-S-H tobermorite. Chemical shrinkage was not assessed.

4.1.2.3.2 Mercury intrusion porosimetry (MIP)

The porosity values and pore size distribution of each paste at 1, 7 and 28 days were determined by MIP analysis through AutoPore III, Micromeritics. After curing in a wet chamber, the pastes samples (27 x 54 mm) were wet cut into 2mm slices using a 0.4mm thick

diamond disc saw (Struers, Miniton).

The slices were immersed in isopropanol for 4 days for hydration stoppage. The volume of isopropanol should be 50 to 100 times that of the sample slice. During this period, the solvent was changed after 24h and 48h. After 48 hours of the last exchange, the slices were dried in a desiccator under a vacuum, with silica gel, for another 48 hours (ZANCHETTA, 2021).

Samples were inserted into the penetrometer and placed in a low-pressure chamber evacuated to a 50 mmHg pressure. The penetrometer was filled with mercury while the pressure was increased up to 0.55 MPa. After that, the penetrometer was moved to the high-pressure chamber. The pore size distribution was estimated by Washburn's equation. We used the surface tension of mercury equal to 0.485 N/m at 25°C (SCRIVENER; SNELLINGS; LOTHENBACH, 2018) and a contact angle of 140° (COOK; HOVER, 1991).

4.1.2.4 Compressive strength and performance indices analysis

4.1.2.4.1 Compressive strength

Fresh pastes were cast into cylindrical molds of reduced dimension (diameter x height): 27x54 mm. Six specimens were molded for each age of interest (6h, 12h, 1, 7 and 28 days). A vibrating table was used for 30 s to ensure proper compaction. The specimens were cured in a controlled room at a temperature of 23±2°C and relative humidity above 95%.

At the age of interest, the specimens were demolded to measure compressive strength. The compressive strength test was performed with a press (DL 10000, EMIC), capacity of 100 kN, resolution of 0.001 kN and loading speed of 0.25 MPa/s.

4.1.2.4.2 CO_2 emissions

The calculation of CO2 emissions for the studied binders are described below. Equation 30 evaluates each binder's environmental impact. CO_2 emissions resulting from crushing and grinding processes were excluded.

$$CO_{2_{binder}} = \sum_{i=1}^{n} M_i \cdot CO_{2\ cement} + \sum_{j=1}^{n} M_j \cdot CO_{2\ SCM} \qquad \text{Equation 30}$$

Where $CO_{2\ binder}$ is the CO_2 emission to obtain one ton of the studied binder; $CO_{2\ cement}$ is the CO_2 emissions associated with HIS-C, MPC and R-PC; $CO_{2\ SCM}$ is the CO_2 emissions from supplementary cementitious material. These parameters unit is CO_2 emission per ton of analyzed powder. M is the mass percentage of the powder to the final binder.

The $CO_{2\ cement}$ used was determined using the method proposed by (QUATTRONE;

ANGULO; JOHN, 2014) and followed the assumptions and values highlighted in (ZANOVELLO et al., 2023). Therefore, HIS-C and R-PC have 846 and 184 $kgCO_2$/ton of cement, respectively.

The $CO_{2\ SCM}$ emissions associated with limestone filler, fly ash, granular blast furnace slag, and calcined clay were 8, 42, 89, and 270 $kgCO_2$/ton of SCM, respectively. The emissions used followed the weight values presented by (MILLER et al., 2018).

4.1.2.4.3 Literature database

Literature data were used to compare engineered cements with blended cements containing conventional supplementary cementitious materials (SCMs). The database comprises six types of cement with different replacement levels (11-50%). These papers were selected because they established a standard consistency and employed a methodology similar to ours to determine dispersant saturation content and the minimum water/binder ratio (ABRÃO et al., 2020; ABRÃO; CARDOSO; JOHN, 2020).

4.2 Results and discussions

4.2.1 Engineered cements

4.2.1.1 Materials characterization

R-PC presented lower density than anhydrous cement (HIS-C and MPC) since it is not constituted by clinker phases but by a complex system of partial and total dehydrated cement phases (ANGULO et al., 2022; BOGAS; CARRIÇO; TENZA-ABRIL, 2020; SERPELL; LOPEZ, 2015). R-PC has a particle size distribution of 3 times greater than HIS-C, while the MPC presents a granulometric profile of 10 times smaller than the HIS-C (Figure 42a). OLF and HIS-C have similar grain sizes. The specific surface area (SSA) via BET for R-PC was 7 and 18 times greater than MPC and HIS-C (Table 22), respectively. The elevated SSA is constantly reported in the literature (BOGAS; CARRIÇO; TENZA-ABRIL, 2020; ZANOVELLO et al., 2023) due to the dehydration process, which promotes intrinsic porosity and morphological changes in the recycled cement grain. HIS-C and OLF have a spherical shape once shape factor is close to 1. MPC and MLF showed values similar to the literature (ABRÃO; CARDOSO; JOHN, 2020; ZANOVELLO et al., 2023). The shape factor of R-PC shows the complex morphology (with high surface area or internal pores) in the material.

Engineered cement formulations exhibit reduced BET-specific surface area (SSA_{BET}) and shape factor when replacing R-PC (Table 22). The particle size distributions of R80-C20 and R75-C10 are bimodal, while R35-C15 has a more unimodal profile (Figure 42b).

Figure 42 - Particle size distribution of the anhydrous materials (a) and engineered cements (b).

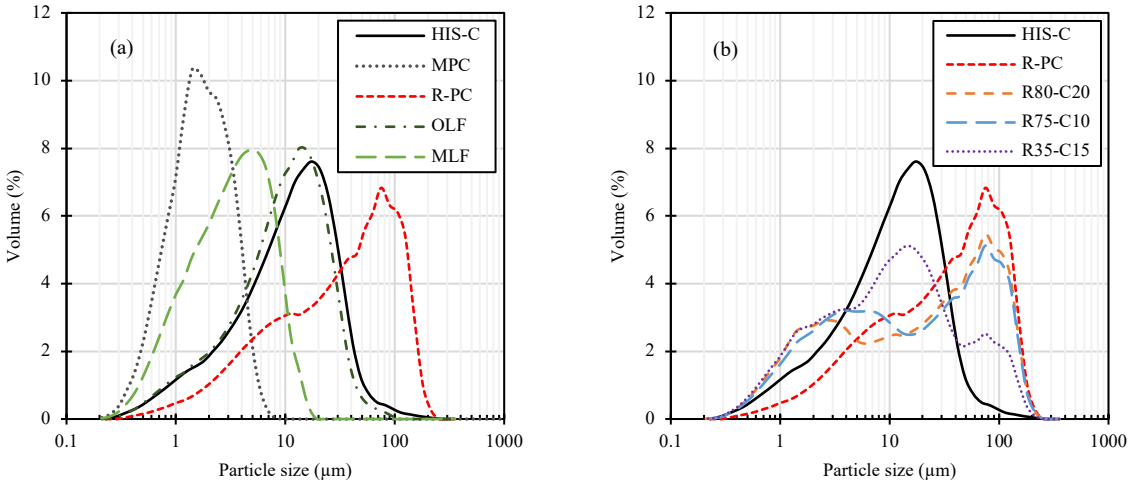

Table 22 - Physical properties of the used cements, fillers and engineered binders.

Parameters	HIS-C	R-PC	MPC	MLF	OLF	R80-C20	R75-C10	R35-C15
ρ (g/cm^3) [a]	3.05	2.65	2.92	2.82	2.79	2.70	2.70	2.76
D_{10} (µm) [b]	1.92	3.58	0.65	0.86	1.82	1.29	1.40	1.26
D_{50} (µm) [b]	10.96	31.67	1.54	3.03	9.48	18.91	15.34	9.80
D_{90} (µm) [b]	29.62	104.35	3.33	7.92	25.12	98.96	96.77	64.71
SSA_{BET} (m^2/g) [c]	1.55	21.64	4.01	3.15	1.02	18.11	17.10	8.69
SSA_{LD} (m^2/g) [d]	0.41	0.24	1.56	1.03	0.48	0.52	0.50	0.57
Shape factor [e]	3.79	91.17	2.57	3.06	2.15	34.61	33.88	15.29
VSA_{BET} (m^2/cm^3) [f]	4.7	57.3	11.7	8.9	2.8	48.9	46.2	24.0
Minimum w/s [g]	-	0.60	-	-	-	0.50	0.50	0.36
Packing density [h]	46.7%	38.6%	-	-	-	42.5%	42.5%	50.2%

[a] *Particle specific gravity from He pycnometer.*
[b] *D-Values obtained by Laser diffraction granulometry.*
[c] *Specific surface area obtained by BET method.*
[d] *Specific surface area obtained by Laser diffraction granulometry.*
[e] *Shape factor calculated from SSA_{BET} and SSA_{LD}.*
[f] *Volumetric surface area obtained by the SSA_{BET} and ρ.*
[g] *Minimum water/solids ratio to obtain a paste (turning point).*
[h] *Packing density estimated by the volume of turning point water and density of engineered binders.*

Minimum water demand (turning point) for paste production was determined for all binders containing R-PC, revealing a linear correlation with SSA_{BET} (results in Table 22). Additionally, the water-to-solids ratio at the turning point relates to the mixture's packing density. As expected, R-PC displays the lowest packing density due to its high SSA and internal porosity. R80-C20 and R75-C10 demonstrate similar turning point water values and packing density, indicating that the partial replacement of MPC with MLF maintains engineered binder properties. Notably, R35-C15 exhibits the highest packing density (surpassing HIS-C), attributed to a substantial filler replacement that enhances packing and reduces SSA.

The R-PC grain presented a total porosity accessible by MIP of 40% (Figure C1). The percentage by pore size was 37% with size > 100nm. R-PC grain mainly contains large capillary pores, with no gel pores. The critical diameter was 14000 nm (1.4 µm). Typically, intergranular pores are larger than capillary pores. Therefore, the addition of R-PC in a cementitious matrix can reduce pore size, despite its contribution to the initial increase in porosity.

4.2.2 Engineered cement pastes

4.2.2.1 Water demand and Rheological analysis

Figure 43 shows the deflocculation curves (apparent viscosity versus dispersant content) of R-PC paste (a) and engineered cement pastes (b). The water/solids ratio was the lowest possible to obtain a paste without dispersant, values presented in the graphic's legend.

After the dispersant saturation content definition, the final composition of the pastes could be defined. Table 21 presents the final composition of HIS-C/P, R-PC/P and engineered cement pastes for a standard consistency (100 ± 10 mm in mini-slump).

Engineered binders exhibited lower water demand compared to the R-PC. The water demand reduction was 14%, 23%, and 36% for R80-C20/P, R75-C10/P, and R35-C15/P, respectively. Remarkably, the water demand for engineered binders closely resembled that of conventional Portland cement.

Figure 43 - Deflocculation curves for recycled Portland cement (a) and engineered cement pastes (b).

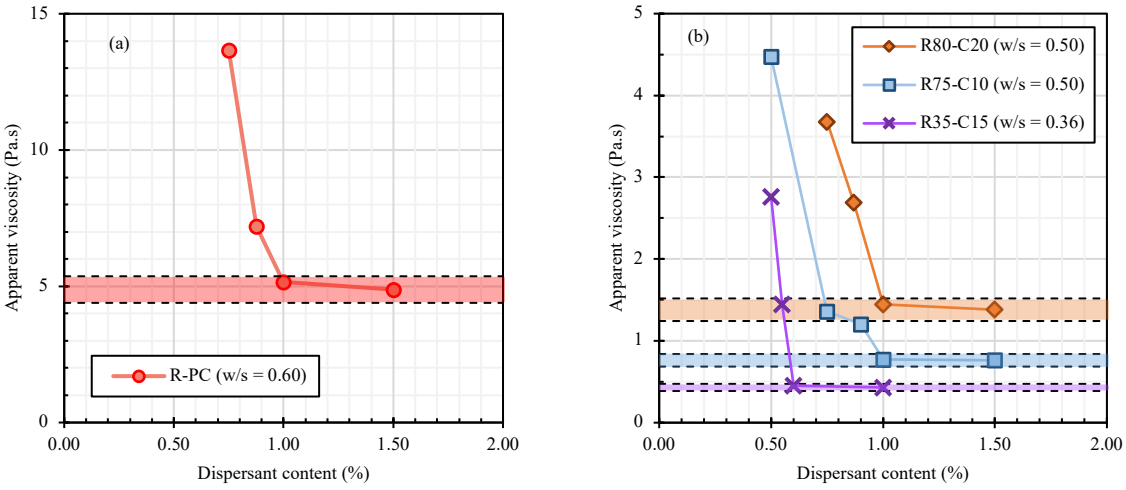

The dispersant saturation content was equal for R-PC, R80-C20/P and R75-C10/P. R35-C15/P showed a 40% reduction in dispersant content compared to the others. The dispersant demand for binders with R-PC was 10 times higher than for HIS-C. The high dispersant demand

for R-PC-based binders has raised financial concerns that can make those binders economically unfeasible. On the other hand, the absolute amount of dispersant was reduced by 3 times compared to previous studies (ZANOVELLO et al., 2023).

Flatt and coauthors (FLATT et al., 2023) emphasized a vision for future binders characterized by reduced clinker content, greater utilization of SCMs, a higher specific surface area (SSA), and an increased solids fraction. This future outlook aligns with the composition of R-PC-based binders. Moreover, Flatt and his colleagues anticipate that the demand for better dispersion, driven by the characteristics of future binders, will lead to the development of more efficient and cost-effective dispersants.

The water demand for binders containing R-PC had a high-fit exponential trend with the specific surface area by BET (Figure 44a). A greater SSA requires more water quantity to envelop the particles and promote fluidity. Furthermore, the dispersant saturation content exhibits a high-fit logarithmic relationship with SSA, requesting a greater dispersant quantity to prevent particle agglomeration (Figure 44b). In summary, the SSA reduction in R-PC-based engineered binders is a pivotal factor in minimizing both water and dispersant demand.

Figure 44 - Specific surface area relation with water demand (a) and dispersant saturation content (b).

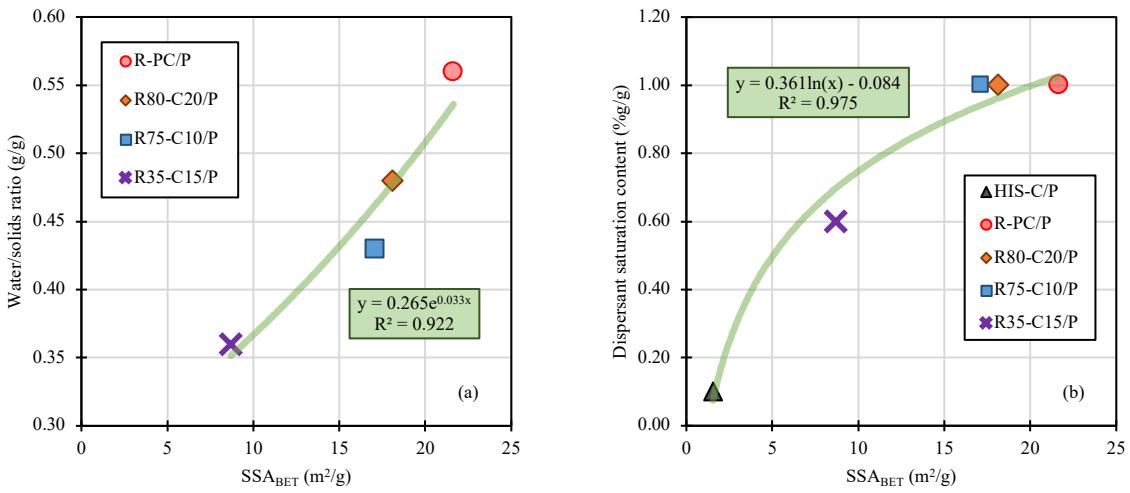

Figure 45 shows the rheological profile of the final pastes. The majority of the pastes had Bingham pseudoplastic behavior, R75-C10/P presented slightly shear thickening behavior with increasing viscosity from 25 to 50s^{-1}. R80-C20/P presented intermediate profile values between HIS-C/P and R-PC/P. Shear stress and viscosity values were similar for R35-C15/P and HIS-C/P.

Figure 45 - Shear rate versus shear stress (a) and apparent viscosity (b) of the final pastes in this work.

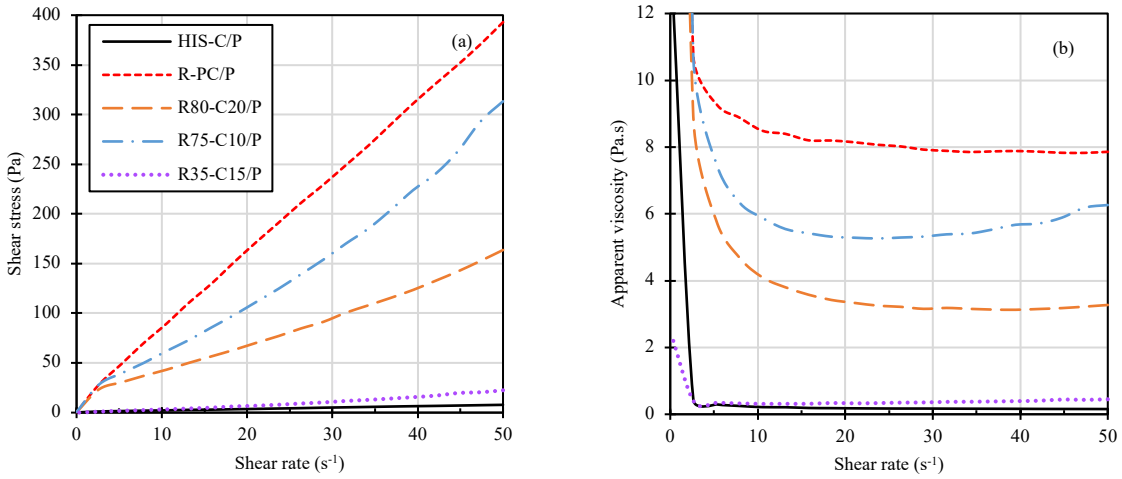

The yield stress presented a high-fit linear relationship with the intergranular friction within the binder matrix. This frictional assessment was quantified by the SSA divided by the water-to-solids ratio, which considers the morphology and water demand of the binders (Figure 46a).

Furthermore, the apparent viscosity at 50s-1 exhibited an exponential correlation with the volumetric surface area (VSA) (Figure 46b). As R-PC has the lowest density and the highest SSA, the apparent viscosity at 50s-1 decreases as R-PC content increases in the pastes. Despite the highest solids concentration, R35-C15/P exhibited the lowest apparent viscosity among engineered binders, akin in magnitude to HIS-C/P.

Figure 46 - Correlation between physical parameters and rheological behavior for (a) interparticle size distance vs. yield stress and (b) volumetric surface area vs. apparent viscosity.

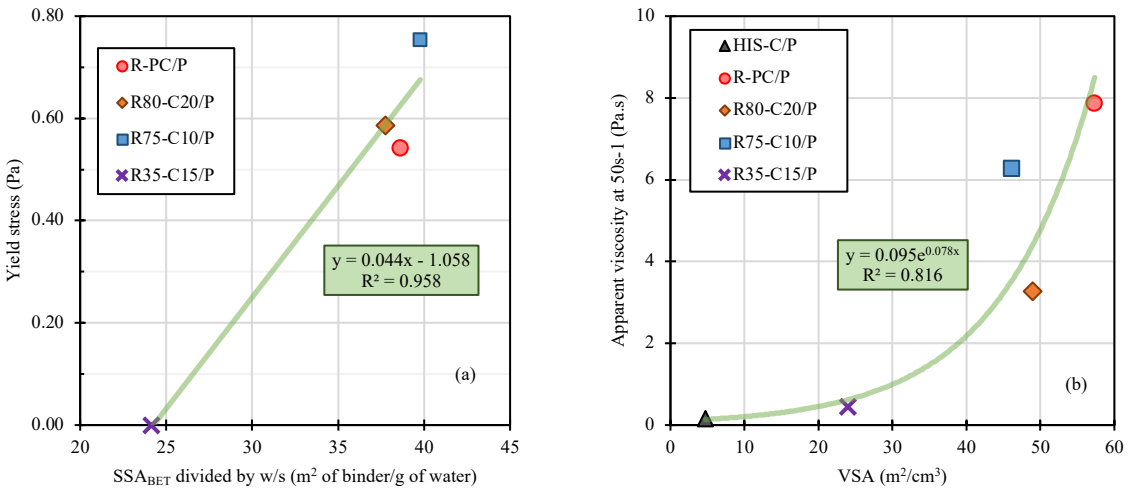

4.2.2.2 Kinetics and Reactivity

Figure 47a highlights the first hour of the (re)hydration process by isothermal calorimetry. An initial peak consistently appears between 5 to 7 minutes in pastes containing R-PC. These high initial peaks are attributed to a wetting mechanism, wherein the adsorption of water in dehydrated phases promotes a fast reformation of phases (mainly recombining water in C-S-H), similar to the 'memory effect' of dehydrated layered double hydroxide (LDH) structures (ANGULO et al., 2022; MASCOLO; MASCOLO, 2015). These behavior and peak intensity values corroborate with (ANGULO et al., 2015b, 2022; BALDUSCO et al., 2019; XU et al., 2023; ZHANG et al., 2018). The wetting peak observed during R-PC rehydration is also attributed to a substantial presence of calcium aluminates within the amorphous phases (BALDUSCO et al., 2019; CARRIÇO; BOGAS; GUEDES, 2020), crystallographic defects in silicates (α'H-C_2S and β-C_2S) (JUILLAND et al., 2010), small quantity of quicklime (CaO) formed in the thermal treatment (ANGULO et al., 2022), and the elevated specific surface area of R-PC (DE ROOIJ; SCHER, 2011; SHUI et al., 2009; WANG; MU; LIU, 2018).

Given the significantly higher specific surface area of R-PC in comparison to the other powders (Figure 47b), it is reasonable to attribute the initial peak and fast phase reformation observed in all engineered cements to the presence of R-PC. De Rooij and Scher (DE ROOIJ; SCHER, 2011) also demonstrated that increasing the surface area of cement leads to higher dissolution rates of phases and higher heat release, independent of the aluminates and silicates content. Therefore, it is reasonable to admit a faster dissolution rate for the Portland cement in the engineered recycled cement pastes due to the presence of the R-PC.

R-PC/P rehydration displays a subtle second peak between 10 and 11 hours (Figure 47c), indicative of a dilution-precipitation mechanism. This mild dilution-precipitation behavior has been documented in the literature (ANGULO et al., 2022; BOGAS et al., 2022; WANG; MU; LIU, 2018; XU et al., 2023). Xu et al. (XU et al., 2023) linked the dilution-precipitation of R-PC to the dehydrated metastable C(-A)-S-H, a distinction from Portland cement, where polycrystalline C_2S predominantly governs the behavior.

Engineered cements showed a behavior mostly similar to R-PC, given their higher content in the binders' compositions, with an initial wetting peak followed by a discrete peak between 4 and 8h. Due to the MPC content, a third peak from dissolution-precipitation was formed around 20-22h, with a delayed deceleration period. HIS-C/P presented the usual behavior of a Portland cement with four hydration stages: dissolution (<15min), induction (<3h), acceleration (3-12h) and deceleration (>12h) (BULLARD et al., 2011; MACIEL et al., 2019; SCRIVENER; JUILLAND; MONTEIRO, 2015).

Figure 47d shows the exponential trend between the combined water determined by TGA (Figure C3 and Table C3) and the cumulative heat for 6h, 12h, 24h and 72h. The (re)formation of phases is directly associated with the heat release over time regardless of the binder composition (e.g., HIS-C, R-PC or ECs). R80-C20/P and R75-C15/P achieved higher values than R-PC. The correlation was initially seen by (ANGULO et al., 2022) for R-PCs having the Portland cement as the maximum limit, and now it was improved by being applied for different ages and the engineered recycled cement binders.

Figure 47e demonstrates the evolution of combined water content over time for each experimental paste. Combined water content is a crucial parameter linked to the (re)formation of phases (reactivity) and microstructure densification. As expected, the R35-C15/P paste exhibited the lowest combined water content at all tested ages due to its lower content of reactive binders (50% in mass); R-PC and HIS-C/P. R75-C10/P paste displayed a higher pattern due to the increase of reactive binders to 85%, mostly influenced by the R-PC behavior. Remarkably, the R80-C20/P paste stood out as the only binder capable of combining water similar to HIS-C/P suggesting that R-PC and MPC react faster when together.

Figure 47f illustrates the relationship between mixing water, for the set rheological condition, and the combined water up to 28 days of age produced by the engineered recycled cements and literature conventional blended cements. The engineered recycled cements were successful in reducing the water demand to levels comparable to those of conventional Portland cements (both neat and blended). Blended cements with dispersant optimization reduced water demand by 16-27%, while engineered mix designs achieved reductions of 14-36% compared to R-PC/P.

The lowest combined water content up to 28 days of age was found in R35-C15/P, attributed to its lower binder content. Only, R80-C20/P exhibited reactivity similar to HIS-C/P, superior to LC^3. Engineered cements with high R-PC content exhibited higher reactivity than conventional blended cements, as R-PC combines water on its own, unlike the majority of conventional SCMs that require prior reactions or specific conditions to initiate their reactions.

The combined water behavior over time and its relationship with reactive binder content have a correlation with porosity refinement and compressive strength evolution, which makes it crucial to understand the volumetric composition of the pastes over time (later seen in 3.2.3 and 3.2.4).

Figure 47 - Heat flux analysis over time: first hour (a) and up to 72 hours (c). Cumulative heat correlations: for the first hour with binder SSA (b) and for 6h to 72h with combined water (d). Combined water over time (e). Combined water at 1, 7 and 28 days relationship with water demand (f).

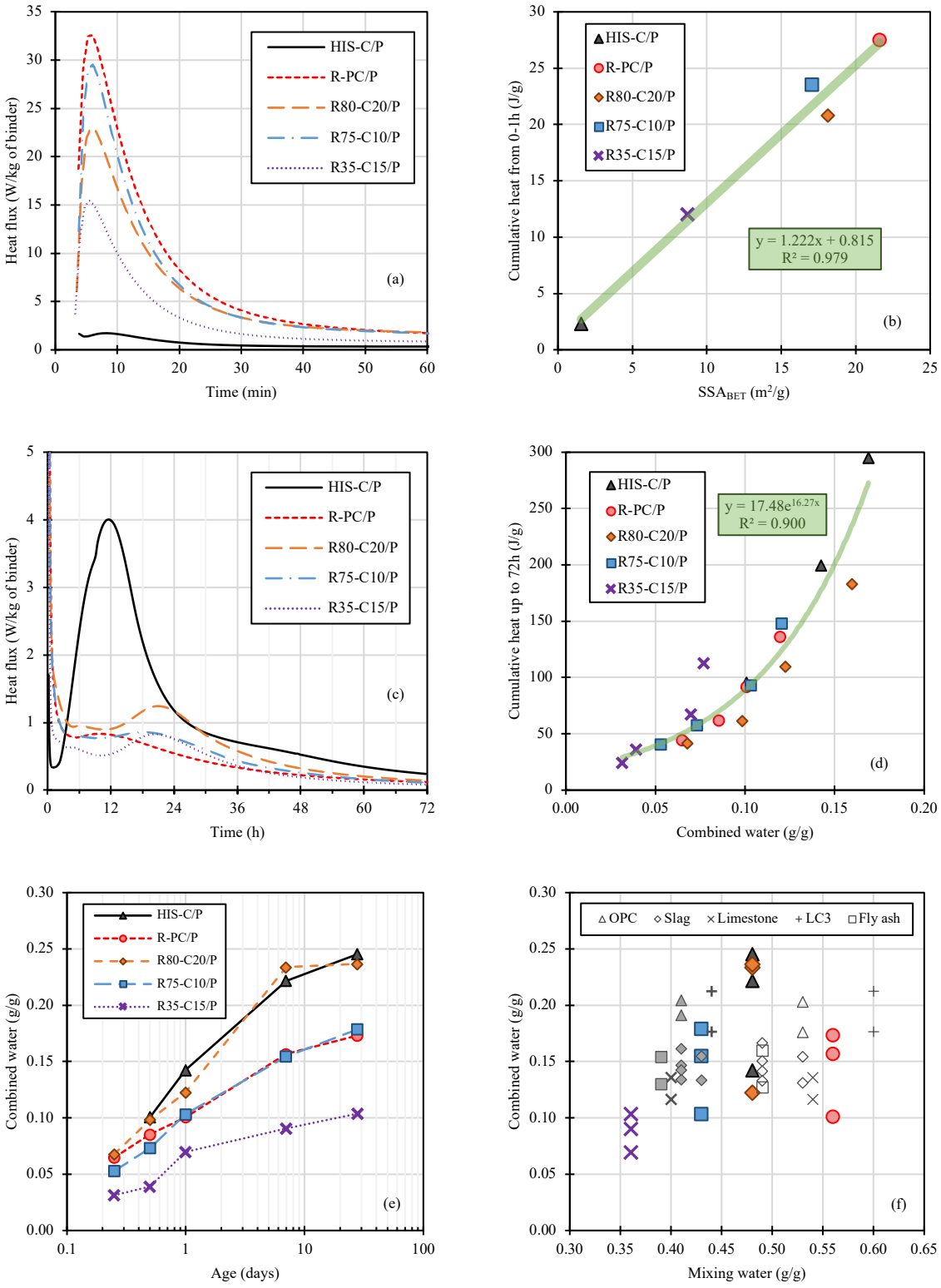

Literature data (ABRÃO et al., 2020; ABRÃO; CARDOSO; JOHN, 2020) from 7 and 28 days are represented by the grey icons, where filled icons indicate the use of superplasticizer, and empty icons indicate its absence.

4.2.2.3 Phases' volumetric composition and porosity over time

The volumetric composition over time of the experimental pastes is shown in Figure 48.

HIS-C/P exhibits the typical pure Portland cement paste system (LOTHENBACH et al., 2008). Initially, there are 32 cm^3 (40%) of solids, composed of clinker Portland, which contains calcium silicates (alite - C_3S, belite - C_2S), calcium aluminates (calcium cyclo-hexaaluminate - C_3A, ferrite - C_4AF), a minor amount of calcium sulfate, and calcite from limestone addition. As a high initial strength cement with 90% g/g of clinker and fine grains, HIS-C/P exhibited fast consumption of calcium silicate and aluminate phases, forming hydrated products, mainly C-S-H and portlandite. This resulted in hydration degrees of 31% at 12 hours, 47% at 1 day, 74% at 7 days, and 82% at 28 days, as indicated in Table C3. The volume of solids increased from 31.9 cm^3 (40%) to 59.4 cm^3 (74%) at 28 days, representing a volume growth of 1.86 times (Figure 49) and resulting in 26% of total porosity, 22% of middle to small-size capillary porosity.

R-PC/P contains only 20 cm^3 (22%) of solids, which is almost half of the amount found in HIS-C/P. This difference is related to the fact that 37% of the volume of recycled cement grain consists of large capillary pores, as shown by the MIP result in Figure B1. Once the cement is hydrated, as demonstrated in the HIS-C/P system, there will be capillary porous that will remain inevitably in the recycled cement. R-PC/P has an initial solids composition consisting of portlandite, C-S-H, calcite, and other calcium-based phases at 42%, 24%, 11%, and 33%, respectively. This composition is supported by the TG/DTG results in the literature (ANGULO et al., 2015b; WANG; MU; LIU, 2018). The R-PC follows a different kinetics compared to pure PC, characterized by a fast reformation of phases, primarily associated with the C-S-H water recombination, as demonstrated in the previous section. Therefore, the hydration degree of R-PC/P is higher than HIS-C/P, especially in the early stages, with 31% at 6 hours, 41% at 12 hours, 49% at 1 day, 76% at 7 days, and 83% at 28 days (Table C3). The R-PC/P system exhibited a solids volume growth of 2.55 times from 0 to 28 days (Figure 49), with initial and final solid volumes of 20.1 cm^3 (22%) and 51.1 cm^3 (57%), respectively. The remaining capillary porosity is 41%, with a predominance of small and large capillary pores, each comprising 18%.

Figure 48 - Volumetric composition in cm^3 for 100g of the studied binder.

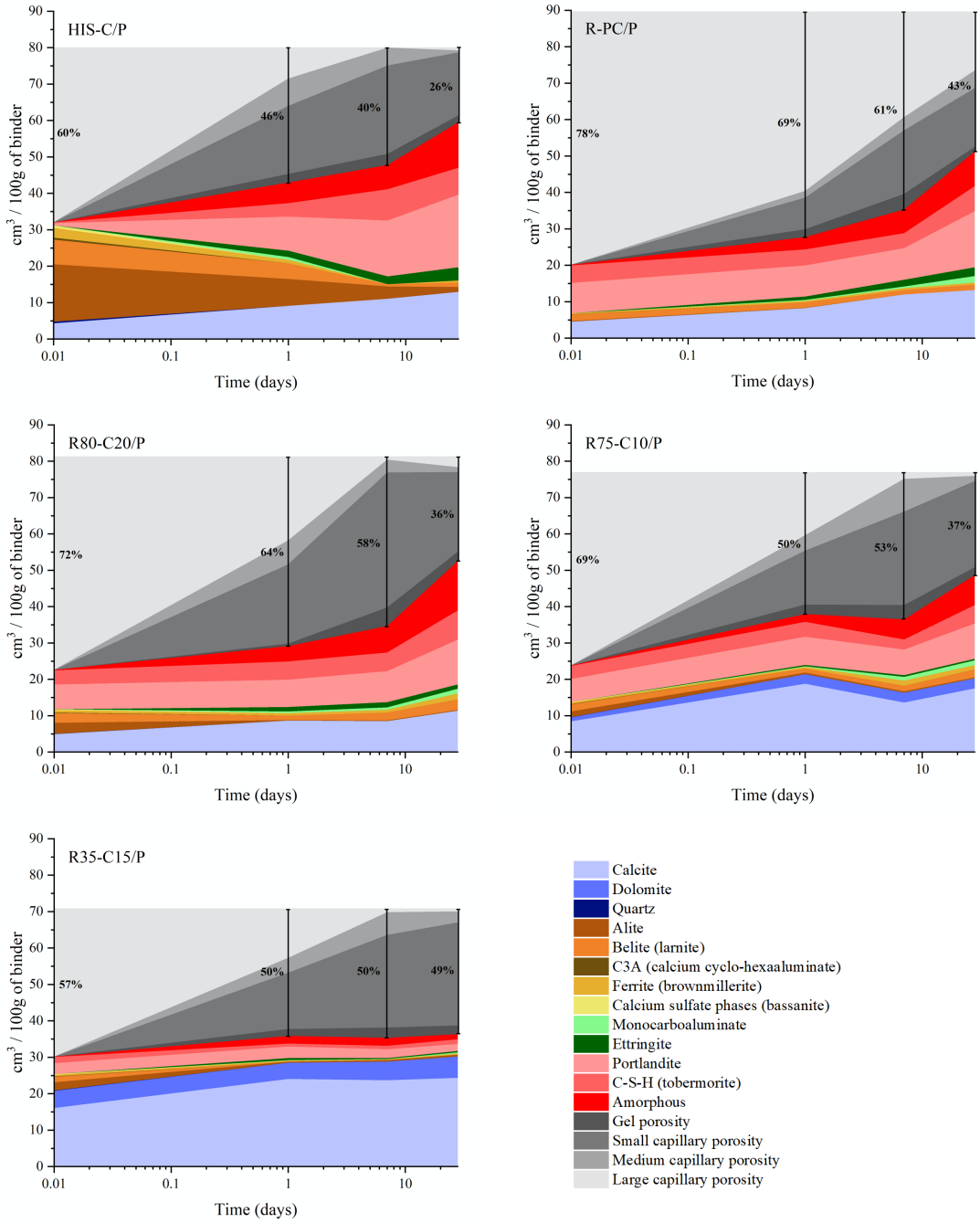

Overall, when compared to HIS-C/P, R-PC/P exhibits a faster (re)hydration process and greater solid volume growth over time. However, it still retains a higher initial and final porosity with a wide and coarser pore size distribution, which directly impacts its mechanical performance.

For engineered systems, the goal was to reduce water demand and improve mechanical performance. Each component used in the binary and ternary blends have different

contributions: (i) R-PC have low CO_2 footprint, hydration faster than HIS-C/P (reforms mostly in the first 12 hours) which is a unique characteristic for an SCM, (ii) the MPC in the system is able to refine the porosity to similar critical diameter of HIS-C/P for low-clinker content (see Figure C4), and (iii) limestone fillers are able to boost packing density.

The increase in the initial volume of solids corresponds to better packing and lower water demand. Specifically, for R80-C20/P, R75-C10/P, and R35-C15/P, the initial volume of solids measured 22.5 cm^3 (28%), 23.8 cm^3 (31%), and 30.1 cm^3 (43%), respectively. Consequently, the initial volumetric solid composition increased from 22% for R-PC/P to 43%, slightly surpassing the packing condition of the HIS-C/P system (39%). However, unlike other engineered blended cements such as reverse filling (ZHENG et al., 2020), nano-engineering (SOBOLEV et al., 2016), high-limestone replacement (DAMINELI, 2013; JOHN et al., 2018; PALM et al., 2016), multiple blends (JEONG et al., 2015; PROSKE et al., 2018), which can achieve residual porosities below 20%, the engineered R-PC-based systems presents barriers to reach such low values due to their inherent internal porosity arising from thermal activation in the recycled cement. The higher volume occupation of R75-C10/P and R35-C15/P correlates in agreement of the R-PC/P content (Figure 49).

Figure 49 - The increase in solid volume over time, measured relative to the initial volume of solids.

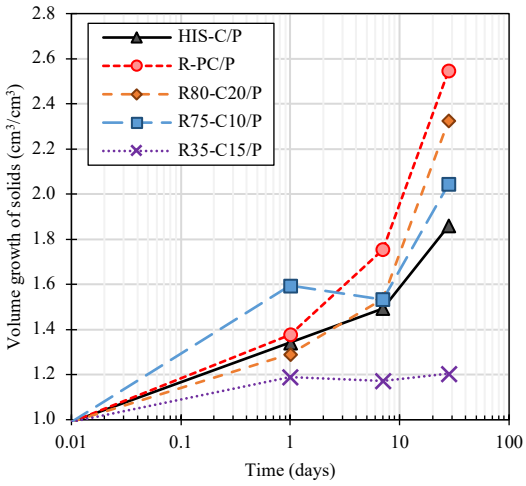

4.2.2.3.1 Porosity refinement

The porosity analysis of the pastes was evaluated through MIP tests conducted at 1, 7 and 28 days. Pore sizes were classified according to (MEHTA; MONTEIRO, 2014): gel pores (<4.5 nm), small capillary pores (4.5–50 nm), medium capillary pores (50–100 nm), and large capillary pores (>100 nm). Figure 50 demonstrates MIP porosity data discretized by pore size ranges for all experimental pastes.

Notably, the majority of pastes displayed a reduction in pore size and total porosity over time, accompanied by a decreasing critical diameter (see Figure C4). HIS-C/P followed a typical pattern of decreasing total porosity and pore refinement, with only small capillary and gel pores at 28 days. HIS-C/P had the lowest critical diameter at 1 day, indicating more effective pore refinement at this age. After 1-day, this difference does not exist more.

Across all ages, R-PC/P consistently demonstrated the largest critical diameter. R-PC/P showed a notable reduction in porosity from 7 to 28 days, mainly due to a decrease in large capillary pores. However, unlike HIS-C/P, R-PC/P maintained a high concentration of large capillary pores at the 28-day. The pore size distribution and critical pore diameter of R-PC/P at 28 days resembled the results of previous research (XU et al., 2023).

Figure 50 - Porosity assessed via MIP and categorized into specific pore size ranges.

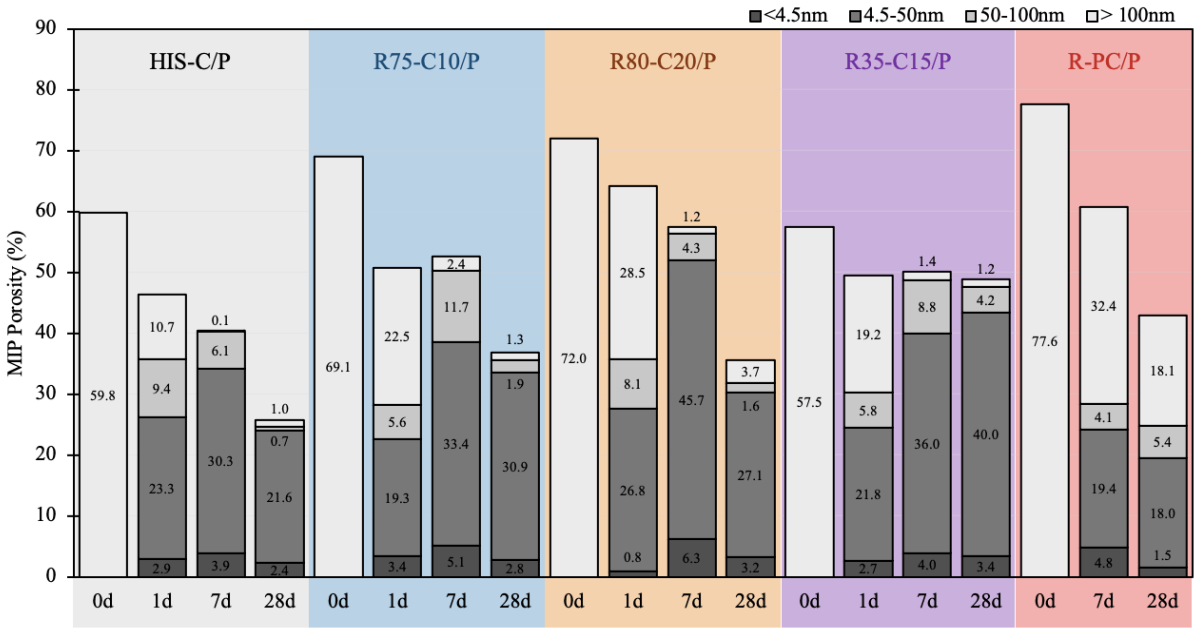

Engineered cement pastes exhibited profiles with multiple peaks, indicating a range of pore sizes. In fact, the microstructure of R-PC encompasses two distinct substructures: one external (with larger capillary pores) and one internal that contains hydration products and smaller capillary pores (XU et al., 2023; ZHANG et al., 2018). All engineered cement pastes had large capillary porosity at 1 day, possibly linked to the internal porosity of R-PC grains and displayed significant pore refinement from 1 to 7 days. After 7 days, the critical diameter of the engineered cement pastes remained similar to HIS-C/P, indicating effective pore refinement.

At 28 days, a consistent decrease in total porosity is evident from 7 to 28 days. R80-C20/P displayed the most refined pore distribution, closely resembling the shape of HIS-C/P

and sharing an equal critical diameter. R75-C10/P exhibited a similar behavior to R80-C20/P but with higher total porosity and critical diameter. Notably, R35-C15/P exhibited minimal changes in total porosity over time, behavior associated with it lower reactive material content. Considering pore size distribution, the engineered cements demonstrated effective refinement compared to R-PC/P, as stablished in the mix design and hypothesis.

The increase of packing density reduced the initial pore size (immediately in contact with water), and smaller pores have been filled more quickly over time.

4.2.2.4 Compressive strength and performance indices analysis

Figure 51 presents the compressive strength for all pastes from 6 hours to 28 days.

Figure 51 - Compressive strength of all pastes at 6h, 12h, and 1,7 and 28 days. HIS-C/P do not have values for 6h because the paste was not completely hardened.

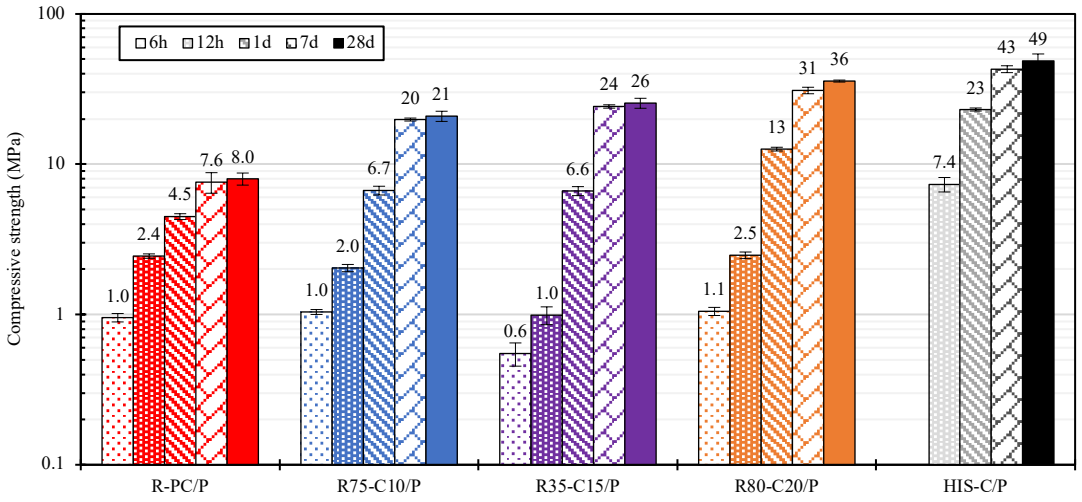

After 6 hours, pastes containing R-PC displayed accelerated hardening and presented near 1 MPa, whereas HIS-C/P had not fully hardened at this stage. The behavior is consistent with the fast reformation of R-PC seen in the calorimetry results (the initial intense peak).

From 6 hours to 12 hours, all R-PC-based pastes roughly doubled their compressive strength. However, HIS-C/P displayed after 12 hours achieved the highest compressive strength compared to the others; 7.4 MPa. Despite R-PC pastes formed more volume of solids (Figure 49), those did not perform better or equal because the initial porosity (water demand and internal porosity) plays a vital role in strength development.

From 12 hours to one day, compressive strength gains highlight the positive impact of the R-PC on the engineered pastes (R75-C10/P, R35-C15/P, and R80-C20/P); 3.4, 6.6 and 5.2, respectively. Those increments were higher than that observed for HIS-C/P (3.3 times).

From 1 to 7 days, where the highest refinement of pore size distribution is observed (Figure 50), the highest percentual strength gain is observed on this timeframe for all pastes. HIS-C/P presented the higher volume of reactive material and lower initial porosity, which resulted in a strength gain of 20 MPa. Engineered recycled cement pastes also have substantial increases of 13.2, 17.6, and 18.4 MPa for R75-C10/P, R35 C15/P, and R80-C20/P, respectively.

From 7 to 28 days, all engineered pastes exhibit the minimal absolute strength gain (lower than 6MPa). This strength evolution behavior offers sustainable and economic advantages. The minimum required structural strength is achieved within the first 7 days, which reduces clinker wastage at later stages.

To evaluate the environmental performance, the compressive strength of the pastes needs to be correlated with the clinker content at different ages (Figure 52a). The clinker contents required for the engineered recycled cements to reach the HIS-C/P strengths for 1, 3, 7, and 28 days are 50%, 31%, 28%, and 28%, respectively. Therefore, it is possible to formulate an engineered cement that matches the strength performance of HIS-C at 3, 7, and 28 days using only 30% clinker, named herein low-CO_2 high-initial strength engineered recycled cements.

Figure 52b compares the relative compressive strength concerning the clinker content of the engineered recycled cement and blended cements with conventional SCMs (e.g., slag, limestone, calcined clay, and fly ash). The relative strength is the strength achieved by the material (paste or mortar) divided by the strength of the Portland cement paste made with water/cement ratio of 0.48 g/g as specified in the Brazilian standard (BRAZILIAN ASSOCIATION OF TECHNICAL STANDARDS, 2019). Cementitious pastes with optimized dispersant content performed better than those without water reduction additive. Blended cements with calcined clay and limestone (LC^3), fly ash, and exclusively limestone accounted for 45% of clinker content by mass. LC^3 with dispersant demonstrated the best performance, with strength similar to neat PC, reaching 97%. Fly ash and limestone performed less favorably than LC^3 and neat PC, achieving 92% and 64% at 28 days. Slag-blended cements had lower replacements (less than 25%) and exhibited performance similar to the Portland cement dilution trend line. R80-C20/P achieved 36 MPa at 28 days, 73% of HIS-C strength with less than 20% of clinker.

Figure 52 - Relationship between clinker content in the binder and compressive strength of the paste from 1 to 28 days (a) and the relative compressive strength of cementitious materials (pastes and mortars) for blended cements and engineered binders at 28 days (b).

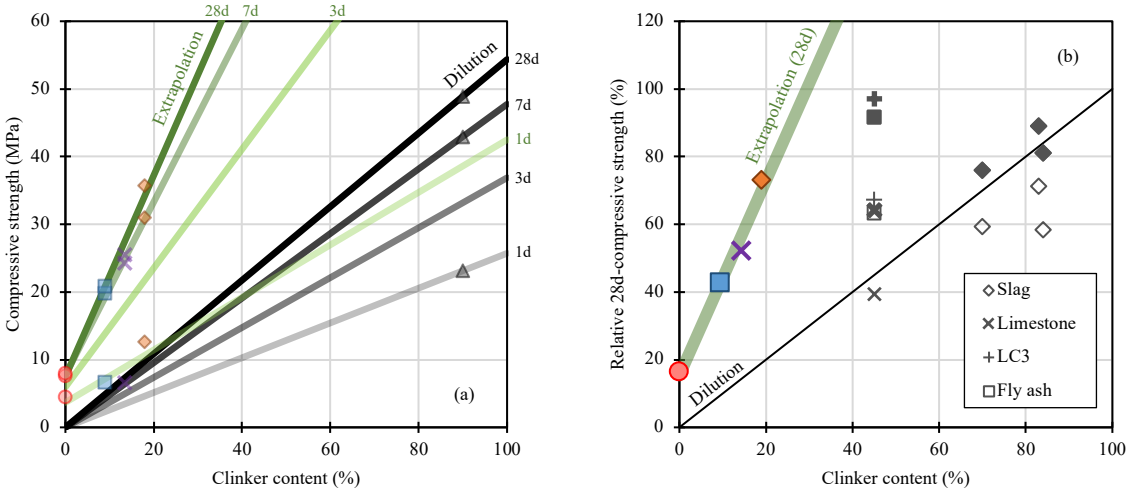

The dilution trend was obtained by linear regression with HIS-C/P data. Extrapolation linear trends are analyzed exclusively in pastes with R-PC. Dilution and extrapolation lines for 3 days were developed with compressive strengths estimated using logarithmic behavior for 12h, 1d and 7d. Extrapolation line fits were higher than 0.98 for all pastes, except for 1d (0.73) indicating R-PC influence in the behavior. Literature data is presented in grey icons (ABRÃO et al., 2020; ABRÃO; CARDOSO; JOHN, 2020). Filled icons denote the use of superplasticizer, while empty icons indicate its absence.

4.2.2.4.1 CO_2 emissions

CO_2 emissions of binder per ton are estimated (Figure 53). The clinker content is also informed. R-PC emits 78% less CO_2 than HIS-C, saving 662 kg of CO_2 per ton of binder, but only 16% of HIS-C strength is achieved. R80-C20/P, R75-C10/P, and R35-C15/P exhibit reductions of 63%, 68%, and 72% in CO_2 emissions compared to HIS-C, respectively; but those recovered 73%, 43%, and 53% of HIS-C strength.

By our estimates, R70-C30 may exhibit similar 28-day compressive strength of neat PC emitting only 383 $kgCO_2$/ton of binder (a 55% CO_2 emission reduction compared to the PC, saving of 463 $kgCO_2$ per ton). It is the highest environmental efficiency when compared to the conventional SCMs blended cements with similar 28-day compressive strength to neat Portland cement (25% slag, 50% fly ash, 50% limestone-calcined clay (LC^3), and 30% carbonated concrete waste fines (CCWF).

Figure 53 - CO_2 emissions per ton of binder, the clinker content is reported in parentheses.

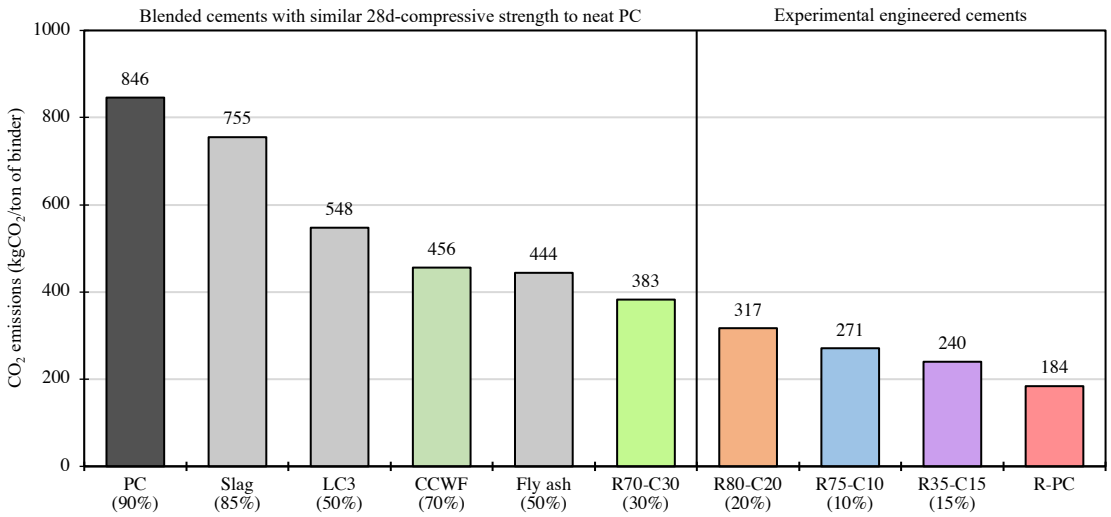

Literature data from (ABRÃO et al., 2020; ABRÃO; CARDOSO; JOHN, 2020). Similar 28d-compressive strength to PC is considered 90% minimum.

4.3 Conclusions

This work developed low-CO_2 high-initial strength engineered recycled cements. Thermoactivated recycled Portland cement (R-PC) blended with limestone fillers and finely-ground clinker Portland cement was used. A mix design using concepts of reverse filling was developed to overcome the recycled cement limitations. The rheological behavior, phases' composition, porosity refinement, mechanical properties of engineered cement pastes were analyzed over time and compared with conventional SCMs blended cements. The CO_2 emissions per ton of binder were also assessed. The following conclusions were drawn:

- The mix design used for the engineered cements (ECs) effectively reduced the surface area and increased the packing density of the systems, leading to a substantial decrease of water and dispersant demands.

- Despite thermoactivated recycled cement (R-PC) has limitations when used as the only binder, which is associated with the internal porosity, high surface area, high water demand, and low mechanical performance, the engineered cements with R-PC have a singular kinetics of reaction with an initial fast reformation, high volume of solids reformed, worldwide availability, and low CO_2 footprint, a unique supplementary cementitious material (SCM) with high potential for circularity in the cement industry.

- The best solution used 80% recycled cement and 20% finely-ground Portland cement achieving 73% of the high-initial strength Portland cement (36 MPa, w/s of 0.48g/g) with 63% reduction in CO_2 emissions (317 kg CO_2/ton of binder), thereby offering the highest environmental efficiency.

- By extrapolating experimental results with engineered cements, we can infer a formulation that matches the high-initial strength of Portland cement using only one-third of the clinker.

5 FUTURE OUTLOOKS

Recycled cement holds large potential for promoting circularity in the cement industry. This strategy can be further improved with the use of fine carbonated concrete waste as a filler, as well as the use of pozzolans to increase pore size refinement. Further studies are encouraged.

The authors do not view the engineering of cements with hydrated cement fines as a potential research avenue, as they exhibit a similar water demand to R-PC but lack reactivity.

The engineered recycled cements displayed a unique strength evolution profile, with 92-95% of its strength achieved within the first 7 days. This enables precise formulation of clinker content to meet initial minimum strength requirements, thereby avoiding the unnecessary use of clinker to provide additional strength over time.

Packing with solid particles is consistently superior to using porous particles. However, it is not possible to completely eliminate the intergranular porosity of R-PC, which consists of larger pores. Therefore, there will always be opportunities for capillary porous solids as SCM since only Portland clinker is employed to refine pore size, allowing quicker filling and lower CO_2 footprint.

REFERENCES

ABRÃO, P. C. R. A. et al. Comparing the Ecoefficiency of Cements Containing Calcined Clay and Limestone Filler. Em: BISHNOI, S. (Ed.). **Calcined Clays for Sustainable Concrete**. RILEM Bookseries. Singapore: Springer Singapore, 2020. v. 25p. 245–255.

ABRÃO, P. C. R. A.; CARDOSO, F. A.; JOHN, V. M. Efficiency of Portland-pozzolana cements: Water demand, chemical reactivity and environmental impact. **Construction and Building Materials**, v. 247, p. 118546, jun. 2020.

ALONSO, C.; FERNANDEZ, L. Dehydration and rehydration processes of cement paste exposed to high temperature environments. **Journal of Materials Science**, v. 39, n. 9, p. 3015–3024, maio 2004.

ALONSO, M. C. et al. Calcium aluminate based cement for concrete to be used as thermal energy storage in solar thermal electricity plants. **Cement and Concrete Research**, v. 82, p. 74–86, abr. 2016.

AMERICAN SOCIETY FOR TESTING AND MATERIALS. **ASTM-109/C 109M-02: Standard test method for compressive strength of hydraulic cement mortars**. , 2002.

ANGULO, S. C. et al. **Rehydration of cement fine: a TG/calorimetry study**. Progress of Recycle in the Built Environment Conference. **Anais**...São Paulo: Martins, I.; Ulsen, C.; Angulo, S.C., 2015a.

ANGULO, S. C. et al. Rehydration of cement fines: a TG/Calorimetry study. **Rehydration of cement fines: a TG/Calorimetry study**, Tchnical paper (IPT). p. 8, 2015b.

ANGULO, S. C. et al. The role of calcium silicates and quicklime on the reactivity of rehydrated cements. **Construction and Building Materials**, v. 340, p. 127625, jul. 2022.

BALDUSCO, R. et al. Dehydration and Rehydration of Blast Furnace Slag Cement. **Journal of Materials in Civil Engineering**, v. 31, n. 8, p. 04019132, ago. 2019.

BAQUERIZO, L. G.; MATSCHEI, T.; SCRIVENER, K. L. Impact of water activity on the stability of ettringite. **Cement and Concrete Research**, v. 79, p. 31–44, jan. 2016.

BENTZ, D. P. Three-dimensional computer simulation of portland cement hydration and microstructure. **Journal of the American Ceramic Society**, p. 20, 1997.

BOGAS, J. A. et al. Hydration and phase development of recycled cement. **Cement and Concrete Composites**, v. 127, p. 104405, mar. 2022.

BOGAS, J. A.; CARRIÇO, A.; PEREIRA, M. F. C. Mechanical characterization of thermal activated low-carbon recycled cement mortars. **Journal of Cleaner Production**, v. 218, p. 377–389, maio 2019.

BOGAS, J. A.; CARRIÇO, A.; TENZA-ABRIL, A. J. Microstructure of thermoactivated recycled cement pastes. **Cement and Concrete Research**, v. 138, p. 106226, dez. 2020.

BONACCORSI, E.; MERLINO, S.; KAMPF, A. R. The Crystal Structure of Tobermorite 14 A (Plombierite), a C-S-H Phase. **Journal of the American Ceramic Society**, v. 88, n. 3, p. 505–512, mar. 2005.

BONAVETTI, V. L.; RAHHAL, V. F.; IRASSAR, E. F. Studies on the carboaluminate formation in limestone filler-blended cements. **Cement and Concrete Research**, v. 31, n. 6, p. 853–859, maio 2001.

BRAZILIAN ASSOCIATION OF TECHNICAL STANDARDS. **ABNT NBR 13: Portland cement — Chemical analysis — Determination of the free calcium oxide by ethylenglycol**. , 2013.

BRAZILIAN ASSOCIATION OF TECHNICAL STANDARDS. **ABNT NBR 16697: Portland cements - Requirements**. , 2018.

BRAZILIAN ASSOCIATION OF TECHNICAL STANDARDS. **ABNT-NBR 7215: Portland cement: determination of compressive strength**. , 2019.

BROUWERS, H. J. H. The work of Powers and Brownyard revisited: Part 1. **Cement and Concrete Research**, v. 34, n. 9, p. 1697–1716, set. 2004.

BRUTON, C. J. et al. Cement Minerals at Elevated Temperature: Thermodynamic and Structural Characteristics. **MRS Proceedings**, v. 333, p. 327, 1993.

BULLARD, J. W. et al. Mechanisms of cement hydration. **Cement and Concrete Research**, v. 41, n. 12, p. 1208–1223, dez. 2011.

CAMETTI, G. et al. De- and re-hydration of scolecite revisited: An in situ single-crystal X-ray study under low and high humidity conditions. **Microporous and Mesoporous Materials**, v. 208, p. 171–180, maio 2015.

CARRIÇO, A. et al. Mortars with thermo activated recycled cement: Fresh and mechanical characterisation. **Construction and Building Materials**, v. 256, p. 119502, set. 2020.

CARRIÇO, A. et al. Shrinkage and sorptivity of mortars with thermoactivated recycled cement. **Construction and Building Materials**, v. 333, p. 127392, maio 2022.

CARRIÇO, A.; BOGAS, J. A.; GUEDES, M. Thermoactivated cementitious materials – A review. **Construction and Building Materials**, v. 250, p. 118873, jul. 2020.

CARRIÇO, A.; REAL, S.; BOGAS, J. A. Durability performance of thermoactivated recycled cement concrete. **Cement and Concrete Composites**, v. 124, n. 104270, nov. 2021.

CASTELLOTE, M. et al. Composition and microstructural changes of cement pastes upon heating, as studied by neutron diffraction. **Cement and Concrete Research**, v. 34, n. 9, p. 1633–1644, set. 2004.

CHEUNG, J.; ROBERTS, L.; LIU, J. Admixtures and sustainability. **Cement and Concrete Research**, v. 114, p. 79–89, dez. 2018.

CHU, S. H. et al. Roles of packing density and slurry film thickness in synergistic effects of metakaolin and silica fume. **Powder Technology**, v. 387, p. 575–583, jul. 2021.

COOK, R. A.; HOVER, K. C. Experiments on the contact angle between mercury and hardened cement paste. **Cement and Concrete Research**, v. 21, n. 6, p. 1165–1175, nov. 1991.

DAI, L. et al. Thermal cycling stability of thermochemical energy storage system Ca(OH)2/CaO. **Applied Thermal Engineering**, v. 133, p. 261–268, mar. 2018.

DAMINELI, B. L. et al. Measuring the eco-efficiency of cement use. **Cement and Concrete Composites**, v. 32, n. 8, p. 555–562, set. 2010.

DAMINELI, B. L. **Conceitos para formulação de concretos com baixo consumo de ligantes: controle reológico, empacotamento e dispersão de partículas.** Doutorado em Engenharia de Construção Civil e Urbana—São Paulo: Universidade de São Paulo, 25 out. 2013.

DAMINELI, B. L. et al. Viscosity prediction of cement-filler suspensions using interference model: A route for binder efficiency enhancement. **Cement and Concrete Research**, v. 84, p. 8–19, jun. 2016a.

DAMINELI, B. L. et al. Viscosity prediction of cement-filler suspensions using interference model: A route for binder efficiency enhancement. **Cement and Concrete Research**, v. 84, p. 8–19, jun. 2016b.

DAMINELI, B. L.; JOHN, V. M.; PILEGGI, R. G. Predicting optimal dispersant (superplasticiser) content for cement–limestone pastes from rheological tests. **Magazine of Concrete Research**, v. 75, n. 4, p. 206–216, fev. 2023.

DE LARRARD, F. **Concrete Mixture Proportioning: a scientific approach**. London: E & FN SPON, 1999.

DE LARRARD, F. **Concrete mixture proportioning: a scientific approach**. [s.l.] CRC Press, 1999.

DE ROOIJ, M. R.; SCHER, S. **The first 24 hours of commercial cement hydration**. 13th Int. Congress of the Chemistry of Cement. **Anais**... Em: 13TH INT. CONGRESS OF THE CHEMISTRY OF CEMENT. Instituto de Ciencias de la Construccíon Eduardo Torroja.Madrid, Spain: Instituto de Ciencias de la Construccíon Eduardo Torroja., 2011.

DE WEERDT, K. et al. Hydration mechanisms of ternary Portland cements containing limestone powder and fly ash. **Cement and Concrete Research**, v. 41, n. 3, p. 279–291, mar. 2011.

DILNESA, B. Z. et al. Stability of Monosulfate in the Presence of Iron. **Journal of the American Ceramic Society**, v. 95, n. 10, p. 3305–3316, out. 2012.

DU, Y. et al. Thermal conductivity of cement paste containing waste glass powder, metakaolin and limestone filler as supplementary cementitious material. **Journal of Cleaner Production**, v. 287, p. 125018, mar. 2021.

ELERT, K.; BEL-ANZUÉ, P.; BURGOS-RUIZ, M. Influence of calcination temperature on hydration behavior, strength, and weathering resistance of traditional gypsum plaster. **Construction and Building Materials**, v. 367, p. 130361, fev. 2023.

EUROPEAN FEDERATION OF CONCRETE ADMIXTURES ASSOCIATIONS LTD. (EFCA). **Concrete admixtures – Plasticisers and Superplasticisers**. , 2015.

EUROPEAN STANDARDS. **EN196-1: Methods of testing cement - Part 1: Determination of strength**. , 2005.

FARAGE, M. C. R.; SERCOMBE, J.; GALLÉ, C. Rehydration and microstructure of cement paste after heating at temperatures up to 300 °C. **Cement and Concrete Research**, v. 33, n. 7, p. 1047–1056, jul. 2003.

FLATT, R. J. Dispersion forces in cement suspensions. **Cement and Concrete Research**, v. 34, n. 3, p. 399–408, mar. 2004.

FLATT, R. J. et al. From physics to chemistry of fresh blended cements. **Cement and Concrete Research**, v. 172, p. 107243, out. 2023.

FLATT, R. J.; BOWEN, P. Electrostatic repulsion between particles in cement suspensions: Domain of validity of linearized Poisson–Boltzmann equation for nonideal electrolytes. **Cement and Concrete Research**, v. 33, n. 6, p. 781–791, jun. 2003.

FORANO, C. et al. Layered Double Hydroxides (LDH). Em: **Developments in Clay Science**. [s.l.] Elsevier, 2013. v. 5p. 745–782.

GUADAGNI, A. **Prontuario dell'ingegnere**. [s.l.] Hoepli editore, 2003.

GUILGE, M. S. **Desenvolvimento de ligante hidráulico a partir de resíduos de Cimento Hidratado, Tijolo Cerâmico e Metacaulinita**. Mestrado em Engenharia de Construção Civil e Urbana—São Paulo: Universidade de São Paulo, 2011.

HANSEN, T. C. Physical structure of hardened cement paste. A classical approach. **Materials and Structures**, v. 19, n. 6, p. 423–436, nov. 1986.

HOU, D. et al. Statistical modelling of compressive strength controlled by porosity and pore size distribution for cementitious materials. **Cement and Concrete Composites**, v. 96, p. 11–20, fev. 2019.

HUNGER, M.; BROUWERS, H. J. H. Flow analysis of water–powder mixtures: Application to specific surface area and shape factor. **Cement and Concrete Composites**, v. 31, n. 1, p. 39–59, jan. 2009.

HUNTZINGER, D. N.; EATMON, T. D. A life-cycle assessment of Portland cement manufacturing: comparing the traditional process with alternative technologies. **Journal of Cleaner Production**, v. 17, n. 7, p. 668–675, maio 2009.

JEONG, Y. et al. Microstructural verification of the strength performance of ternary blended cement systems with high volumes of fly ash and GGBFS. **Construction and Building Materials**, v. 95, p. 96–107, out. 2015.

JOHN, V. M. et al. Fillers in cementitious materials — Experience, recent advances and future potential. **Cement and Concrete Research**, v. 114, p. 65–78, dez. 2018.

JOHN, V. M. et al. Rethinking cement standards: Opportunities for a better future. **Cement and Concrete Research**, v. 124, p. 105832, out. 2019.

JUILLAND, P. et al. Dissolution theory applied to the induction period in alite hydration.

Cement and Concrete Research, v. 40, n. 6, p. 831–844, jun. 2010.

KIM, T. et al. Strength and pore characteristics of OPC-slag cement paste mixed with polyaluminum chloride. **Construction and Building Materials**, v. 223, p. 616–628, out. 2019.

KWAN, A. K. H.; LI, L. G. Combined effects of water film, paste film and mortar film thicknesses on fresh properties of concrete. **Construction and Building Materials**, v. 50, p. 598–608, jan. 2014.

LAM, L.; WONG, Y. L.; POON, C. S. Degree of hydration and gel/space ratio of high-volume fly ash/cement systems. **Cement and Concrete Research**, v. 30, n. 5, p. 747–756, maio 2000.

LIMA PACHECO, A. A. et al. Rehydration of katoite as a layered double hydroxide: an in situ study. **RILEM Technical Letters**, v. 6, p. 8–16, 16 mar. 2021.

LOTHENBACH, B. et al. Influence of limestone on the hydration of Portland cements. **Cement and Concrete Research**, v. 38, n. 6, p. 848–860, jun. 2008.

LOTHENBACH, B.; NONAT, A. Calcium silicate hydrates: Solid and liquid phase composition. **Cement and Concrete Research**, v. 78, p. 57–70, dez. 2015.

LOTHENBACH, B.; SCRIVENER, K.; HOOTON, R. D. Supplementary cementitious materials. **Cement and Concrete Research**, v. 41, n. 12, p. 1244–1256, dez. 2011.

LÜ, L.; HE, Y.; HU, S. Structural characteristics of dehydrated phase of hardened cement paste and its rehydrating ability. **J. Chinese Ceram.**, 2008.

LU, L.; HE, Y.; HU, S. Binding materials of dehydrated phases of waste hardened cement paste and pozzolanic admixture. **Journal of Wuhan University of Technology-Mater. Sci. Ed.**, v. 24, n. 1, p. 140–144, fev. 2009.

MACIEL, M. H. **Influência do ligante pré-hidratado nas propriedades de suspensões de cimento Portland.** Mestrado em Engenharia de Construção Civil e Urbana—São Paulo: Universidade de São Paulo, 25 out. 2017.

MACIEL, M. H. et al. Monitoring of Portland cement chemical reaction and quantification of the hydrated products by XRD and TG in function of the stoppage hydration technique. **Journal of Thermal Analysis and Calorimetry**, v. 136, n. 3, p. 1269–1284, maio 2019.

MARCHON, D.; FLATT, R. J. Mechanisms of cement hydration. Em: **Science and Technology of Concrete Admixtures**. Zurich: Pierre-Claude Aïtcin Robert Flatt, 2016. p. 129–145.

MASCOLO, G.; MASCOLO, M. C. On the synthesis of layered double hydroxides (LDHs) by reconstruction method based on the " memory effect ". **Microporous and Mesoporous Materials**, v. 214, p. 246–248, set. 2015.

MATSCHEI, T.; LOTHENBACH, B.; GLASSER, F. P. Thermodynamic properties of Portland cement hydrates in the system CaO–Al2O3–SiO2–CaSO4–CaCO3–H2O. **Cement and Concrete Research**, v. 37, n. 10, p. 1379–1410, out. 2007.

MEHTA, P. K.; MONTEIRO, P. J. M. **Concrete: Microstructure, Properties, and Materials**.

4. ed. California: Mc Graw Hill Education, 2014.

MENÉNDEZ, E.; ANDRADE, C.; VEGA, L. Study of dehydration and rehydration processes of portlandite in mature and young cement pastes. **Journal of Thermal Analysis and Calorimetry**, v. 110, n. 1, p. 443–450, out. 2012.

MILLER, S. A. et al. Carbon dioxide reduction potential in the global cement industry by 2050. **Cement and Concrete Research**, v. 114, p. 115–124, dez. 2018.

NEVILLE, A. M.; BROOKS, J. J. **Concrete technology**. England: Longman Scientific & Technical, 1987. v. 438

OLIVEIRA, I. R. DE et al. **Dispersão e empacotamento das partículas: princípios e aplicações em processamento cerâmico.** São Paulo: Fazendo Arte, 2000.

OLIVEIRA, F. C. et al. Probabilistic functions of mechanical properties of plain cement pastes determined by a reduced-size test. **Construction and Building Materials**, v. 286, p. 122907, jun. 2021.

PALM, S. et al. Cements with a high limestone content – Mechanical properties, durability and ecological characteristics of the concrete. **Construction and Building Materials**, v. 119, p. 308–318, ago. 2016.

POWERS, T. C. Structure and Physical Properties of Hardened Portland Cement Paste. **Journal of the American Ceramic Society**, v. 41, n. 1, p. 1–6, jan. 1958.

POWERS, T. C.; BROWNYARD, T. L. Studies of the physical properties of hardened Portland cement paste. **Relation of physical characteristics of the paste to compressive strength**, 1947.

PROSKE, T. et al. Concretes made of efficient multi-composite cements with slag and limestone. **Cement and Concrete Composites**, v. 89, p. 107–119, maio 2018.

QUATTRONE, M.; ANGULO, S. C.; JOHN, V. M. Energy and CO2 from high performance recycled aggregate production. **Resources, Conservation and Recycling**, v. 90, p. 21–33, set. 2014.

RAKI, L.; BEAUDOIN, J. J.; MITCHELL, L. Layered double hydroxide-like materials: nanocomposites for use in concrete. **Cement and Concrete Research**, v. 34, n. 9, p. 1717–1724, set. 2004.

REAL, S. et al. Influence of the Treatment Temperature on the Microstructure and Hydration Behavior of Thermoactivated Recycled Cement. **Materials**, v. 13, n. 18, p. 3937, 5 set. 2020.

REN, H. et al. Thermal characterization and kinetic analysis of nesquehonite, hydromagnesite, and brucite, using TG–DTG and DSC techniques. **Journal of Thermal Analysis and Calorimetry**, v. 115, n. 2, p. 1949–1960, fev. 2014.

RICHARDSON, I. G. The calcium silicate hydrates. **Cement and Concrete Research**, v. 38, n. 2, p. 137–158, fev. 2008.

RUSSELL, N. **Understanding the rheology of concrete**. Oxford: Woodhead Publ., 2012.

SALOMÃO, R. et al. Hydrotalcite synthesis via co-precipitation reactions using MgO and Al(OH)3 precursors. **Ceramics International**, v. 37, n. 8, p. 3063–3070, dez. 2011.

SCRIVENER, K. L.; JOHN, V. M.; GARTNER, E. M. Eco-efficient cements: Potential economically viable solutions for a low-CO2 cement-based materials industry. **Cement and Concrete Research**, v. 114, p. 2–26, dez. 2018.

SCRIVENER, K. L.; JUILLAND, P.; MONTEIRO, P. J. M. Advances in understanding hydration of Portland cement. **Cement and Concrete Research**, v. 78, p. 38–56, dez. 2015.

SCRIVENER, K.; SNELLINGS, R.; LOTHENBACH, B. (EDS.). **A Practical Guide to Microstructural Analysis of Cementitious Materials**. 0. ed. [s.l.] CRC Press, 2018.

SERPELL, R.; LOPEZ, M. Reactivated cementitious materials from hydrated cement paste wastes. **Cement and Concrete Composites**, v. 39, p. 104–114, maio 2013.

SERPELL, R.; LOPEZ, M. Properties of mortars produced with reactivated cementitious materials. **Cement and Concrete Composites**, v. 64, p. 16–26, nov. 2015.

SERPELL, R.; ZUNINO, F. Recycling of hydrated cement pastes by synthesis of α′H-C2S. **Cement and Concrete Research**, v. 100, p. 398–412, out. 2017.

SHAW, S.; HENDERSON, C. M. B.; KOMANSCHEK, B. U. Dehydrationrrecrystallization mechanisms, energetics, and kinetics of hydrated calcium silicate minerals: an in situ TGArDSC and synchrotron radiation SAXSrWAXS study. p. 19, 2000.

SHUI, Z. et al. Rehydration reactivity of recycled mortar from concrete waste experienced to thermal treatment. **Construction and Building Materials**, v. 22, n. 8, p. 1723–1729, ago. 2008.

SHUI, Z. et al. Cementitious characteristics of hydrated cement paste subjected to various dehydration temperatures. **Construction and Building Materials**, v. 23, n. 1, p. 531–537, jan. 2009.

SHUI, Z. et al. Preparation of new cementitious system using fly ash and dehydrated autoclaved aerated concrete. **Journal of Wuhan University of Technology-Mater. Sci. Ed.**, v. 29, n. 4, p. 726–732, ago. 2014.

SHUI, Z.; YU, R.; DONG, J. Activation of Fly Ash with Dehydrated Cement Paste. **ACI Materials Journal**, p. 6, 2011.

SILVA, A. G.; DE ALENCAR LOTUFO, R.; FLORES, F. C. **Classification of microstructures by morphological analysis and estimation of the hydration degree of cement paste in concrete**. Proceedings. XV Brazilian Symposium on Computer Graphics and Image Processing. **Anais**... Em: 15TH BRAZILIAN SYMPOSIUM ON COMPUTER GRAPHICS AND IMAGE PROCESSING. Fortaleza-CE, Brazil: IEEE Comput. Soc, 2002. Disponível em: <http://ieeexplore.ieee.org/document/1167136/>. Acesso em: 26 out. 2022

SNELLINGS, R. et al. RILEM TC-238 SCM recommendation on hydration stoppage by solvent exchange for the study of hydrate assemblages. **Materials and Structures**, v. 51, n. 6, p. 172, dez. 2018.

SOBOLEV, K. et al. Nano-Engineered Cements with Enhanced Mechanical Performance.

Journal of the American Ceramic Society, v. 99, n. 2, p. 564–572, fev. 2016.

SPLITTGERBER, F.; MUELLER, A. **Inversion of the cement hydration as a new method for identification and/or recycling**. . Em: INTERNATIONAL CONGRESS ON THE CHEMISTRY OF CEMENT. Durban, South Africa: Unpublished, jan. 2003. Disponível em: <http://rgdoi.net/10.13140/2.1.2201.3766>

STATISTA. **Cement production worldwide from 1995 to 2021**. , 2020. Disponível em: <https://www.statista.com/statistics/1087115/global-cement-production-volume/>

T. C. POWERS AND T. L. BROWNYARD. Studies of the Physical Properties of Hardened Portland Cement Paste. **ACI Journal Proceedings**, v. 43, n. 9, 9 jan. 1946.

TAYLOR, H. F. W. **Cement chemistry**. London: Thomas Telford, 1997. v. 2

TEIXEIRA, J. E. S. L. et al. Estudo do comportamento reológico de pastas cimentícias utilizando reômetro de cisalhamento dinâmico. **Revista Ibracon de Estruturas e Materiais**, v. 7, n. 6, p. 922–939, dez. 2014.

TRINKS, W. et al. **Industrial furnaces**. [s.l.] John Wiley & Sons, 2003. v. 1

UNITED NATIONS. **World population prospects**. [s.l.] Department of Economic and Social Affairs, 2019. v. Population Division

VYŠVAŘIL, M. et al. Physico-mechanical and microstructural properties of rehydrated blended cement pastes. **Construction and Building Materials**, v. 54, p. 413–420, mar. 2014.

WANG, J. Modeling of concrete dehydration and multhiphase transfer in nuclear containment concrete wall during loss of cooling accident. p. 212, 2016.

WANG, J.; LACARRIÈRE, L.; SELLIER, A. Multicomponent modelling of cement paste dehydration under different heating rates. **Materials and Structures**, v. 52, n. 1, p. 6, fev. 2019.

WANG, J.; MU, M.; LIU, Y. Recycled cement. **Construction and Building Materials**, v. 190, p. 1124–1132, nov. 2018.

WONG, H. H. C.; KWAN, A. K. H. Packing density of cementitious materials: part 1—measurement using a wet packing method. **Materials and Structures**, v. 41, n. 4, p. 689–701, maio 2008.

XINWEI, M.; ZHAOXIANG, H.; XUEYING, L. Reactivity of Dehydrated Cement Paste from Waste Concrete Subjected to Heat Treatment. p. 6, 2010.

XU, L. et al. A systematic review of factors affecting properties of thermal-activated recycled cement. **Resources, Conservation and Recycling**, v. 185, p. 106432, out. 2022.

XU, L. et al. Investigations on the rehydration of recycled blended SCMs cement. **Cement and Concrete Research**, v. 163, p. 107036, jan. 2023.

XUAN, D. X.; SHUI, Z. H. Rehydration activity of hydrated cement paste exposed to high temperature. **Fire and Materials**, v. 35, n. 7, p. 481–490, nov. 2011.

YI, S.-T.; YANG, E.-I.; CHOI, J.-C. Effect of specimen sizes, specimen shapes, and placement directions on compressive strength of concrete. **Nuclear Engineering and Design**, v. 236, n. 2, p. 115–127, jan. 2006.

YU, P.; KIRKPATRICK, J. R. Thermal dehydration of tobermorite and Jennite. Concrete Science and Engineering. v. 1, n. 3, p. 185–191, 1 set. 1999.

YU, R.; SHUI, Z. Influence of agglomeration of a recycled cement additive on the hydration and microstructure development of cement based materials. **Construction and Building Materials**, v. 49, p. 841–851, dez. 2013.

ZANCHETTA, L. DE M. **Efeito do teor de filer calcário na microestrutura de materiais cimentícios: uma análise multiescala.** Doutorado em Engenharia de Construção Civil e Urbana—São Paulo: Universidade de São Paulo, 10 set. 2021.

ZANOVELLO, M. et al. Strength-porosity correlation and environmental analysis of recycled Portland cement. **Resources, Conservation and Recycling**, v. 190, p. 106763, mar. 2023.

ZHANG, L. et al. Modification and enhancement of mechanical properties of dehydrated cement paste using ground granulated blast-furnace slag. **Construction and Building Materials**, v. 164, p. 525–534, mar. 2018.

ZHANG, Q.; YE, G. Microstructure Analysis of Heated Portland Cement Paste. **Procedia Engineering**, v. 14, p. 830–836, 2011.

ZHANG, Q.; YE, G. Dehydration kinetics of Portland cement paste at high temperature. **Journal of Thermal Analysis and Calorimetry**, v. 110, n. 1, p. 153–158, out. 2012.

ZHANG, Q.; YE, G. Quantitative analysis of phase transition of heated Portland cement paste. **Journal of Thermal Analysis and Calorimetry**, v. 112, n. 2, p. 629–636, maio 2013.

ZHANG, Q.; YE, G.; KOENDERS, E. Investigation of the structure of heated Portland cement paste by using various techniques. **Construction and Building Materials**, v. 38, p. 1040–1050, jan. 2013.

ZHANG, Y. et al. Ink-bottle Effect and Pore Size Distribution of Cementitious Materials Identified by Pressurization–Depressurization Cycling Mercury Intrusion Porosimetry. **Materials**, v. 12, n. 9, p. 1454, 5 maio 2019.

ZHENG, K. et al. Reverse filling cementitious materials based on dense packing: The concept and application. **Powder Technology**, v. 359, p. 152–160, jan. 2020.

ZHOU, Q.; LACHOWSKI, E. E.; GLASSER, F. P. Metaettringite, a decomposition product of ettringite. **Cement and Concrete Research**, v. 34, n. 4, p. 703–710, abr. 2004.

ZHUTOVSKY, S.; SHISHKIN, A. Recycling of hydrated Portland cement paste into new clinker. **Construction and Building Materials**, v. 280, p. 122510, abr. 2021.

SUPPLEMENTARY MATERIAL A: SCALE FACTOR INDEX

Oliveira et al. (2021) (OLIVEIRA et al., 2021) presents results of tensile strength in cubic shaped pastes from the literature as a function of cube size (Figure A1a) to express a scale effect . The axes were converted to logarithm and the exponential trend was found (Figure A1b). Tensile values were found for the cube dimensions of interest 20 to 70 mm through Equation A1. Afterwards, the strength values were divided according to the reference dimension 27 mm. In this way, the shape factor index was created (Figure A2).

Figure A1 - Experimental and literature data in relation to the observation scale for tensile strength (a) and mathematical procedure for trend identification (b)

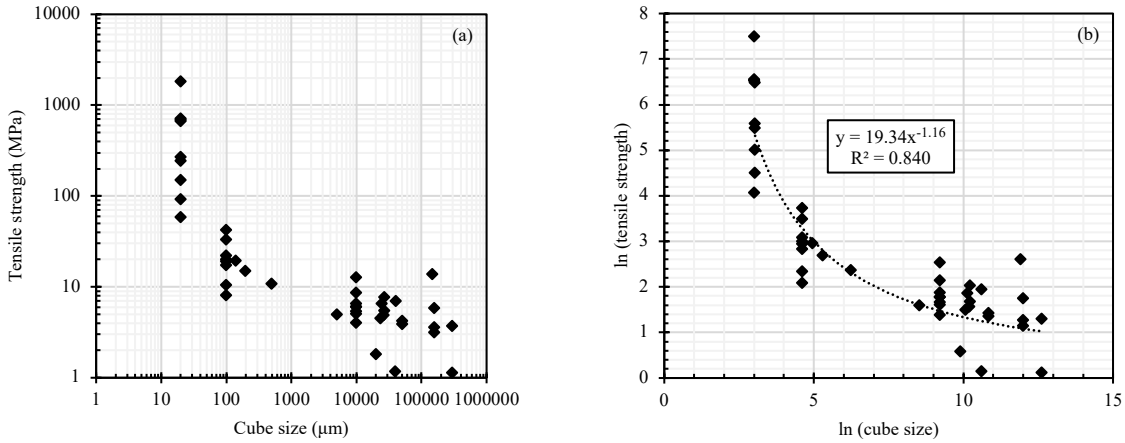

Where "σ_s" is the tensile strength in MPa and "d" is the side of the cube in mm.

$$\sigma_s = e^{19.336\,[\ln(1000d)]^{-1.16}} \qquad \text{Equation A1}$$

Figure A2 - Shape factor index for different cube sizes

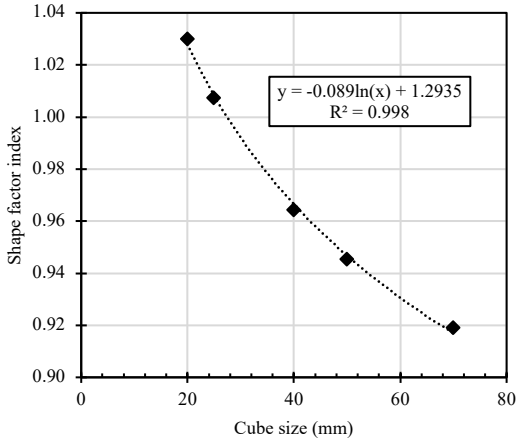

SUPPLEMENTARY MATERIAL B: MIX DESIGN OF ENGINEERED CEMENTS

The steps for determining the initial mix design proportions of engineered cements are described in Table B1.

Table B1 - Mix design steps for engineered cements development.

Steps	Input data	Output data	Assumptions
Volumetric composition of precursor paste at 28d	HIS-C density (3.05 g/cm^3) w/s ratio (0.45 g/g) HIS-C combined water (0.245 g/g)	Hydrated solids volume (65%) Porosity of precursor paste (35%)	Powers' simplified equations (Equations B1-B4).
Porosity of R-PC	R-PC density (2.65 g/cm^3) Turning-point water (0.60 g/g)	Dehydrated solids volume (39%) Intragranular porosity (21%) Intergranular porosity (40%)	The turning point measures the R-PC porosity (intra and inter). There are only intragranular pores, after dehydration.
Volumetric composition of R-PC paste at 28d	R-PC density (2.65 g/cm^3) w/s ratio (0.60 g/g) R-PC combined water (0.173 g/g)	Rehydrated solids (52%) Intragranular porosity (16%) Intergranular porosity (32%)	Powers' simplified equations (Equations B1-B4). Intra and inter porosities are reduced proportionally.
Volumetric composition of EC paste at 28 and 0d	Porosity of precursor paste (35%) MPC combined water (0.245 g/g)	Hydrated solids and filler contents for each scenario strategy: (i) R80-C20: 13% of hydrated solids filled by MPC hydration. (ii) R75-C10: 13% of hydrated solids filled half by MPC hydration and half by MLF. (iii) R35-C15: 50% of R-PC replaced by OLF and 13% of hydrated solids filled half by MPC hydration. EC pastes volume discretized by R-PC, MPC, MLF, OLF and water	Define the hydrated solids and filler content needed to achieve the precursor paste porosity in EC paste. The hydrated solids only fill the inter porosity of the R-PC paste. R-PC was adopted equal to dehydrated solids. MPC was determined using the hydrated solids volume growth by Powers for HIS-C paste. Porosity is occupied by water.
Final mass composition of EC pastes	R-PC density (2.65 g/cm^3) MPC density (2.92 g/cm^3) MLF density (2.82 g/cm^3) OLF density (2.79 g/cm^3)	R-PC, MPC, LFs and water mass contents	Volume x specific gravity = Mass

$$V_{paste} = V_{solids} + V_{water} \quad \text{Equation B1}$$

$$V_{hydrates\ solids} = V_{solids} + 0.75w_n \quad \text{Equation B2}$$

$$V_{pores} = V_{paste} - V_{hydrate\ solids} \quad \text{Equation B3}$$

$$P = V_{pores}/V_{paste} \quad \text{Equation B4}$$

Figure B1 - Schematical representation of volumetric percentual composition of hydrated precursor paste at 28 days, R-PC grain and rehydrated R-PC paste at 28 days.

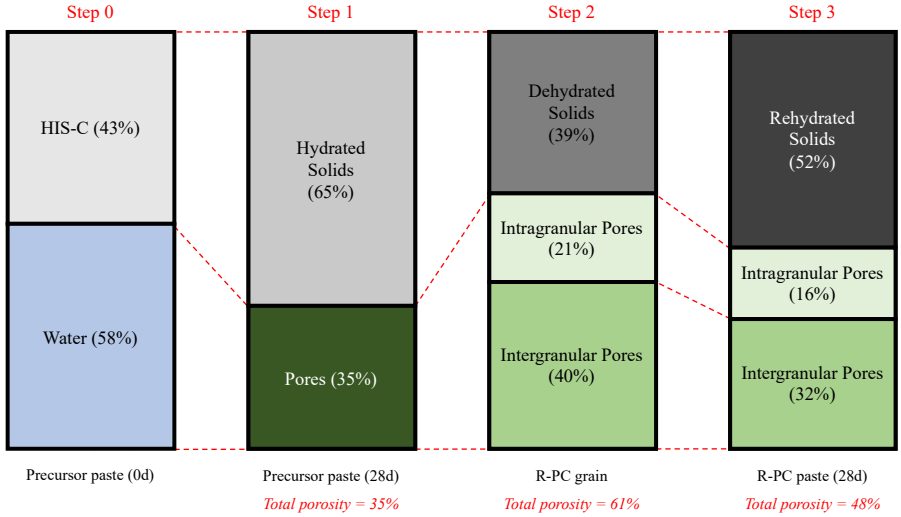

Figure B2 - Schematical representation of volumetric percentual composition of each engineered cement pastes.

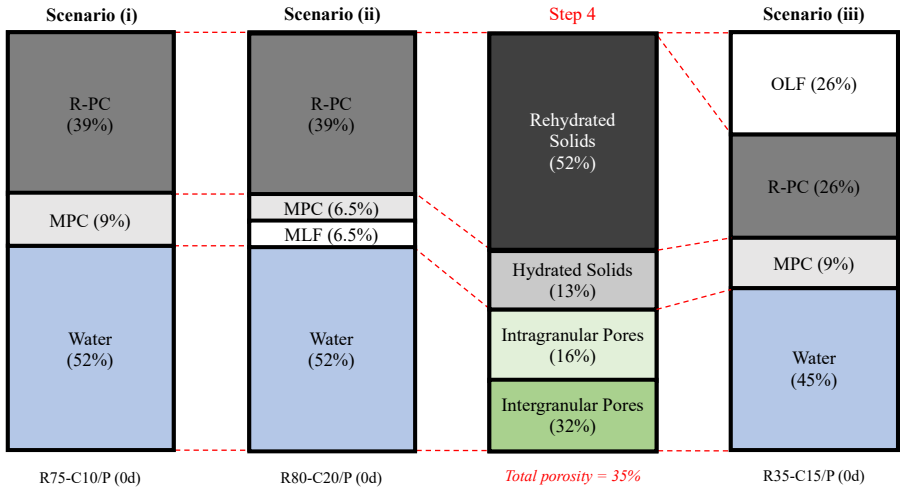

Table B2 presents the designed and real engineered cement pastes. All the pastes demand more water than designed.

Table B2 - Estimated and real engineered cement pastes.

Paste	R-PC	MPC	MLF	OLF	w/s $_{estimated}$	w/s $_{real}$	SP (%)
R80-C20/P	80%	20%			0.42	0.48	1.00
R75-C10/P	75%	10%	15%		0.38	0.43	1.00
R35-C15/P	35%	15%		50%	0.30	0.36	0.60

Mix design concepts illustration

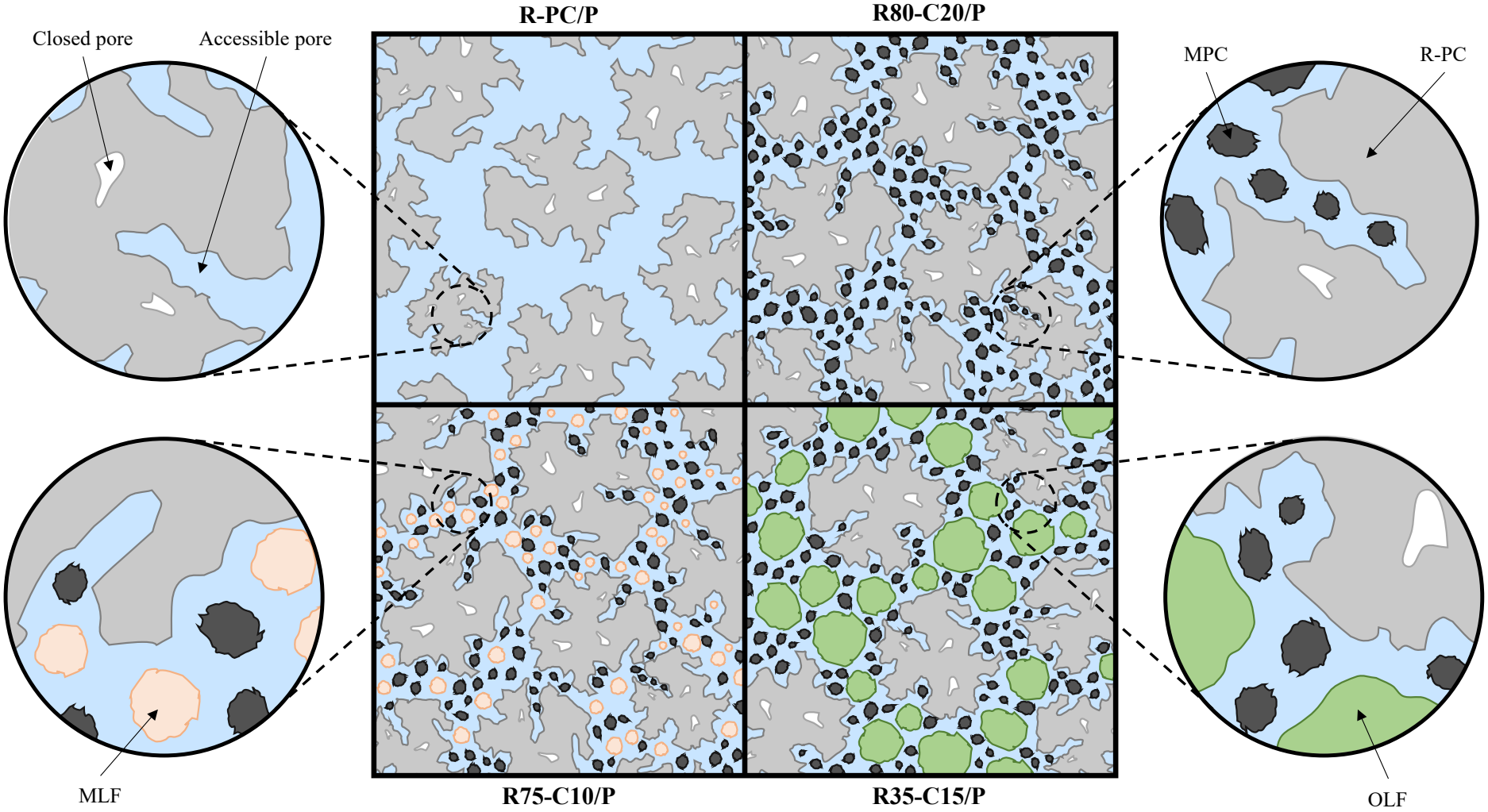

SUPPLEMENTARY MATERIAL C: CHARACTERIZATION OF POWDERS AND PASTES

Table C1 presents the phases, crystal system, formula and parameters of the unitary cells used for the Rietveld refinement.

Table C1 - Rietveld refinement information.

Phase	Crystal system	Formula	COD
Alite	Monoclinic	Ca_3SiO_5	96 154 0705
Alite	Triclinic	Ca_3SiO_5	96 901 6126
Aluminate	Cubic	$Ca_3Al_2O_6$	96 100 0040
Bassanite	Monoclinic	$CaSO_4 \cdot 0.5H_2O$	96 901 2210
Brownmillerite	Orthorhombic	Ca_2AlFeO_5	96 120 0010
Brownmillerite	Orthorhombic	Ca_2AlFeO_5	96 901 6629
Calcite	Hexagonal	$CaCO_3$	96 900 0967
Calcite	Hexagonal	$CaCO_3$	96 900 9669
Dolomite	Hexagonal	$CaMg(CO_3)_2$	96 900 1010
Ettringite	Hexagonal	$C_3A \cdot 3CaSO_4 \cdot 32H_2O$	96 901 2923
Larnite	Monoclinic	Ca_2SiO_4	96 901 2790
Larnite	Monoclinic	Ca_2SiO_4	96 901 2791
Larnite	Monoclinic	Ca_2SiO_4	96 901 2793
Magnesium calcite	Hexagonal	$C_6O_{18}Ca_{5.64}Mg_{0.36}$	96 721 4218
Monocarboaluminate	Anorthic	$3CaO \cdot Al_2O_3 \cdot CaCO_3 \cdot 11H_2O$	96 100 0460
Portlandite	Hexagonal	$Ca(OH)_2$	96 100 1769
Portlandite	Hexagonal	$Ca(OH)_2$	96 152 9753
Portlandite	Hexagonal	$Ca(OH)_2$	96 900 0114
Quartz	Hexagonal	SiO_2	96 101 1177
Tobermorite	Anorthic	$Ca_5Si_6O_{18}$	96 900 5448

Mercury intrusion Porosimetry result of R-PC is presented in Figure C1.

Figure C1 - Pore size distribution for R-PC grain through MIP.

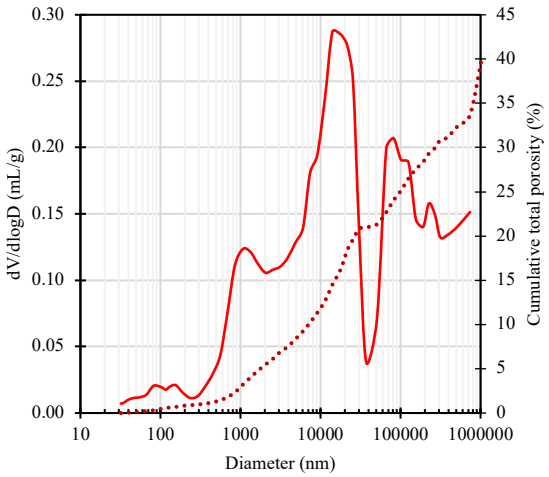

TG/DTG results of anhydrous materials are shown in Figure C2.

Figure C2 - TG/DTG results of cements (a,b) and limestone fillers (c,d) used in this work.

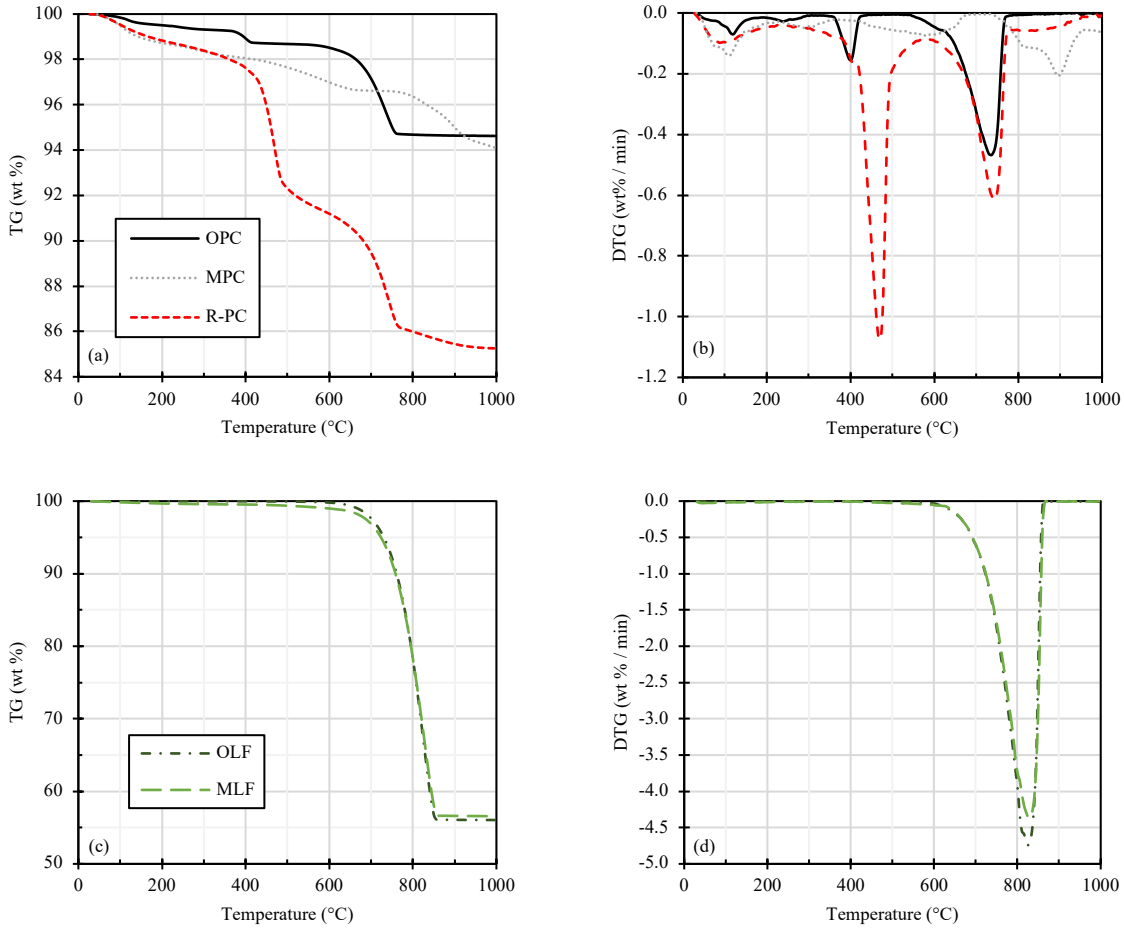

Table C2 - Chemical notation, molecular weight, molar volume and density of each phase used in the QXRD.

Phases	Chemical Notation	M [g/mol]	V° [cm³/mol]	Density [g/cm³]
C_3S	Ca_3SiO_5	228.33	73[a]	3.13
C_2S	Ca_2SiO_4	172.25	52[a]	3.31
C_3A	$Ca_3Al_6O_{12}$	474.12	89[a]	5.33
C_4AF	$Ca_2(Al,Fe)_2O_5$	325.82	130[a]	2.51
Bassanite	$CaSO_4{\cdot}0.5H_2O$	145.16	54[b]	2.68
Calcite	$CaCO_3$	100.09	37[c]	2.71
Dolomite	$CaMg(CO_3)_2$	184.41	64[d]	2.87
Monocarboaluminate	$Ca_3Al_2(OH)_6(CO_3){\cdot}4H_2O$	408.35	150[a]	2.72
Ettringite	$Ca_6Al_2(SO_4)_3(OH)_{12}{\cdot}26H_2O$	1255.29	707[a]	1.78
Portlandite	$Ca(OH)_2$	74.10	33[c]	2.25
C-S-H (tobermorite)	$Ca_5Si_6O_{16}(OH)_2{\cdot}4H_2O$	731.04	59[c]	12.39

[a] Molar volume calculated by unit cell or density given in (TAYLOR, 1997).
[b] Average value based on Mineralogy database and (ELERT; BEL-ANZUÉ; BURGOS-RUIZ, 2023).
[c] Data from PSI-GEMS dataset presented at (MATSCHEI; LOTHENBACH; GLASSER, 2007).
[d] Data from (MATSCHEI; LOTHENBACH; GLASSER, 2007).

Figure C3 - TG and DTG results for HIS-C/P (a,b), R-PC/P (c,d), R80-C20/P (e,f), R75-C10/P (g,h) and R35-C15/P (i,j).

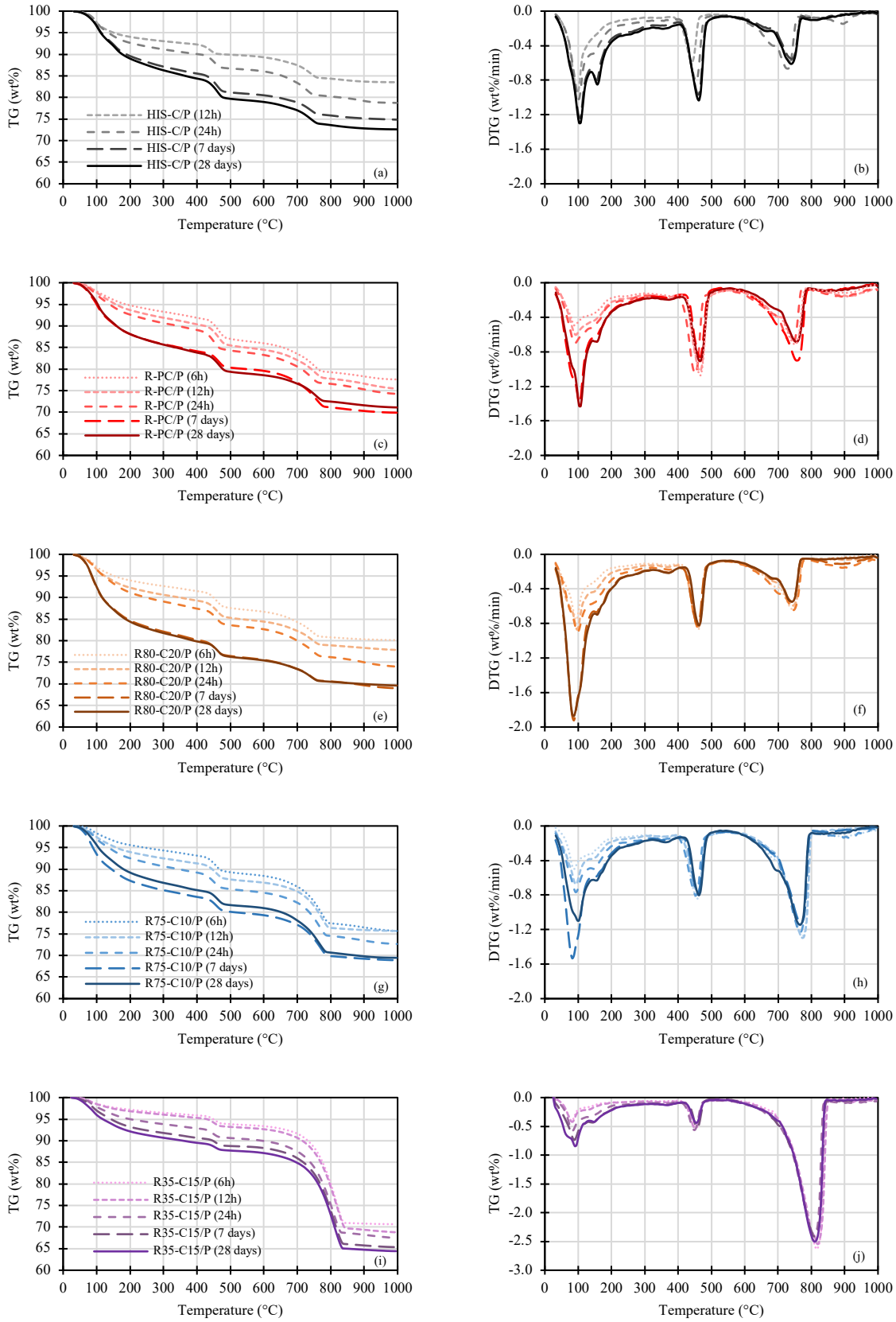

Table C3 synthetize the important mass losses and combined water by the TG/DTG results of the pastes of this work at different ages.

Table C3 - TG analysis of engineered cement pastes at different ages.

Paste	Age	Mass loss (% g/g)					Wn [f]	α [g]
		W_{25}-W_{330} [a]	W_{330}-W_{430} [b]	W_{430}-W_{550} [c]	W_{550}-W_{1000} [d]	LOI [e]		
HIS-C/P	0h	0.72	0.58	0.06	4.05	5.40	0.014	
	12h	7.19	1.30	1.82	6.16	16.48	0.101	33.8
	1d	9.21	1.25	3.10	7.70	21.26	0.142	47.5
	7d	13.37	1.70	4.08	5.99	25.14	0.222	74.2
	28d	14.31	1.99	4.36	6.73	27.39	0.245	81.9
R-PC/P	0h	1.73	0.91	5.73	6.36	14.73	0.091	
	6h	7.10	1.49	4.96	8.85	22.41	0.065	31.3
	12h	8.54	1.63	4.89	9.50	24.55	0.085	40.9
	1d	9.80	2.04	4.33	9.58	25.76	0.101	48.6
	7d	14.72	1.58	3.71	10.10	30.10	0.157	75.5
	28d	14.88	1.87	4.29	7.85	28.89	0.173	83.2
R80-C20/P	0h	1.73	0.78	4.71	5.73	12.96	0.078	
	6h	7.68	1.28	3.91	6.99	19.86	0.068	22.4
	12h	9.75	1.50	3.91	6.99	22.14	0.098	32.3
	1d	11.40	1.68	3.77	9.17	26.02	0.123	40.6
	7d	18.45	1.92	3.62	7.03	31.02	0.234	77.2
	28d	18.80	1.84	3.50	6.25	30.39	0.237	78.2
R75-C10/P	0h	1.54	0.72	4.40	11.49	18.15	0.072	
	6h	6.02	1.39	3.74	13.19	24.33	0.053	25.4
	12h	7.85	1.39	3.53	11.56	24.33	0.073	34.9
	1d	9.78	1.80	3.45	12.31	27.34	0.103	49.3
	7d	15.33	1.56	3.36	10.86	31.11	0.155	74.2
	28d	13.67	1.61	3.35	11.91	30.54	0.179	85.6
R35-C15/P	0h	1.08	0.40	2.23	24.03	27.75	0.036	
	6h	3.78	0.62	2.06	22.90	29.35	0.031	24.4
	12h	4.19	0.83	2.06	24.19	31.26	0.039	30.7
	1d	6.44	0.89	2.40	22.90	32.63	0.070	55.1
	7d	8.42	1.10	1.92	23.31	34.74	0.091	71.7
	28d	9.65	1.03	1.92	23.03	35.63	0.104	81.9

[a] *Decomposition of C-S-H, monosulfoaluminate and ettringite.*
[b] *Decomposition of brucite.*
[c] *Decomposition of portlandite (CH). Portlandite (% g/g) = water loss (% g/g) × (74/18).*
[d] *Decomposition of not well crystalline calcite ($CaCO_3$). Calcite (% g/g) = CO_2 loss (% g/g) × (100/44).*
[e] *Loss on ignition (LOI).*
[f] *Combined water content (g/g).*
[g] *Hydration degree (%)*

The combined water content at 90 days was estimated using a logarithmic trend as follows: 0.299 g/g for HIS-C/P, 0.208 g/g for R-PC/P, 0.303 g/g for R80-C20/P, 0.209 g/g for R75-C10/P, and 0.127 g/g for R35-C15/P.

Figure C4 - Differential intrusion volume against pore diameter (dV/dlogD) was measured for the experimental pastes at 1, 7, and 28 days. It's important to note that the R-PC/P result is missing at 1 day due to the paste's inability to withstand the stress required for slicing during sample preparation.

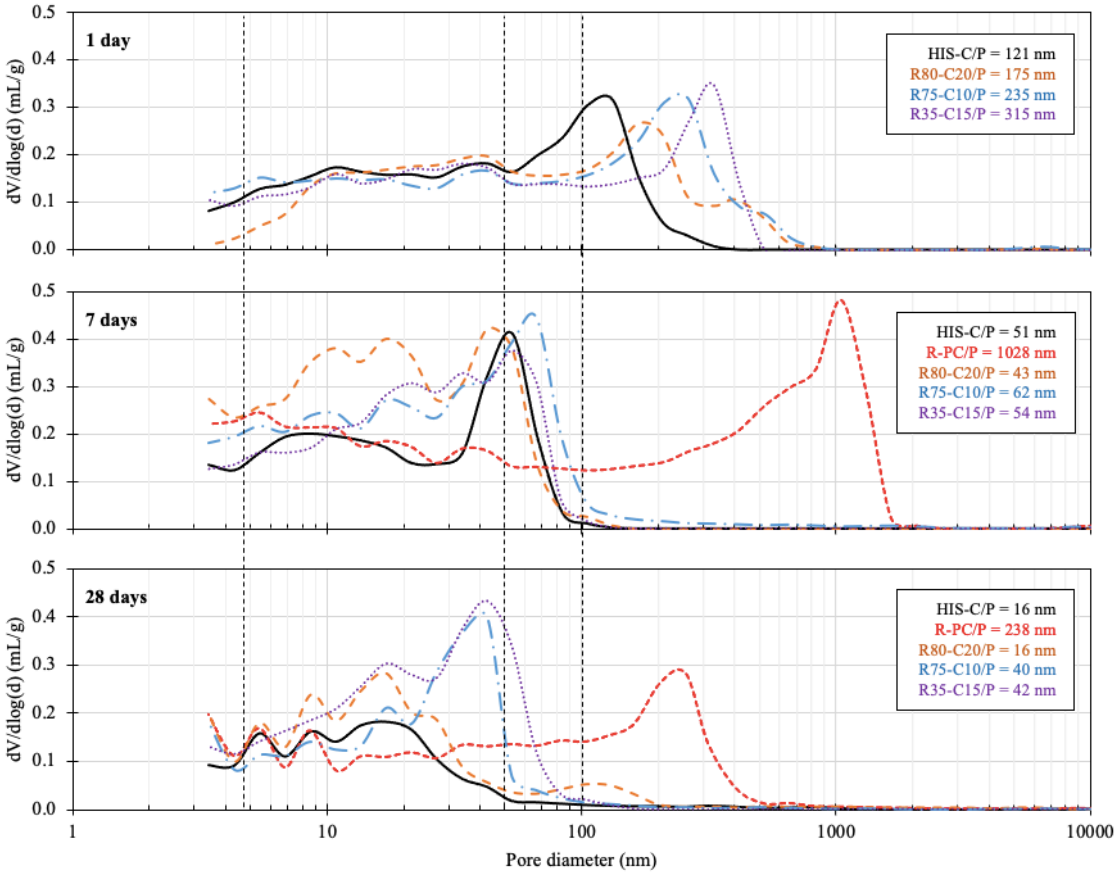

Figure C5 - Compressive strength relation with critical diameter (a) and total porosity (b) determined by MIP.